European Journal of Medicinal Chemistry 221 (2021) 113512

Contents lists available at ScienceDirect

European Journal of Medicinal Chemistry

journal homepage: http://www.elsevier.com/locate/ejmech

Development of tricyclic *N*-benzyl-4-hydroxybutanamide derivatives as inhibitors of GABA transporters mGAT1-4 with anticonvulsant, antinociceptive, and antidepressant activity

Paula Zaręba [a, *], Kinga Sałat [a], Georg C. Höfner [b], Kamil Łątka [a], Marek Bajda [a], Gniewomir Latacz [a], Krzysztof Kotniewicz [a], Anna Rapacz [a], Adrian Podkowa [a], Maciej Maj [c], Krzysztof Jóźwiak [c], Barbara Filipek [a], Klaus T. Wanner [b], Barbara Malawska [a], Katarzyna Kulig [a, 1]

[a] Faculty of Pharmacy, Jagiellonian University Medical College, 9 Medyczna St, 30–688, Kraków, Poland
[b] Department of Pharmacy, Center for Drug Research, Ludwig-Maximilians-Universität München Butenandtstr, 5-13, 81377, Munich, Germany
[c] Department of Biopharmacy, Medical University of Lublin, ul. W. Chodzki 4a, 20-093, Lublin, Poland

ARTICLE INFO

Article history:
Received 21 November 2020
Received in revised form
20 April 2021
Accepted 22 April 2021
Available online 4 May 2021

Keywords:
GABA transporter
mGAT1
mGAT2
mGAT3
mGAT4
GAT inhibitors
N-benzylamides
[^{3}H]GABA uptake
Molecular docking
Molecular dynamics
Anticonvulsant activity
Antinociceptive activity
Antidepressant-like properties

ABSTRACT

γ-Aminobutyric acid (GABA) neurotransmission has a significant impact on the proper functioning of the central nervous system. Numerous studies have indicated that inhibitors of the GABA transporters mGAT1-4 offer a promising strategy for the treatment of several neurological disorders, including epilepsy, neuropathic pain, and depression. Following our previous results, herein, we report the synthesis, biological evaluation, and structure-activity relationship studies supported by molecular docking and molecular dynamics of a new series of *N*-benzyl-4-hydroxybutanamide derivatives regarding their inhibitory potency toward mGAT1-4. This study allowed us to identify compound **23a** (*N*-benzyl-4-hydroxybutanamide bearing a dibenzocycloheptatriene moiety), a nonselective GAT inhibitor with a slight preference toward mGAT4 (pIC_{50} = 5.02 ± 0.11), and compound **24e** (4-hydroxy-*N*-[(4-methylphenyl)-methyl]butanamide bearing a dibenzocycloheptadiene moiety) with relatively high inhibitory activity toward mGAT2 (pIC_{50} = 5.34 ± 0.09). In a set of *in vivo* experiments, compound **24e** successively showed predominant anticonvulsant activity and antinociception in the formalin model of tonic pain. In contrast, compound **23a** showed significant antidepressant-like properties in mice. These results were consistent with the available literature data, which indicates that, apart from seizure control, GABAergic neurotransmission is also involved in the pathophysiology of several psychiatric diseases, however alternative mechanisms underlying this action cannot be excluded. Finally, it is worth noting that the selected compounds showed unimpaired locomotor skills that have been indicated to give reliable results in behavioral assays.

1. Introduction

γ-Aminobutyric acid (GABA, **1**, Fig. 1) is the main inhibitory neurotransmitter found in the central nervous system (CNS) of diverse species [1]. A growing body of research has shown that pathologically decreased GABA concentrations in the synaptic cleft are involved in the etiology of several neurological and psychiatric disorders, including epilepsy [2–5], neuropathic pain (NP) [6–8], depression [1], anxiety [9], and Parkinson's [10], Huntington's [11], and Alzheimer's diseases [12]. For years, a number of mechanisms influencing the imbalance between inhibitory and excitatory neurotransmission have been studied. Among these mechanisms, regulation of the synthesis, release, and removal of synaptically released GABA is of fundamental importance for the maintenance of brain function at all levels. As a result, numerous studies have confirmed that inhibition of membrane-bound GABA transporters (GATs) is a successful approach for the enhancement of decreased GABA function. GABA transporters of the solute carrier family 6

* Corresponding author. 9 Medyczna Street, 30–688, Kraków, Poland.
E-mail address: paula.zareba@uj.edu.pl (P. Zaręba).
[1] Author is deceased.

https://doi.org/10.1016/j.ejmech.2021.113512
0223-5234/

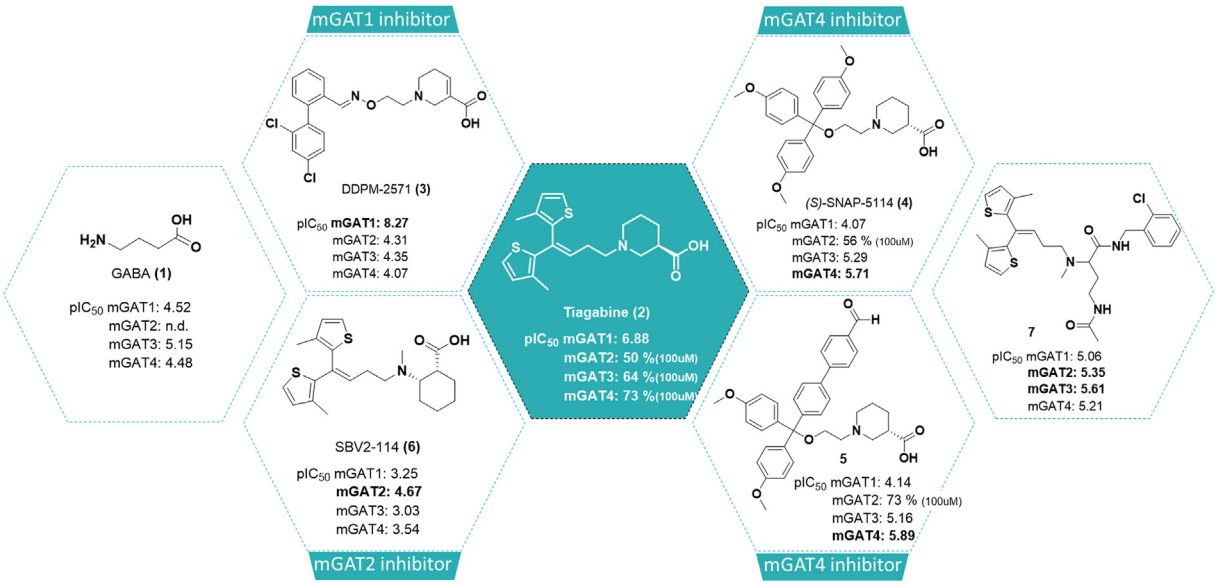

Fig. 1. Structure of a GABA transport substrate – GABA (**1**), which itself is a potent inhibitor of [^{3}H]-GABA uptake [44], and known GAT inhibitors with their inhibitory activities toward GABA transporters and their pIC_{50} values: tiagabine (**2**) [29], DDPM-2571 (**3**) [29], (*S*)-SNAP-5114 (**4**) [35], **5** [36], SBV2-114 (**6**) [22], **7** [45] n.d. – not described.

(SLC6) are divided into four types, and have been cloned from mouse, rat, and human tissues [13]. It has been established that mouse GAT1 (mGAT1), GAT2 (mGAT2), GAT3 (mGAT3), and GAT4 (mGAT4) correspond to human and rat GAT1, BGT1 (betaine/GABA transporter 1), GAT2, and GAT3, respectively [2]. However, the species-dependent nomenclature can seem rather confusing; thus, the International Union of Basic and Clinical Pharmacology (IUPHAR) has proposed standardization of the terminology as follows: GAT1 (SLC6A1), GAT2 (SLC6A13), GAT3 (SLC6A11), and BGT1 (SLC6A12) [14]. In our current study, we utilized the mGAT1–mGAT4 nomenclature since we used *in vitro* assays based on GABA transporters cloned from mouse cells and *in vivo* mouse models of seizures, pain, depression, and anxiety. The four GAT subtypes differ in their expression and pharmacological roles. mGAT1 and mGAT4 are the most prevalent GAT and are almost exclusively located in the CNS. mGAT1 is distributed throughout the brain, with a high density in the neocortex, hippocampus, cerebellum, and basal ganglia. mGAT4 is predominantly observed at high concentrations in astrocytes and at lower densities in the spinal cord, brain stem, thalamus, and hypothalamus [13,14]. The high levels of brain mGAT1 and mGAT4 cause these transporters to play an important role in the inactivation of GABA and have been identified as a main pharmacological target. In contrast, the betaine-GABA transporter (mGAT2) and mGAT3 represent potentially minor prospective significance for the inactivation of GABAergic neurotransmission in the CNS since it was demonstrated that both are primarily expressed in peripheral organs and only at a low level in the brain [15–19]. However, BGT1 is still under investigation [20–24]. The effective development and registration of tiagabine (**2**, Fig. 1), a selective mGAT1 inhibitor, has made mGAT1 a well-known anticonvulsant target [25,26]. Furthermore, evidence from both clinical and preclinical studies have noted the importance of tiagabine (**2**) in anxiety, pain, and depression [27,28]. Other selective or nonselective mGAT1 inhibitor representatives, in particular the guvacine analog DDPM-2571 (**3**, Fig. 1) [29] and *N*-substituted nipecotic acid analog (*S*)-SNAP-5114 (**4**, Fig. 1) [30], have also been used as pharmacological tools to evaluate their CNS effects and the biological functions of diverse GABA transporters [31]. DDPM-2571 (**3**), a prominent mGAT1 inhibitor with the highest selectivity and affinity of mGAT1 inhibitors to date, presents antidepressant-like, anxiolytic-like, and antinociceptive properties [32]. (*S*)-SNAP-5114 (**4**), the first potent and slightly selective mGAT3/4 inhibitor, was described as an effective anticonvulsive and antinociceptive agent against different types of pain, including acute, persistent, and chronic pain [2,30,31,33,34]. However, with respect to the poor chemical stability of (*S*)-SNAP-5114 (**4**), which led to limitations in *in vivo* studies, modification of its lipophilic scaffold was found to be a promising strategy to improve selectivity toward mGAT1-4. As a consequence, performed studies allowed us to obtain, among others, compound **5** (Fig. 1) with higher inhibitory potency toward mGAT4 than lead molecule **4** with comparable subtype selectivity [35,36]. Compound **5** became a relevant molecule for the future development of more potent and selective mGAT4 inhibitors. Furthermore, several reports have indicated that SBV2-114 (**6**) has demonstrated moderate potency with improved selectivity toward BGT1 [20,37–40]. Even so, in a recent study, SBV2-114, the *cis*-cyclohexyl-β-amino acid **6**, has attracted attention as a potential target for seizure management [41]. As pointed out above, despite the low density of BGT1 in the brain, its inhibitors appear to be attractive for the elucidation of the pharmacological activity of BGT1 inhibitors. However, it should be noted that obtaining highly selective GAT inhibitors is difficult due to the high sequence identities of mGAT2-4 [17,42,43].

Based on the above considerations, GABA uptake inhibitors were found to be beneficial for the treatment of different disorders involving GABAergic neurotransmission. In this context, our previous work identified compound **7** (Fig. 1) which shows higher inhibitory potency toward mGAT3 (pIC_{50} = 5.61) than the well-known mGAT3/4 inhibitor – (*S*)-SNAP-5114 (**4**, pIC_{50} (mGAT3) = 5.29). In parallel, two selected structural analogs of **7** displayed an analgesic effect in two mouse models of chronic pain induced by streptozotocin (STZ) and oxaliplatin administration [45]. These results encouraged us to extend the development of novel GABA uptake inhibitors. Thus, in the present study, a set of new 4-hydroxybutanamide, 4-aminobutanamide, and 4-acetamidobutanamide derivatives was designed and synthesized. The subject of this study was to transform the diaromatic moiety of the parent compounds **8** [46] and **9** [47] into tricyclic systems

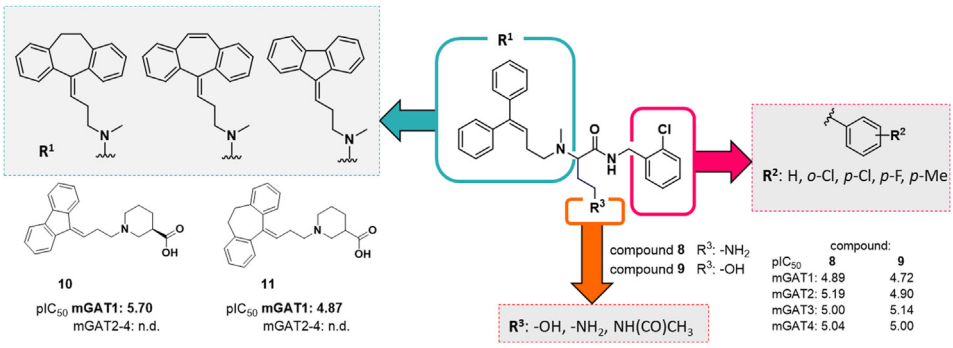

Fig. 2. The general structures of the target compounds based on modification of parent compounds **8** [46] and **9** [47] and known tricyclic derivatives of nipecotic acid **10** [49], and **11** [49].

(Fig. 2). We investigated the diverse lipophilic and electronegative side chains present in the structures of reference compounds, *i.e.,* dibenzocycloheptadiene and fluorene moieties (**10** [48] and **11** [49]) or dibenzocycloheptatriene moiety. Other modifications included the introduction of substituents into the benzyl fragment of the molecules, such as a chlorine atom at the *ortho* or *para* position or a fluorine atom or methyl group at the *para* position (Fig. 2). The whole novel series of butanamide derivatives were tested for their inhibitory potency at mGAT1-4. In addition, to explore the molecular interactions of target compounds with GABA transporters, we performed computational docking and molecular dynamics studies. Finally, to confirm the therapeutic potential of the obtained compounds, we tested lead compounds in animal seizure models. Additionally, bearing in mind the wide spectrum of indications of tiagabine (**2**) we also studied the antinociceptive, antidepressant-like, and anxiolytic-like activity for selected compounds.

2. Results

2.1. Chemistry

2.1.1. Synthesis of the 4-hydroxybutanamide derivatives 22a–e, 23a–e and 24a–e

The synthetic procedure for the 4-hydroxybutanamide derivatives **22a**–**e**, **23a**–**e**, and **24a**–**e** is outlined in Scheme 1. The primary strategy used for the synthesis of target compounds involved *N*-alkylation of the amine building blocks **15**, **16**, and **17** [50] with the appropriate alkyl halide, such as 3-bromodihydrofuran-2(3*H*)-one (**18**), to form **19**–**21**. As the initial step for the synthesis of building blocks with a tricyclic system, **15**, **16**, and **17** [50] and the corresponding bromides **12**–**14** [51] were obtained as described previously and further converted to suitable amines **15** [50], **16**, and **17** by a previously used general method [47]. Using *N*-benzylamine and its derivatives, aminolysis reactions [47,52] of intermediates **19**–**21** afforded the designed 4-hydroxybutanamide derivatives **22a**–**e**, **23a**–**e**, and **24a**–**e**.

2.1.2. Synthesis of the 4-aminobutanamide and 4-acetamidobutanamide derivatives 27a–e and 28a–e

The designed 4-aminobutanamide and 4-acetamidobutanamide derivatives **27a**–**e** and **28a**–**e** were prepared in accordance with previously described synthetic procedures [45]. As outlined in Scheme 2, in the first step, the introduction of a suitable tricyclic system with a butenyl linker into position 2 of the *N*-benzyl-2-bromo-4-(1,3-dioxo-2,3-dihydro-1*H*-isoindol-2-yl)butanamide derivatives (**25a**–**e**) was performed to obtain compounds **26a**–**e**. Subsequent hydrolysis of the phthalimide group yielded the desired 4-aminobutanamide derivatives **27a**–**e**. 4-Amino derivatives **27a**–**e** were then converted into suitable 2-substituted 4-acetamidobutanamide derivatives **28a**–**e** *via* an *N*-acylation reaction [45]. All compounds were synthesized as racemic mixtures.

2.2. In vitro evaluation and structure–activity relationships

The inhibitory potencies of all the obtained final compounds **22a**–**e**, **23a**–**e**, **24a**–**e**, **27a**–**e**, and **28a**–**e** were determined for the four mouse GABA transporter subtypes (mGAT1–4). The assay was based on [^{3}H]GABA uptake using human embryonic kidney cells (HEK-293) stably expressing mouse GABA transporters according to the literature [26]. The specific affinity to mGAT1 was determined by a competitive MS Binding Assay with NO711 as an unlabeled marker quantified by LC–ESI–MS/MS [53]. The compounds that could reduce GABA uptake or NO711 binding by at least 50% at an inhibitor concentration of 100 μM were considered active. The pIC_{50} or pK_i values from the [^{3}H]GABA uptake or MS Binding Assays were determined in triplicate in three independent experiments. If the test compounds at a screening concentration of 100 μM could not reduce [^{3}H]GABA uptake or NO711 binding below 50% ($pIC_{50} = 4.00$), the percent of remaining [^{3}H]GABA uptake or NO711 binding was given (in the presence of 100 μM inhibitor).

The influence on the inhibitory activity of the more rigid side chain of the *N*-benzyl-4-hydroxybutanamide derivatives toward mGAT1-4 was determined with reference to parent compounds **8** and **9** (Fig. 2). As seen from the *in vitro* data in Table 1 and Fig. 3, exchange of the diaryl moiety in parent compounds **8** and **9** into a tricyclic moiety generally led to increased GABA uptake inhibition, except for compounds with fluorene moiety (**22a**–**e**) that displayed reduced activity especially toward mGAT1-2 and mGAT4. It was found that the type of bridge connecting both aryl groups together and the substituents at position 4 of butanamide are substantial for GABA uptake inhibition. Among all the investigated 4-hydroxybutanamide derivatives with a tricyclic system, an optimal bridge seemed to be obtained with the dibenzocycloheptadiene derivatives **24a**–**e**. For compounds **24d** and **24e** with an ethylene bridge linking the two aryl groups together, we observed a noticeable increased activity in favor of mGAT2. The most potent mGAT2 inhibitor was compound **24e**, with a methyl group in the *para* position of the benzyl moiety (pIC_{50} 5.34). However, connecting both aromatic rings with a direct covalent bond caused a decrease in the activity of the obtained compounds **22a**–**e** to pIC_{50} 4.35–4.60 for mGAT4 compared to the nonrigid analogs **8** and **9** to pIC_{50} 5.00–5.06 for mGAT4, and maintenance of the preference for mGAT3 was observed but on a slightly lower level (pIC_{50} 4.70–4.99 and 5.00–5.14 for mGAT3, respectively; Table 1, Fig. 3). In addition, introduction of a double bond between C10 and C11 in the linker of

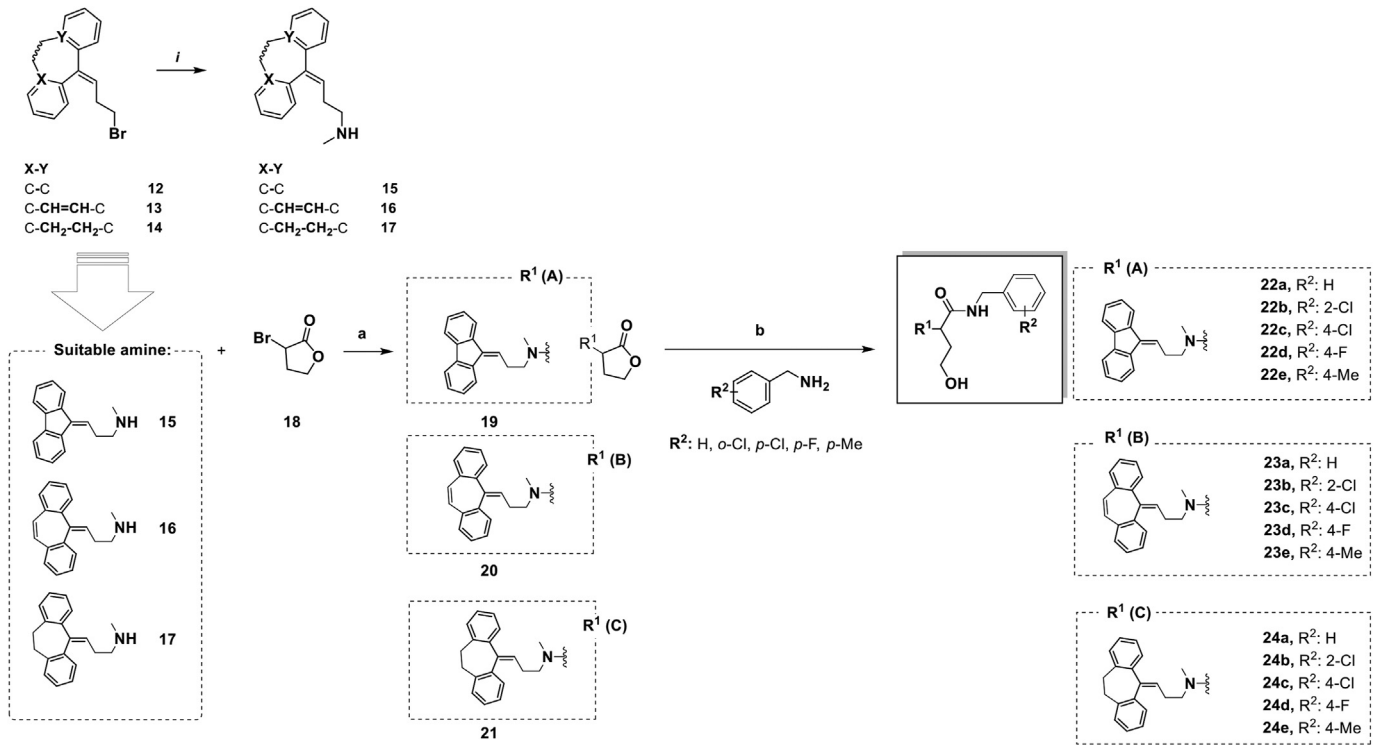

Scheme 1. Synthesis route for the 2-substituted derivatives of 4-hydroxybutanamide **22a**–**e**, **23a**–**e**, and **24a**–**e**. Reagents and conditions: (*i*) $MeNH_2$ solution (33 wt % in absolute ethanol), rt, 24 h; (a) tetra-n-butylammonium bromide (TBAB), K_2CO_3, CH_3CN, 15 min at 0 °C and 16 h at rt; (b) argon, dry THF, reflux, 48 h.

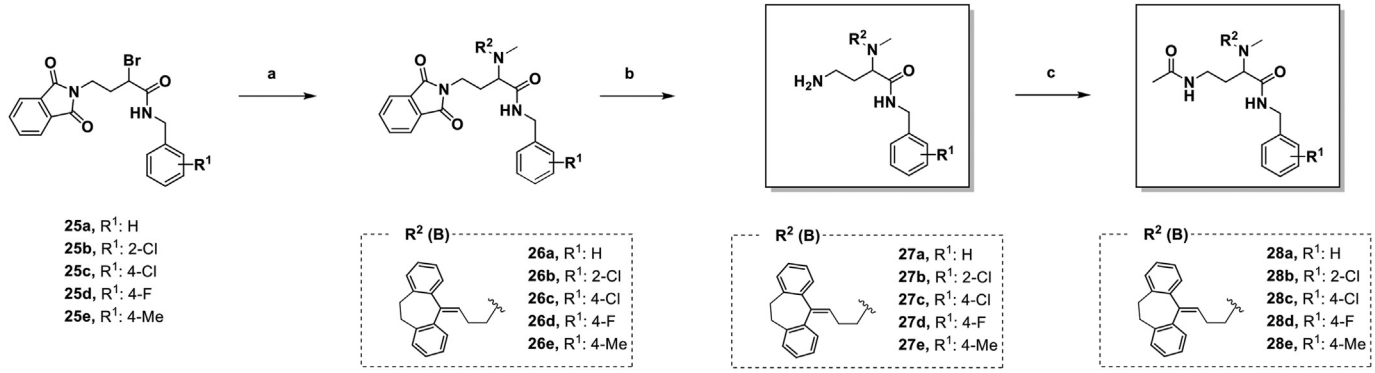

Scheme 2. Synthesis route for the 4-aminobutanamide and 4-acetamidobutanamide derivatives **27a**–**e** and **28a**–**e**. Reagents and conditions: (a) amine (**17**), KI, K_2CO_3, MeCN, reflux, 24 h; (b) NH_2NH_2 (50%–60%), EtOH, 2 h at 60 °C and 5 h at rt; (c) DMAP, DCC, CH_3COOH, DCM, 10 min at 0 °C and 20 h at rt.

the tricyclic moiety (**23a**–**e**) showed lower activity to pIC_{50} 4.16–4.68 for mGAT1 compared with their structural analogs **24a**–**e**; their pIC_{50} values ranged from 4.70 to 5.00 for mGAT1. Relatively good inhibitory activity against mGAT4 were obtained as a result of replacing the hydroxyl group in the dibenzocycloheptadiene derivatives (**24a**–**e**) with an amino group at the 4-position of butanamide (**27a**–**e**); their pIC_{50} values ranged from 5.19 to 5.36 for mGAT4. Among 4-aminobutanamide derivatives, compound **27d**, with a fluorine atom in the *para* position of the benzyl moiety, showed the highest pIC_{50} value toward mGAT4 (**27d**, pIC_{50} 5.36). In turn, in the group of 4-acetamidobutanamide derivatives (**28a**–**e**), notably a decrease in inhibitory activity toward mGAT2 was observed although the preference for mGAT1 and mGAT3-4 was maintained compared to 4-hydroxybutanamide derivatives (**24a**–**e**). Nevertheless, an acetamide derivative with a methyl group at the 4-position of the benzyl moiety (**28e**, pIC_{50} 5.25) retained activity toward mGAT3 at the same level as its structural analog with a free amino group at the 4-position (**27e**, pIC_{50} 5.32, Table 1, Fig. 3).

2.3. Molecular modeling

In order to elucidate how the obtained compounds interact with GABA transporters, we conducted molecular docking and molecular dynamics studies using homology models of the targets. For this purpose, we used previously developed models of human GAT-1, GAT-2, GAT-3 and BGT-1 which correspond to mouse GAT-1, GAT-3, GAT-4 and GAT-2, respectively [43]. Mouse and human GABA transporters have very high homology of the amino acid sequence [55–59]. The differences mainly concern the amino acid residues at the N- and C-terminus, away from the ligand binding sites. In addition, previous studies indicate that the activity of compounds is

Table 1
Inhibitory potencies (pIC_{50} ± SEM) toward mGAT1–4 obtained from the [^{3}H]GABA uptake experiments and binding affinities (pK_i ± SEM) toward mGAT1 from the MS Binding Assays of the obtained compounds. [54]

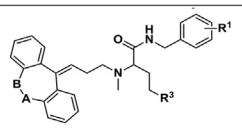

Compound	R^1	R^3	A-B	pIC_{50}[a] ± SEM mGAT1	mGAT2	mGAT3	mGAT4	pK_i[a] ± SEM mGAT1
22a	H	OH	bond	4.62 ± 0.05	4.75 ± 0.09	4.90 ± 0.09	4.60 ± 0.06	75%
22b	2-Cl	OH	bond	4.48 ± 0.09	4.59 ± 0.08	4.79 ± 0.11	4.57 ± 0.10	93%
22c	4-Cl	OH	bond	4.37 ± 0.05	4.49 ± 0.04	4.99 ± 0.02	4.35 ± 0.08	91%
22d	4-F	OH	bond	4.43 ± 0.01	4.59 ± 0.11	4.87 ± 0.06	4.45 ± 0.08	90%
22e	4-Me	OH	bond	4.50 ± 0.11	4.52 ± 0.02	4.70 ± 0.11	4.51 ± 0.08	99%
23a	H	OH	CH=CH	4.66 ± 0.09	4.81 ± 0.09	4.87 ± 0.02	5.02 ± 0.11	75%
23b	2-Cl	OH	CH=CH	4.68 ± 0.05	5.17 ± 0.05	5.05 ± 0.06	5.02 ± 0.04	69%
23c	4-Cl	OH	CH=CH	4.16 ± 0.05	4.84 ± 0.01	4.87 ± 0.08	4.80 ± 0.09	63%
23d	4-F	OH	CH=CH	4.66 ± 0.10	4.99 ± 0.10	4.91 ± 0.02	4.87 ± 0.06	71%
23e	4-Me	OH	CH=CH	4.56 ± 0.09	5.01 ± 0.08	4.77 ± 0.05	5.04 ± 0.06	55%
24a	H	OH	CH_2–CH_2	4.70 ± 0.09	5.04 ± 0.03	4.94 ± 0.07	4.77 ± 0.02	51%
24b	2-Cl	OH	CH_2–CH_2	4.60 ± 0.10	4.96 ± 0.06	4.90 ± 0.08	4.80 ± 0.09	82%
24c	4-Cl	OH	CH_2–CH_2	5.00 ± 0.10	5.11 ± 0.10	4.86 ± 0.09	4.80 ± 0.07	79%
24d	4-F	OH	CH_2–CH_2	4.66 ± 0.02	5.24 ± 0.03	4.78 ± 0.07	4.88 ± 0.10	81%
24e	4-Me	OH	CH_2–CH_2	4.85 ± 0.05	**5.34 ± 0.09**	4.90 ± 0.04	4.97 ± 0.10	53%
27a	H	NH_2	CH_2–CH_2	5.09 ± 0.05	5.02 ± 0.06	5.01 ± 0.09	5.33 ± 0.10	4.78 ± 0.07
27b	2-Cl	NH_2	CH_2–CH_2	5.18 ± 0.11	4.87 ± 0.05	5.09 ± 0.08	5.31 ± 0.02	4.87 ± 0.07
27c	4-Cl	NH_2	CH_2–CH_2	5.20 ± 0.05	4.96 ± 0.08	5.29 ± 0.07	5.25 ± 0.08	4.60 ± 0.09
27d	4-F	NH_2	CH_2–CH_2	5.20 ± 0.06	4.93 ± 0.09	5.32 ± 0.09	**5.36 ± 0.06**	4.96 ± 0.05
27e	4-Me	NH_2	CH_2–CH_2	5.14 ± 0.06	4.95 ± 0.05	5.32 ± 0.02	5.19 ± 0.10	5.14 ± 0.04
28a	H	$NH(CO)CH_3$	CH_2–CH_2	4.54 ± 0.07	4.43 ± 0.01	4.75 ± 0.08	4.75 ± 0.04	77%
28b	2-Cl	$NH(CO)CH_3$	CH_2–CH_2	4.54 ± 0.01	4.58 ± 0.16	4.75 ± 0.04	4.73 ± 0.05	87%
28c	4-Cl	$NH(CO)CH_3$	CH_2–CH_2	4.55 ± 0.05	4.32 ± 0.22	4.84 ± 0.11	4.90 ± 0.03	90%
28d	4-F	$NH(CO)CH_3$	CH_2–CH_2	4.86 ± 0.11	4.71 ± 0.09	4.95 ± 0.10	4.94 ± 0.08	71%
28e	4-Me	$NH(CO)CH_3$	CH_2–CH_2	4.86 ± 0.08	4.81 ± 0.21	5.25 ± 0.06	4.87 ± 0.08	69%
Tiagabine (**2**) [26]				**6.88 ± 0.12**	52%	64%	73%	7.43 ± 0.11[54]
DDPM-2571 (**3**)[29]				**8.27 ± 0.03**	4.31	4.35	4.07	8.29 ± 0.02
(*S*)-SNAP-5114 (**4**) [26]				4.07 ± 0.09	56%	**5.29 ± 0.04**	**5.81 ± 0.10**	n.d.
5 [36]				4.14	73%	**5.16 ± 0.05**	**5.89 ± 0.07**	77%
SBV2-114 (**6**) [22]				3.25 ± 0.04	4.67 ± 0.07	3.03 ± 0.07	3.54 ± 0.05	n.d.
7 [45]				5.06 ± 0.02	**5.35 ± 0.08**	**5.61 ± 0.07**	5.21 ± 0.05	68%
8 [46]				4.89 ± 0.10	5.19 ± 0.01	5.00 ± 0.04	5.04 ± 0.06	4.96 ± 0.09
9 [47]				4.72 ± 0.07	4.90 ± 0.13	5.14 ± 0.10	5.00 ± 0.04	54%
10 [49]				5.70[b]				
11 [49]				4.87[b]				

[a]Data are given as the mean ± SEM of three independent experiments that were performed in triplicate. The percent results represent [^{3}H]GABA uptake or NO711 binding in the presence of 100 μM inhibitor. Data without SEM implies that only one experiment was performed in triplicate. [b]Inhibition of GABA uptake in synaptosomes. n.d. – not described.

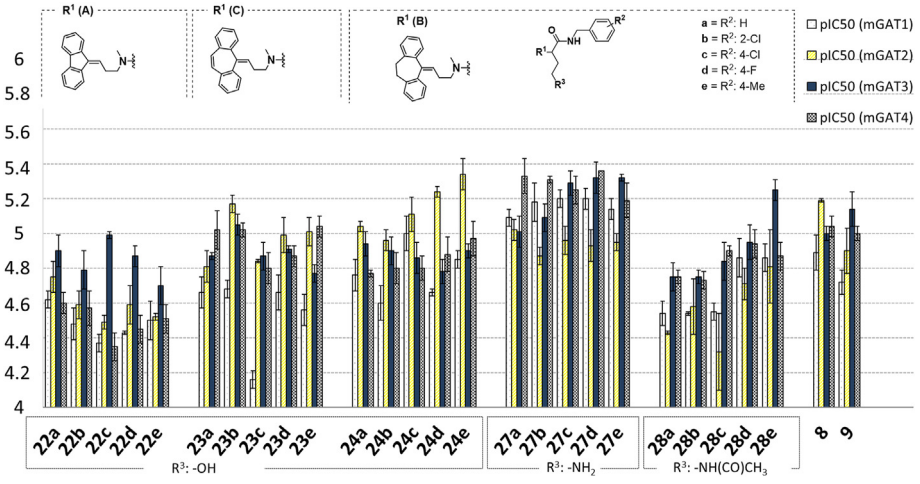

Fig. 3. Bar graph showing the pIC_{50} values of compounds **22a**–**e**, **23a**–**e**, **24a**–**e**, **27a**–**e**, and **28a**–**e** compared to the values of the parent compounds **8** and **9**.

very similar toward the transporters from both species [60]. All models were built with the SWISS-MODEL server based on the crystal structure of the *Drosophila melanogaster* dopamine transporter as a template. As the activity of compounds was investigated for the racemates, we considered both the *R*- and *S*- isomer in the molecular modeling studies. The general orientation of both stereoisomers was similar due to the large conformational freedom of the fragment containing the chiral carbon atom. For each type of the transporter, we present with details this isomer which obtained higher docking score and a more coherent binding mode (for information about absolute configuration see Fig. 4). Even though the stereoisomers of compounds differ from each other in value of scoring function, there is no clear trend and the differences are too small to indicate which isomer is more active.

The results indicated that all studied compounds bind mainly within the vestibule of the transporters (Fig. 4). It is a different binding mode from that observed for reference compounds (e.g. tiagabine, (*S*)-SNAP-5114) described in our previous work [43]. In their case, the nipecotic acid fragment was located within the main binding site (S1), where the carboxylic group interacted with the sodium ion (Na1). In turn, the aromatic groups reached the S2 site in the vestibule which is situated above the extracellular gate (Suppl. Fig. S1). The compounds investigated here represent a different chemotype and contain the *N*-benzylamide group instead of an acid group. Such extension of the molecule limits the interactions within the S1 site.

In most poses for all derivatives and each type of GAT, the dibenzocycloheptatriene, dibenzocycloheptadiene and fluorene fragments are located closest to the entrance to the transporter. These moieties form hydrophobic interactions mainly with: PHE294, TYR452 and MET458 in GAT-1; PHE293 and TYR453 in BGT-1; TYR448, TYR449, TYR515 and MET454 in GAT-2; and PHE531, TYR469, TYR535 and MET474 in GAT-3. The planar fluorene moiety creates weaker hydrophobic interactions and does not fit the described cavities as well as the larger coplanar dibenzocycloheptatriene and dibenzocycloheptadiene moieties. In addition, the poses obtained for compounds with fluorene fragments were less coherent, which is reflected in the lower activity of these derivatives. The main core containing the tertiary amine and amide moieties is arranged along the vestibule, and the benzyl group is directed toward the S1 site, which is located inside this site or near the extracellular gate. The exact arrangements of the main core and benzyl group vary depending on the type of GABA transporter.

The prediction of protonation states at physiological pH (7.4) indicates that in the case of 4-aminobutanamide derivatives, protonated primary amines and non-protonated tertiary amine are the dominant forms. For GAT-1, GAT-2 and GAT-3, the location of the positive charge makes it possible to create a beneficial salt bridge between the protonated amine of the ligand and the carboxyl group of an aspartic acid residue (ASP451 in GAT-1; ASP447 in GAT-2; ASP467 in GAT-3) while at the same time reach the main binding site (S1) through the benzyl group. The abovementioned salt bridge with the aspartic acid residue that is part of the extracellular gate seems to be one of the key interactions for ligand binding. This salt bridge was very stable during the molecular dynamics simulations carried out for the GAT-1, GAT-2, and GAT-3 complexes with representatives of the most active compounds, *i.e.*, **27c**, **27e** and **27d**, respectively (Fig. 5). In turn, the benzyl moieties can form hydrophobic interactions with TYR60, TYR140, LEU300 and LEU136 in GAT-1; PHE288, TYR129, LEU294 and LEU125 in GAT-2; and

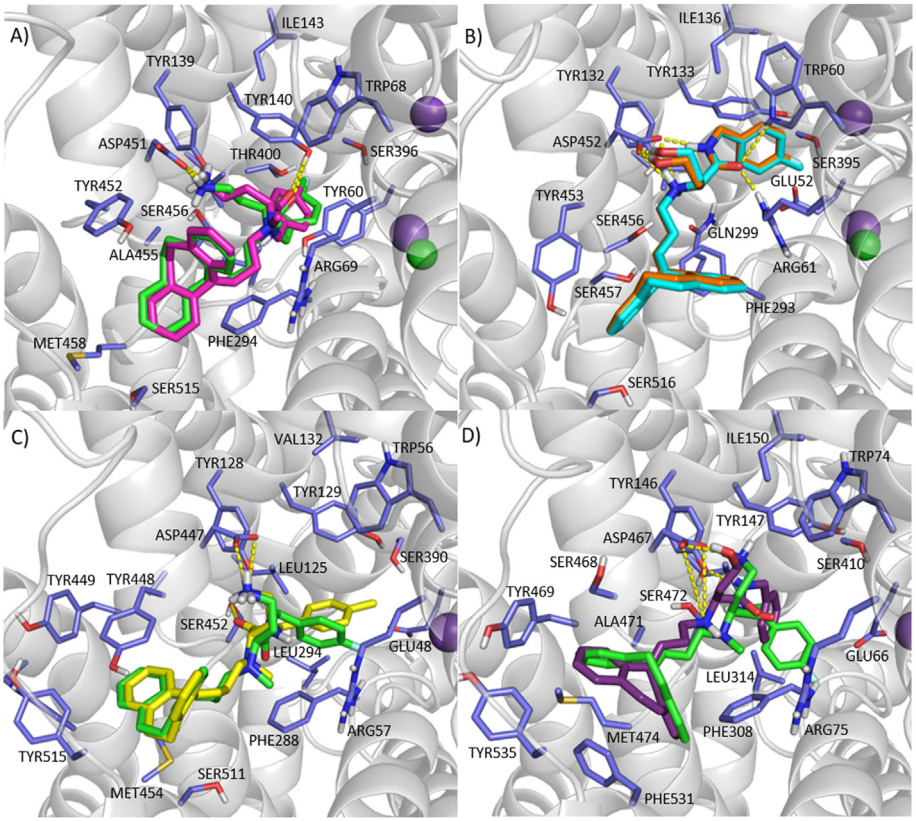

Fig. 4. Binding modes of compounds **(*R*)-27d** (green) and **(*R*)-27c** (pink) in GAT-1 (panel A); compounds **(*R*)-24d** (orange) and **(*R*)-24e** (blue) in BGT-1 (panel B); compounds **(*S*)-27d** (green) and **(*S*)-27e** (yellow) in GAT-2 (panel C); and compounds **(*S*)-23a** (purple) and **(*S*)-27d** (green) in GAT-3 (panel D). Ionic interactions and hydrogen bonds are represented by yellow dashes.

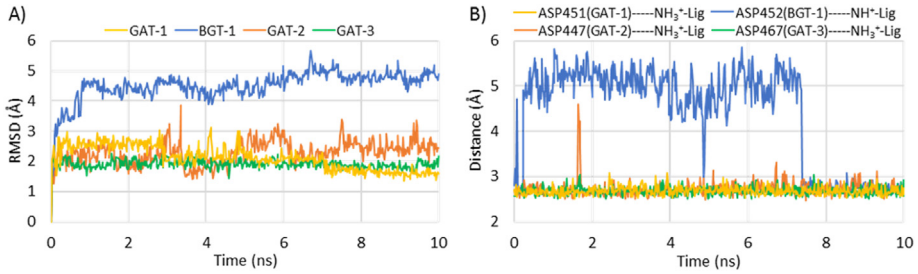

Fig. 5. RMSD changes for the compounds over the course of the molecular dynamics simulations (panel A). Distance changes between the carboxyl moiety of the aspartic acid residue from the extracellular gate and protonated amino group of each ligand, during molecular dynamics simulations (panel B). Analyzed ligand-protein complexes: GAT-1 – **(*R*)-27c**; BGT-1 – **(*R*)-24e**; GAT-2 – **(*S*)-27e**; and GAT-3 – **(*S*)-27d**.

LEU314, LEU143, PHE308 and TYR147 in GAT-3. Such a favorable arrangement may explain the increased activity of the 4-amino derivatives toward GAT-1, GAT-2 and GAT-3. For the 4-hydroxybutanamide and 4-acetamidobutanamide derivatives, in the absence of a primary amine, the tertiary amine is protonated. Different positions of the positive charge make it difficult to form a salt bridge with aspartic acid while maintaining the beneficial interactions from the benzyl fragment. However, the 4-hydroxy and 4-acetamido compounds can create ionic bonds between the amine group and aspartic acid residue and hydrogen bonds with the carboxyl group of the aforementioned residue through the hydroxyl group (Fig. 4D, compound **23a**) or, less frequently, the acetamide group.

During the molecular dynamics calculations for the complexes of **27e** with GAT-2 and **27d** with GAT-3, the formation of a hydrogen bond between the amide group of the compounds and the hydroxyl group of residue SER452 (GAT-2) or SER472 (GAT-3) was observed. In the case of GAT-1, the amide group of **27c** initially formed a hydrogen bond with the TYR140 hydroxyl group and then moved toward the nonhelical fragment of the TM1 domain, forming water-mediated hydrogen bonds with atoms on the GLY65 and ASN66 main chains.

In the case of BGT-1 transporters, it was observed that the tested compounds bind higher in the vestibule, as shown in Fig. 4B with two of the most active compounds toward BGT-1, **24d** and **24e**. Such binding implies a different placement of the benzyl group. Initially, this group interacts mainly with TYR133, LEU56 and ILE136, and then, over the course of the simulation (carried out for compound **24e**), the benzyl group moves toward TYR132, creating π-π interactions with this residue. Therefore, the benzyl group does not reach the S1 site, unlike it does in other types of GABA transporters. Another relatively active compound, **24d**, is almost identically placed within BGT-1 compared to **24e**. This arrangement seems to be beneficial because the S1 site in BGT-1 is highly polar due to the presence of the residues GLU52, GLU126 and GLN299. The upper position of the compound in the vestibule also enables the creation of a salt bridge between ASP452 and the protonated tertiary amine of the 4-hydroxybutanamide derivatives. During MD simulations, this salt bridge was initially broken, resulting in ionic interactions. However, at the end of the simulation, the salt bridge was restored. 4-Hydroxybutanamide derivatives additionally form two hydrogen bonds with ASP452 via hydroxyl and amide groups (Fig. 4B). The 4-aminobutanamide derivatives generally have a similar arrangement within BGT-1 but form one hydrogen bond less with ASP452 because at physiological pH, the tertiary amine moiety of the 4-aminobutanamide derivatives is deprotonated, so it cannot be a hydrogen bond donor. This result is similar to the case of the 4-acetamidobutanamide derivatives. The acetamide group of these compounds does not form a hydrogen bond with ASP452 due to steric hindrance. In addition, the poses of these compounds are less coherent, which may explain their lower activity. The reported binding mode within BGT-1 for the most active compound (**24e**) was generally preserved during the course of the molecular dynamics simulations. A significant shift from the original position was observed only for the benzyl group as described above.

2.4. Hepatotoxicity and cytotoxicity

From all final compounds, we selected two representative derivatives (**23a** and **24e**) for *in vitro* studies in order to verify their safety in the HepG2 and HEK-293 cell lines for the purpose of testing the selected compounds *in vivo*. Compound **24e** was selected as one of two compounds with the highest activity toward mGAT2 ($pIC_{50} = 5.34 \pm 0.09$, Table 1, Fig. 3). Compound **23a** displayed balanced activity as a nonselective GAT inhibitor with a slight preference toward mGAT4 and was obtained using a simpler and more effective synthesis procedure than the 4-aminobutanamide analogs. Thus, initially, the HepG2 *hepatoma* cell-based hepatotoxicity assay was used to investigate the safety of compounds **23a** and **24e**. The results revealed that neither of the selected compounds induced significant hepatotoxicity after 72 h of incubation at concentrations up to 25 μM. A statistically significant ($p < 0.0001$) decrease in HepG2 cell viability was observed for **23a** and **24e** only at the highest concentrations of 50 and 100 μM (Fig. 6A).

Compound **24e** was slightly more toxic compared with **23a**, as it completely eradicated cell viability at 50 μM, whereas **23a** was showed 72% viability compared to the control (1% DMSO in culture media). In general, taking into account the results for the reference cytostatic drug doxorubicin at 1 μM, the tested compounds showed weak (**23a**) or moderate (**24e**) hepatotoxic effects. It is crucial to note that we did not observe a statistically significant decrease in HepG2 cell viability for concentrations corresponding to the IC_{50} values obtained for individual GAT subtypes (IC_{50} values in the range of 4–14 μM for compounds **23a** and **24e**). Analogical studies were conducted with the use of the HEK-293 cell line. In general, both compounds showed stronger toxic effects compared to the results from the HepG2 assay, as a significant ($p < 0.0001$) decrease in HEK-293 cell viability was observed not only at the concentrations of 50 and 100 μM but also at 25 μM. Interestingly, a significant ($p < 0.05$) slight induction in cell proliferation was observed after treatment with 1 μM **23a** and **24e**. Nevertheless, the observed antiproliferative effects at 25 μM were still weaker than those for the cytostatic drug doxorubicin at 1 μM. Therefore, we assumed that selected compounds showed an acceptable level of safety and an appropriate *in vitro* profile for further verification of their anticonvulsant, antinociceptive, antidepressant-like, and anxiolytic-like properties in mouse models of seizures, pain, depression, and anxiety.

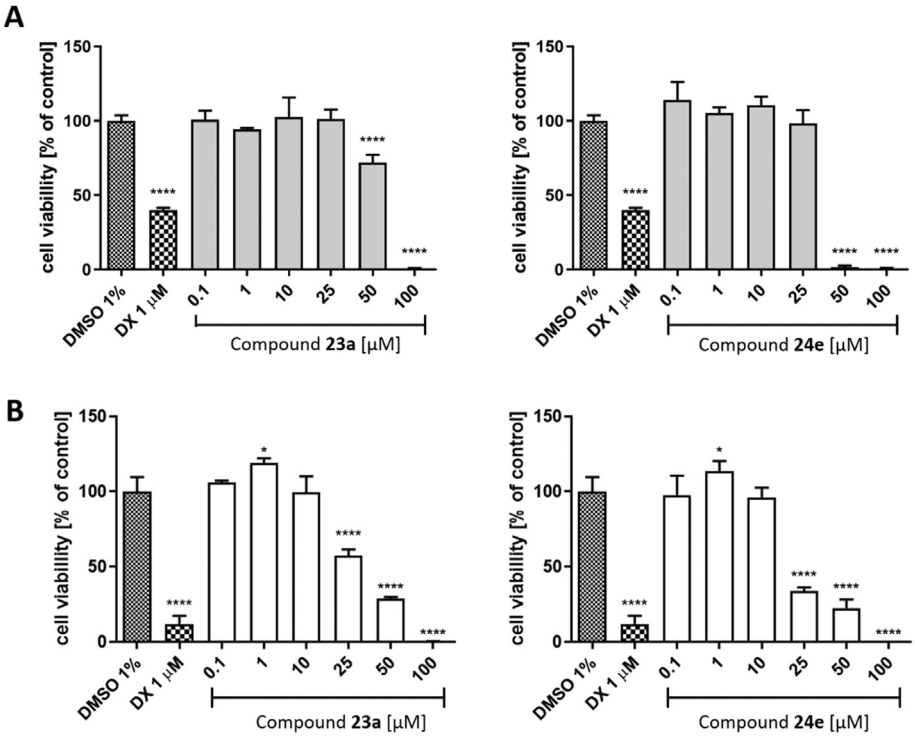

Fig. 6. The influence of **23a**, **24e**, and the reference cytostatic drug doxorubicin (DX) on the viability of *hepatoma* HepG2 cells (panel A) and HEK-293 cells (panel B) after 72 h of incubation. Statistical significance (*p < 0.05, ****p < 0.0001) was analyzed by GraphPad Prism 8.0.1 software using one-way ANOVA and Bonferroni's multiple comparison post hoc test.

2.5. In vivo pharmacological evaluation

2.5.1. Anticonvulsant activity

2.5.1.1. Electroconvulsive threshold (ECT) test. In the ECT test (Fig. 7A), both compounds **23a** and **24e** used at the dose of 100 mg/kg elevated the threshold for electroconvulsions and **24e** was particularly efficacious in this assay (elevation of seizure threshold: **23a**: 43% and **24e**: 90% vs. vehicle-treated mice). In our previous studies [28,32], we tested selective GAT1 inhibitors, *i.e.*, tiagabine at a dose of 100 mg/kg (*i.p.*), which was only weakly effective in elevating the threshold for electroconvulsions (31.6% vs. control), and DDPM-2571 at the maximal tolerated dose (10 mg/kg, *i.p.*). The latter did not elevate the electroconvulsive threshold. The mixed GAT3/4 inhibitor (*S*)-SNAP-5114 (100 mg/kg, *i.p.*), was also not effective in this assay [46].

2.5.1.2. Maximal electroshock seizure (MES) test. In the MES test, neither **23a** nor **24e**, both examined at 100 mg/kg, were effective (Fig. 7B). As in the control group, seizures were observed in 83% of the mice tested. Additionally, the reference compounds tested in our previous studies, tiagabine, DDPM-2571 and (*S*)-SNAP-5114, were not effective in the MES test, either [28,32,46].

2.5.1.3. Pentylenetetrazole-induced seizures (PTZ). In the pentylenetetrazole test, the dose 100 mg/kg of both compounds **23a** and **24e** was tested. One-way ANOVA revealed an overall treatment effect on the latency to the first clonus ($F[2,27] = 3.411$, $p < 0.05$) and on the number of seizure episodes ($F[2,29] = 5.126$, $p < 0.05$). Post hoc analyses showed that compared to the control group, **24e** significantly prolonged the mean latency to the occurrence of the first clonus ($p < 0.05$, Fig. 8A). This compound also reduced the number of seizure episodes, but this activity did not reach statistical significance (Fig. 8B). Compound **23a** at 100 mg/kg was not effective in this assay (Fig. 8A and B).

In our previous studies, tiagabine revealed protective anticonvulsant properties against PTZ-induced seizures. In comparison to the control group, it prolonged the latency to first clonus at a wide range of doses (6.25–50 mg/kg, *i.p.*) and reduced the number of seizure episodes in PTZ-treated mice [28]. DDPM-2571, compared to vehicle, significantly prolonged the latency to seizure onset at doses of 1 mg/kg - 10 mg/kg. It also reduced the number of seizure episodes at doses of 0.5 mg/kg - 10 mg/kg [32]. (*S*)-SNAP-5114 at doses of 30 and 100 mg/kg was not effective in this assay (unpublished data), which is in line with previously reported data [61].

2.5.1.4. Pilocarpine-induced seizures. In the pilocarpine-induced model of seizures, one-way ANOVA showed a statistically significant effect of treatment on the latency to *status epilepticus* ($F[2,28] = 5.249$, $p < 0.05$). In this test, compared to the control group, none of the compounds was effective at the dose 100 mg/kg (*i.p.*); **24e** significantly ($p < 0.01$) reduced the latency to the occurrence of *status epilepticus,* while **23a** did not affect the latency to *status epilepticus* in pilocarpine-treated mice (Fig. 9).

In our previous studies, intraperitoneal administration of tiagabine at a dose of 50 mg/kg prolonged the latency to prodromal seizure symptoms, latency to the occurrence of *status epilepticus* and latency to death [28]. In the pilocarpine test, pretreatment with DDPM-2571 significantly prolonged the latency to *status epilepticus* at doses of 5 and 10 mg/kg [32]. (*S*)-SNAP5114 at doses of 100 and 200 mg/kg (*i.p.*) prolonged the latency to *status epilepticus* and latency to death [46].

2.5.2. Antinociceptive activity

2.5.2.1. Hot plate test. In the hot plate test, both compounds **23a** and **24e** were tested at a dose of 30 mg/kg. One-way ANOVA did not demonstrate an overall effect of treatment ($F[2,21] = 0.8202$,

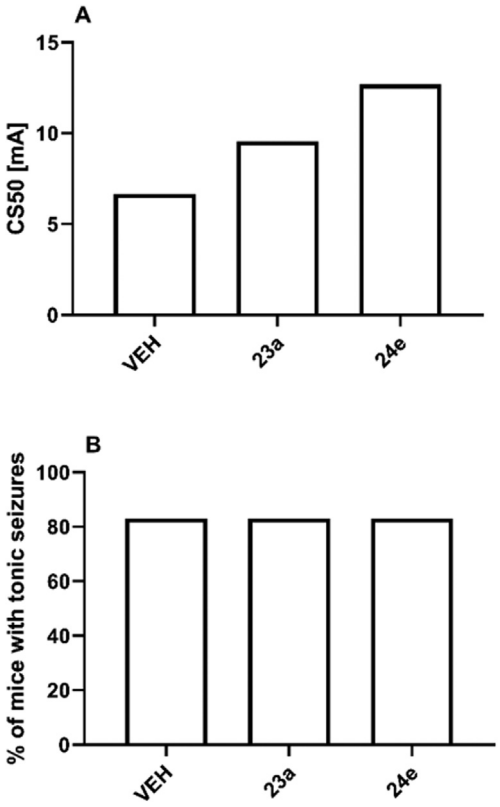

Fig. 7. Effect of compounds **23a** and **24e** (100 mg/kg, *i.p.*) on the threshold for electroconvulsions measured in the mouse ECT test (panel A), and anticonvulsant activity of compounds **23a** and **24e** (100 mg/kg, *i.p.*) measured in the maximal electroshock seizure (MES) test (panel B). Results are shown as median current strength (CS_{50}: current intensity required to induce tonic hind limb extension in 50% of the mice challenged; panel A) or % of mice with tonic hind limb extension in each group (panel B); n = 6.

p > 0.05). Although both **23a** and **24e** showed a tendency to prolong the latency pain reaction, these results did not reach statistical significance (Fig. 10).

Our previous studies showed that in the hot plate test, tiagabine at a dose of 8 mg/kg significantly prolonged the latency to nociceptive response [28]. DDPM-2571 prolonged the latency to pain reaction at doses of 1 mg/kg, 2.5 mg/kg and 5 mg/kg [32]. (*S*)-SNAP-5114 did not demonstrate antinociceptive activity in the hot plate test [46].

2.5.2.2. Formalin test. In the formalin test, as in the hot plate test, both examined compounds **23a** and **24e** were tested at a dose of 30 mg/kg. In the neurogenic phase, one-way ANOVA did not reveal an overall treatment effect ($F[2,18] = 3.161$, $p > 0.05$), but an overall treatment effect was observed in the second phase of the formalin test ($F[2,17] = 8.915$, $p < 0.01$). As demonstrated in Fig. 11A, in the neurogenic phase, only **24e** reduced the duration of the nocifensive response ($p < 0.05$ vs. control). Both **23a** and **24e** showed antinociceptive properties in the second phase of the formalin test ($p < 0.05$ and $p < 0.01$ vs. control, respectively, Fig. 11B).

Previously, we demonstrated that tiagabine at a dose of 8 mg/kg attenuated the nociceptive response in both phases of the formalin test. Compared to the control, it reduced the duration of the nocifensive response by 81.7% and 95.9% in the acute and late phases of the formalin test, respectively [28]. In the formalin test, in the first (neurogenic) phase of the test, DDPM-2571 did not demonstrate antinociceptive properties. In contrast, DDPM-2571 was highly effective in the second phase of this test, attenuating nocifensive behavior in a dose-dependent manner [32]. (*S*)-SNAP-5114 was not effective in this assay (unpublished data).

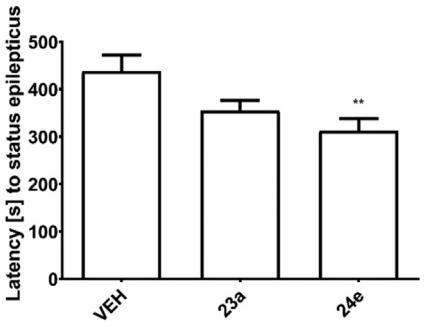

Fig. 9. Anticonvulsant activity of the test compounds **23a** and **24e** (100 mg/kg, *i.p.*) measured in a mouse pilocarpine model of seizures. Results are shown as mean latency [s] (±SEM) to *status epilepticus*. Statistical analysis: one-way analysis of variance (ANOVA), followed by Dunnett's post hoc comparison. Significance vs. vehicle-treated group: $p < 0.01$; n = 10–12.

2.5.3. Antidepressant-like activity

2.5.3.1. Forced swim test. In the forced swim test, one-way ANOVA revealed an overall effect of treatment ($F[6,49] = 5.144$, $p < 0.001$). Compared to the control group, **23a** showed dose-dependent, statistically significant antidepressant-like activity in this test (Fig. 12A). Compound **24e** was also effective in the forced swim test, but its significant antidepressant-like activity was shown only at the dose of 30 mg/kg ($p < 0.05$ vs. control, Fig. 12A).

Previously, tiagabine (doses: 8 and 30 mg/kg, *i.p.*) significantly

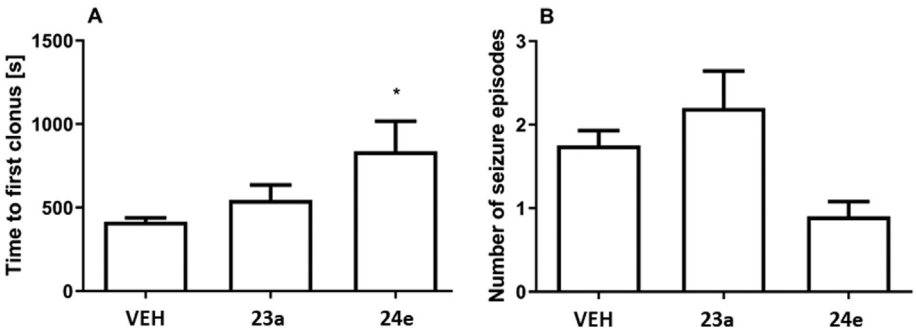

Fig. 8. Effects of the tested compounds **23a** and **24e** (100 mg/kg, *i.p.*) on latency to first clonus (panel A) and the number of seizure episodes (panel B) in a PTZ-induced seizure model. Results are shown as mean latency [s] to the occurrence of seizures (±SEM, panel A) and mean number of seizure episodes (±SEM, panel B). Statistical analysis: one-way ANOVA followed by Dunnett's post hoc test. Significance vs. control group: *$p < 0.05$; n = 10–12.

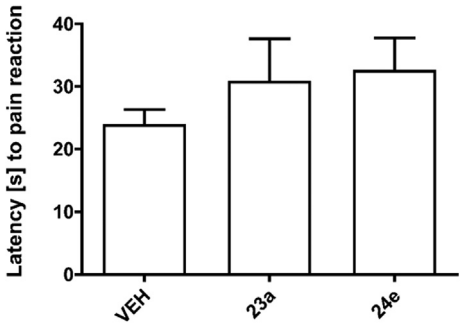

Fig. 10. Antinociceptive activity of the compounds **23a** and **24e** (30 mg/kg, *i.p.*) in the hot plate test. Results are shown as latency to pain reaction [s] (±SEM) in response to thermal stimulus (55 °C). Statistical analysis: one-way analysis of variance (ANOVA), followed by Dunnett's post hoc comparison: $p > 0.05$; $n = 8$.

reduced immobility by 59% and 97.4%, respectively vs. the control [28]. In the forced swim test, DDPM-2571 significantly reduced the duration of immobility at doses of 2.5 and 5 mg/kg [32]. (*S*)-SNAP5114 (30 mg/kg, *i.p.*) also slightly but statistically significantly reduced immobility by 20% vs. control mice [46].

2.5.3.2. Tail suspension test. Since 30 mg/kg dose of **23a** and **24e** showed significant antidepressant-like activity in the forced swim test, this dose was also assessed for its ability to reduce immobility in the tail suspension test. One-way ANOVA showed an overall effect of treatment ($F [2,19] = 5.211$, $p < 0.05$). Dunnett's post hoc test showed a significant effect from both compounds on the duration of immobility in this test ($p < 0.05$, Fig. 12B). These results confirmed the antidepressant-like activity of **23a** and **24e** observed in the forced swim test. Previously, we established that tiagabine, DDPM-2571 and (*S*)-SNAP-5114 were not effective in this assay (unpublished data).

2.5.4. Anxiolytic-like activity

2.5.4.1. Four-plate test. In the four-plate test, one-way ANOVA did not show an overall effect of treatment ($F [2,25] = 2.247$, $p > 0.05$). Neither **23a** nor **24e** used at the dose 30 mg/kg (*i.p.*) were effective in this assay (Fig. 13A).

In our previous studies with this same test, we demonstrated potential anxiolytic properties of tiagabine (8 mg/kg, *i.p.*). Compared to the control group, tiagabine increased the mean number of punished crossings by 79% [28]. In the four-plate test, DDPM-2571 at the dose of 5 mg/kg significantly increased the mean number of punished crossings compared to the control group [32]. (*S*)-SNAP-5114 was effective at a dose of 30 mg/kg (unpublished data).

2.5.4.2. Elevated plus maze. In the elevated plus maze test, one-way ANOVA did not show an overall effect of treatment on the time spent in open arms ($F [2,26] = 0.7630$, $p > 0.05$) or % entry into the open arms ($F [2,23] = 3.384$, $p > 0.05$). The results obtained in this test confirmed that neither **23a** nor **24e** at the dose of 30 mg/kg possessed anxiolytic-like properties in mice and they did not influence either time spent in open arms (Fig. 13B) or % of open arm entries (Fig. 13C).

In our previous studies, tiagabine (8 mg/kg, *i.p.*) prolonged the time spent in the open arms of the elevated plus maze and raised the ratio of the number of entries into the open arms to the number of entries to all arms of the maze in a statistically significant manner [28]. In the elevated plus maze test, the dose of 5 mg/kg DDPM-2571, compared to the control, increased the % time spent in

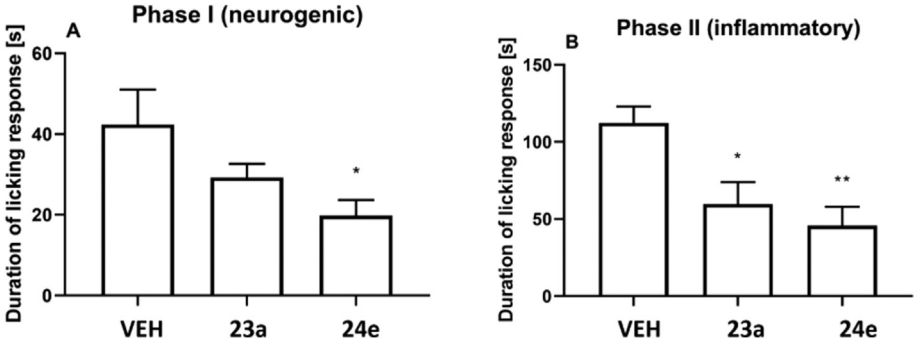

Fig. 11. Antinociceptive activities of compounds **23a** and **24e** used at 30 mg/kg (*i.p.*) in the mouse formalin test. The results are shown as the duration of the licking/biting response [s] (±SEM) in the formalin-injected paw during the neurogenic phase (0–5 min, panel A) and inflammatory phase (15–30 min, panel B) of the test. Statistical analysis: one-way ANOVA followed by Dunnett's post hoc comparison. Significance vs. vehicle-treated group in the respective phase: *$p < 0.05$, **$p < 0.01$; $n = 6–8$.

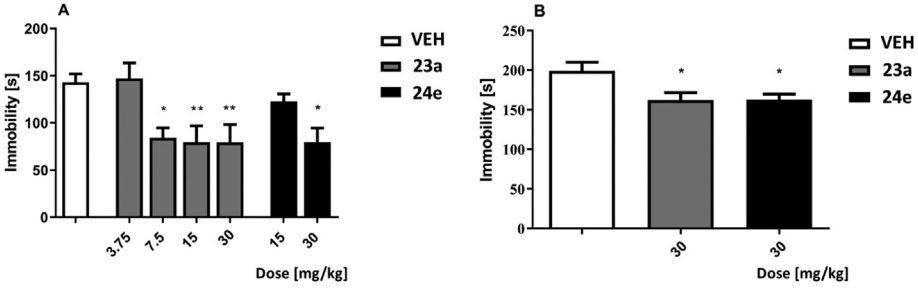

Fig. 12. Antidepressant-like activity of compounds **23a** and **24e** in the forced swim test (panel A) and in the tail suspension test (panel B). The results are shown as the duration of immobility [s] (±SEM) in drug-treated and vehicle-treated mice. Statistical analysis: one-way ANOVA followed by Dunnett's post hoc comparison. Significance vs. vehicle-treated group: *$p < 0.05$, **$p < 0.01$; $n = 7–9$.

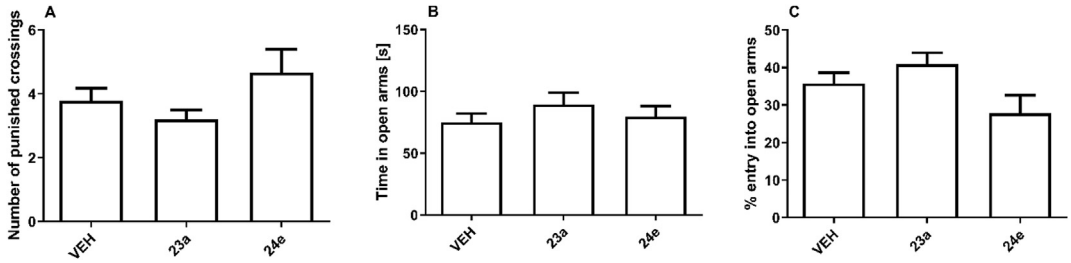

Fig. 13. Anxiolytic-like activity of compounds **23a** and **24e** used at the dose of 30 mg/kg (*i.p.*) in the mouse four-plate test (panel A) and in the elevated plus maze test (panels B and C). Results are shown as mean number of punished crossings (±SEM) in drug-treated and vehicle-treated groups (panel A), time [s] spent in open arms (±SEM, panel B) or % entry into open arms (panel C). Statistical analysis: one-way ANOVA, followed by Dunnett's post hoc comparison: $p > 0.05$; $n = 7–10$.

the open arms of the elevated plus maze and reduced the % time spent in the closed arms. Compared to vehicle-treated animals, DDPM-2571 also increased the number of entries into the open arms [32]. (*S*)-SNAP-5114 (30 mg/kg, *i.p.*) was not effective in this test (data unpublished).

2.5.5. Locomotor activity test

In the locomotor activity test, repeated measures ANOVA showed an overall treatment effect on the locomotor activity of animals ($F[2,105] = 6.505$, $p < 0.01$). The time effect and drug × time interaction were not significant ($F[4,105] = 0.8336$, $p > 0.05$ and $F[8,105] = 0.5726$, $p > 0.05$, respectively). As shown in Fig. 14, **23a** reduced the locomotor activity of mice only between the 24th and 30th min of the test ($p < 0.05$ vs. control). Compound **24e** at a dose of 30 mg/kg did not affect the locomotor activity of mice.

In our previous studies, intraperitoneal tiagabine significantly reduced locomotor activity at doses of 8 and 30 mg/kg [28]. DDPM-2571 at doses of 5 mg/kg and 10 mg/kg did not affect the locomotor activity of mice [32]. Similarly, (*S*)-SNAP-5114 (30 mg/kg, *i.p.*) did not affect the locomotor activity of the animals (unpublished data).

3. Discussion

We designed a novel series of mGAT1-4 ligands from a group of GABA derivatives. SAR studies and molecular modeling confirmed that the introduction of a dibenzocycloheptadiene moiety connected with a propylene chain on the nitrogen atom in the second position of *N*-benzyl-4-hydroxybutanamide derivatives increases the GABA uptake inhibitory activity. 4-Hydroxybutanamide

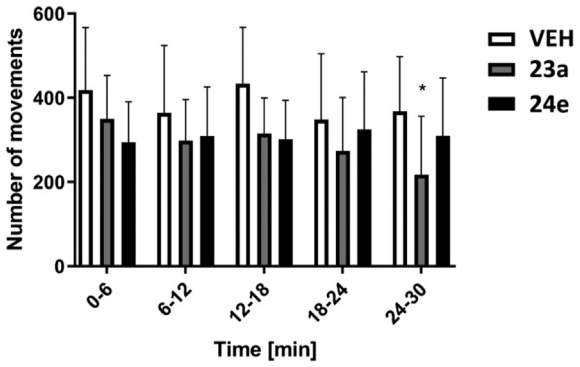

Fig. 14. Influence of the test compounds **23a** and **24e** used at the dose of 30 mg/kg on the locomotor activity of mice. The results are shown as the mean number of light-beam crossings (±SEM) measured at selected time intervals: 0–6 min, 6–12 min, 12–18 min, 18–24 min and 24–30 min. Statistical analysis of the results was conducted using repeated measures ANOVA followed by Bonferroni's multiple comparison test; $n = 8$.

derivatives with dibenzocycloheptadiene moieties (**24a**–**e**) were found to be the most potent mGAT2 inhibitors. Based on molecular modeling studies, we assume that this could be a result of the formation of two additional hydrogen bonds with mGAT2 (BGT-1) via hydroxyl and amide groups in comparison with the 4-aminobutanamide derivatives (**27a**–**e**), which form only one hydrogen bond. On the other hand, among all the compounds, relatively high inhibitory activity toward mGAT3/4 with moderate mGAT1 binding affinities displayed compounds **27a**–**e**. This may be the result of the appropriate position of the positive charges on **27a**–**e**, which makes the creation of a beneficial salt bridge with an aspartic acid residue in mGAT1/3/4 possible to reach the main binding site (S1) through the benzyl group. As one of the most potent mGAT2 inhibitors, we identified compound **24e** with pIC_{50} 5.34 ± 0.09. An additional compound that revealed attractive and well-balanced activity toward mGAT4 was **23a**. Both compounds **23a** and **24e** showed rather weak hepatotoxic and cytotoxic effects against *hepatoma* HepG2 and HEK-293 cells, respectively, and thus were selected for *in vivo* studies. In a set of *in vivo* experiments, the pharmacological properties of novel GAT inhibitors were demonstrated. The selected compounds (**23a** and **24e**) had varied anticonvulsant, antinociceptive and antidepressant-like properties in mice. However, neither test compound demonstrated anxiolytic-like activity in mice. Numerous GAT1 inhibitors are regarded as potential drug candidates for the treatment of epilepsy, and tiagabine, a selective GAT1 inhibitor, has been used for the treatment of partial seizures in humans [62,63]. Of note, this drug shows effectiveness only in selected mouse models of seizures [28]. Hence, in our research, to increase the complementarity of the methods, we used a variety of behavioral tests that assessed the potential anticonvulsant properties of **23a** and **24e**. The ECT test is a model that mimics partial tonic-clonic seizures in men [64]. Both **23a** and **24e** elevated the seizure threshold for electroconvulsions, but **24e** was more potent than **23a**. In the MES test, which reflects human grand mal epilepsy [65], neither **23a** nor **24e** revealed anticonvulsant activity. Additionally, the pilocarpine model did not show anticonvulsant properties from either **23a** or **24e**. Since previously tested GAT1 inhibitors (tiagabine, DDPM-2571) were more effective in this seizure model, it can be concluded that GAT1 inhibition rather than the inhibition of other GAT isoforms plays a role in the abolition of seizures induced by pilocarpine. In contrast, **24e** showed anticonvulsant properties in the PTZ test. Considering the pharmacological effects of **23a** and **24e** and their anticonvulsant activity, we were interested in whether the observed effects could be a result of synergistic effects between GABA reuptake and the calcium influx inhibition. Although, it is assumed that drugs acting by blockade of voltage-gated sodium and to a lesser degree calcium channels (with the exception of ethosuximide) are effective in MES test, but not in PTZ model [66,67], our studies showed that in the MES test, which reflects human *grand mal* epilepsy,

neither **23a** nor **24e** revealed anticonvulsant activity. In contrast, **24e** showed anticonvulsant properties in the PTZ test, additionally, **23a** and **24e** showed rather low ability to inhibit the calcium influx at the concentration of 10 μM (40 ± 9 and 48 ± 18, respectively vs. nimodipine as a reference 59 ± 6, Table S1 in Supplementary materials). Bearing that in mind, we can speculate that the influence of the test compounds **23a** or **24e** on calcium channels might be excluded as a potential mechanism responsible for their anticonvulsant action. Taken together, in this part of the present research, various mouse models of seizures were utilized to study the anticonvulsant properties of **23a** and **24e**. Notably, these screening assays not only identified a potential lead compound with anticonvulsant properties (**24e**) but also allowed us to predict its efficacy against different types of seizures in humans [68]. The PTZ model of clonic seizures generally describes nonconvulsive (absence or myoclonic) seizures in humans [69]. The efficacy of **24e** in the PTZ model suggests that this compound might be potentially effective in absence seizures in humans.

In the present study, we also demonstrated the antinociceptive properties of **23a** and **24e** in the formalin test but not in the hot plate test. Compound **24e** attenuated pain responses in both phases of the formalin test, while **23a** was effective only in the late phase. The formalin model of tonic pain reflects persistent pain, which is regarded to be dependent on sensory C-fiber activation (acute/early phase of this test) and inflammation and sensitization within the spinal cord dorsal horn and brain (the second phase of the test). This finding predicts that **24e** might have a wider spectrum of antinociceptive activity than **23a**. Obtained results attracted our attention since they are found to be similar to those obtained for ReN 1869, a tricyclic derivative of nipecotic acid, presented by Novo Nordisk [70]. Interestingly, ReN 1869 is a selective histamine H_1 receptor antagonist possessing antinociceptive activity in tests of chemical nociception in rodents, e.g., the formalin test but not in thermal tests, e.g., the hot plate test. Therefore, we decided to describe in detail and justified our concerns regarding the obtained *in vivo* effects and the activity toward GATs. For that account, we decided for screening our selected compounds (**23a** and **24e**) to assess their affinity toward histamine H_1 receptors in the Eurofins CEREP, France. The obtained results confirmed their potential antihistaminic activity. Compounds binding, calculated as a % inhibition of control specific binding at 10 μM, was impressively high: H_1 (*h*) antagonist radioligand 98% (**23a**) and 99% (**24e**, see Supporting Information Table S1). In this particular case, we have provided evidence that the antinociceptive properties of **23a** and **24e** could result from their dual activity toward GAT transporters and histamine H_1 receptors. These interesting results constitute only a very primary *in vitro* screening. Further investigation to determine pK_i values as well as the functional assays for the H_1 receptors is recommended in the next stage of our research in the future. Furthermore, available literature data indicate that, apart from seizure control, GABAergic neurotransmission is also involved in the pathophysiology of several psychiatric diseases, including anxiety and depression, and GAT inhibitors might be potentially useful for the treatment of these disorders [71–74]. Our present study did not confirm the anxiolytic-like activity of both compounds tested, but these compounds, in particular **23a** and to a lesser degree **24e**, showed significant antidepressant-like properties in the two mouse models used for antidepressant drug screening, i.e., the forced swim test and the tail suspension test. Additionally, the effects of **23a** and **24e** on locomotor activity were assessed. Unimpaired locomotion is pivotal to obtain reliable results in behavioral assays. In particular, it is sometimes difficult to differentiate between antinociceptive effects and anxiety- or depression-related behavioral activities of drugs from indices related to impaired locomotion. The lack of significant influence from both **23a** and **24e** on the motor skills of the animals seems to be a beneficial property of these compounds, as it precludes false positive interpretation of data obtained in the behavioral models used in the present study. Of note, selective GAT1 inhibitors or GAT1 knockout mice were previously reported to possess anxiolytic-like and antidepressant-like properties in animal models. Our present research could indicate the potential role of non-GAT1 inhibitors in the treatment of depression or the obtained physiological effects could result from activity at other neurotransmitter systems or being synergistic effects between different systems. To verify the antidepressant-like properties obtained from these *in vivo* tests we performed a pan-screening of **23a** and **24e** on other targets in preliminary studies. Thus, we decided to evaluate **23a** and **24e** for their specific affinity to three monoamine transporters: serotonin (hSERT), noradrenaline (hNET) and dopamine (hDAT) that were determined by a competitive MS Binding Assay with the triple reuptake inhibitor (1*R*,3*S*)-indatraline as native marker quantified by LC–ESI–MS/MS [75,76]. As a result, **23a** and **24e** did not show affinities to monoamine reuptake transporters at the concentration of 100 nM. For detailed data, see Supporting Information Table S1). Based on the obtained results we could expect that obtained significant antidepressant-like properties for **23a** and to a lesser degree for **24e** could not result in synergistic effects between GABA neurotransmitter systems and NET and SERT inhibition. Finally, assays performed by Eurofins Pharma Discovery Services toward serotonin 5-HT_{2A} receptor shed light on the potential mechanism responsible for antidepressant-like effects observed for the obtained compounds. It turned out that the novel compounds showed inhibition of control specific binding at 10 μM toward 5-HT_{2A} receptor (see Supporting Information Table S1).

4. Conclusion

Our current SAR studies identified a new series of *N*-benzyl-4-hydroxybutanamide derivatives with inhibitory potency toward mGAT1-4. Interesting results obtained in the primary *in vitro* screening highlight the need for further investigation to produce a clear explanation of the pharmacological activity of presented herein GAT inhibitors. Finally, the broad studies containing experimental data presented in this article will shed light on a different structural model of known GAT inhibitors and their pharmacological profile.

5. Experimental section

5.1. Chemistry

Solvents for the reactions, such as THF and methylene chloride, were dried, distilled, and collected under an argon atmosphere before use. THF was distilled from a mixture of sodium and benzophenone, while methylene chloride was distilled from calcium hydride. Thionyl chloride and TEA were distilled under vacuum before use. Purification of the chemical compounds by column chromatography was carried out using silica gel (mesh: 0.063–0.200 mm, Sigma-Aldrich) as a stationary phase. The reactions were monitored by thin-layer chromatography (aluminum sheets precoated with silica gel 60 F254 (Merck) and visualized via UV light (254 nm). In addition, the TLC plate was stained with a 0.5% solution of ninhydrin in *n*-propanol or in a solution of 5% $(NH_4)_6Mo_7O_{24}$ and 0.2% $Ce(SO_4)_2$ in 5% H_2SO_4. The retention factor (R_f) was defined using the following solvent systems: S_1 (chloroform/acetone 1:1 v/v), S_2 (hexane/ethanol/TEA 7:2:1 v/v/v), S_3 (DCM/acetone 7:3 v/v), S_5 (PE/EtOAc 1:1 v/v), S_7 (DCM/acetone 7:3 v/v), S_9 (DCM/acetone 9:1 v/v), and S_{10} (NH_3/methanol/DCM/petroleum ether 9:45:120:18 v/v/v/v). ^1H NMR and ^{13}C NMR spectra

were recorded using Varian Mercury-VX 300, with ^{1}H at 300.08 MHz and ^{13}C at 75.46 MHz. The chemical shifts (δ) are reported in ppm and were calculated in relation to the frequency of the deuteron field stabilization signal. Coupling constants, *J*, are reported in Hz. The purities of the final compounds were recorded using an Acquity™ UPLC (Waters, Milford, MA, USA) coupled to a tandem quadrupole (TQD, Waters) mass spectrometer (electrospray ionization (ESI) mode-tandem quadrupole). Chromatographic separations were carried out using an Acquity UPLC bridged ethyl hybrid (BEH) C_{18} column; 2.1 × 100 mm, 1.7 μm particle size, equipped with Acquity UPLC BEH C18 VanGuard precolumn; 2.1 × 5 mm, 1.7 μm particle size. All of the final compounds showed purities of >95%. Elemental analyses (C, H, N, and S) were carried out on a Vario Elementar EL III (Elementar Analysensysteme, Hanau, Germany) and determined to be within 0.4% of the theoretical values.

5.1.1. [3-(9H-fluoren-9-ylidene)propyl](methyl)amine (**15**)

A mixture of 9-(3-bromopropylidene)-9*H*-fluorene (**12**, 25.6 mmol, 7.3 g) and a 33% solution of methylamine in ethanol (35 mL) was stirred at room temperature for 48 h. After the reaction was complete, water (20 mL) was added to the residue, and the product was extracted with DCM (2 × 15 mL). The combined organic fractions were dried over Na_2SO_4, and the obtained product was purified by column chromatography over silica gel (started with S_3: DCM/acetone = 7:3 and changed eluent to S_{10}: 25% NH_3/methanol/DCM/petroleum ether = 9:45:120:18) to yield **15** (3.73 g, 62%, R_f = 0.56 (S_{10})) as a yellow oil. Formula $C_{17}H_{17}N$, MW 235.33. ^{1}H NMR ($CDCl_3$) δ ppm 2.51 (s, 3 H (*Me*)), 2.92–2.97 (m, 2 H ($NHCH_2CH_2$)), 3.00–3.06 (m, 2 H ($NHCH_2$)), 6.74 (t, *J* = 7.18 Hz, 1 H (C=C*H*)), 7.27–7.40 (m, 4 H (*Ar*)), 7.64–7.89 (m, 4 H (*Ar*)).

5.1.2. Methyl(3-{tricyclo[9.4.0.0^{3,8}]pentadeca-1(11),3,5,7,9,12,14-heptaen-2-ylidene}propyl)amine (**16**)

A mixture of 2-(3-bromopropylidene)tricyclo[9.4.0.0^{3,8}]pentadeca-1(11),3,5,7,9,12,14-heptaene (**13**, 30 mmol, 9.3 g) and a 33% solution of methylamine in ethanol (41 mL) was stirred at room temperature for 48 h. After the reaction was complete, water (25 mL) was added to the residue, and the product was extracted with DCM (2 × 15 mL). The combined organic fractions were dried over Na_2SO_4, and the obtained product was purified by column chromatography over silica gel (started with S_3: DCM/acetone = 7:3 and changed eluent to S_{10}: 25% NH_3/methanol/DCM/petroleum ether = 9:45:120:18) to yield **16** (6.5 g, 83%, R_f = 0.81 (S_{10})) as a yellow oil. Formula $C_{19}H_{19}N$, MW 261.37. ^{1}H NMR ($CDCl_3$) δ ppm 2.30 (m, 5 H ($H_3C-NH-CH_2-CH_2$-)), 2.61 (td, *J* = 6.86, 4.49 Hz, 2 H (-CH_2-NH-)), 5.53 (dd, *J* = 8.03, 6.91 Hz, 1 H (C=C*H*)), 6.86 (d, *J* = 1.03 Hz, 2 H (ArC*HCH*Ar)), 7.21–7.37 (m, 8 H (*Ar*)).

5.1.3. General procedure (GP1) for the synthesis of 3-substituted oxolan-2-one derivatives **19**–**21**

A mixture of anhydrous K_2CO_3 (1 equiv), the suitable amine (1 equiv) and tetrabutylammonium bromide (TBAB, 0.1 equiv) in acetonitrile was stirred at 0 °C for 15 min. Then, a solution of 3-bromooxolan-2-one (**18**) (1 equiv) was added dropwise followed by stirring for an additional 20 h at room temperature. After the reaction was complete, the precipitate was filtered off, and the filtrate was concentrated under vacuum. The crude product was purified by column chromatography over silica gel.

5.1.3.1. 3-{[3-(9H-Fluoren-9-ylidene)propyl](methyl)amino}oxolan-2-one (**19**).

Synthesis followed GP1 with **15** (8.17 mmol, 1.84 g), 3-bromooxolan-2-one (**18**) (8.18 mmol, 0.80 g), TBAB (0.82 mmol, 0.26 g), and anhydrous K_2CO_3 (8.10 mmol, 1.12 g) in acetonitrile (10 mL). The crude product was purified by column chromatography over silica gel (S_9: DCM/acetone = 9:1) to yield **19** (1.82 g, 73%, R_f = 0.71 (S_1: chloroform/acetone = 1:1)) as a yellow oil. Formula $C_{21}H_{21}NO_2$, MW 319.16. ^{1}H NMR (300 MHz, $CDCl_3$) δ ppm 2.30–2.38 (m, 2 H (NCH_2CH_2)), 2.50 (s, 3 H (*Me*)), 2.91–3.00 (m, 2 H (OCH_2CH_2)), 3.02–3.11 (m, 2 H (CH_2N)), 4.07–4.25 (m, 2 H (NC*H*; OCH_2)), 4.33–4.43 (m, 1 H (OCH_2)), 6.77 (t, *J* = 6.92 Hz, 1 H (C = C*H*)), 7.24–7.40 (m, 4 H (*Ar*)), 7.65–7.72 (m, 2 H (*Ar*)), 7.75 (dt, *J* = 7.37, 1.06 Hz, 1 H (*Ar*)), 7.83–7.88 (m, 1 H (*Ar*)).

5.1.3.2. 3-[Methyl(3-{tricyclo[9.4.0.0^{3,8}]pentadeca-1(11),3,5,7,9,12,14-heptaen-2-ylidene}propyl)amino]oxolan-2-one (**20**).

Synthesis followed GP1 with **16** (15 mmol, 3.89 g), 3-bromooxolan-2-one (**18**) (15 mmol, 2.47 g), TBAB (1.5 mmol, 50 mg), and anhydrous K_2CO_3 (15 mmol, 2.08 g) in acetonitrile (25 mL). The crude product was purified by column chromatography over silica gel (S_9: DCM/acetone = 9:1) to yield **20** (4.23 g, 98%, R_f = 0.72 (S_1: chloroform/acetone = 1:1)) as a yellow oil. Formula $C_{23}H_{23}NO_2$, MW 345.44. ^{1}H NMR (300 MHz, $CDCl_3$) δ ppm 2.10–2.23 (m, 2 H (-CH_2-CH_2-N)), 2.24–2.45 (m, 5 H (*Me,* N–CH–CH_2-)), 2.53–2.66 (m, 1 H (N–CH_2-)), 2.66–2.80 (m, 1 H (-CH_2-N)), 3.50–3.66 (m, 1 H (N–C*H*-)), 4.08–4.17 (m, 1 H (O–CH_2-)), 4.25–4.37 (m, 1 H (O–CH_2-)), 5.56 (dd, *J* = 8.21, 6.54, 4.49 Hz, 1 H (C=C*H*-)), 6.85 (s, 2 H (-C*H*-C*H*-)), 7.20–7.39 (m, 8 H (*Ar*)).

5.1.3.3. 3-[Methyl(3-{tricyclo[9.4.0.0^{3,8}]pentadeca-1(11),3,5,7,12,14-hexaen-2-ylidene}propyl)amino]oxolan-2-one (**21**).

Synthesis followed GP1 with **17** (15 mmol, 3.95 g), 3-bromooxolan-2-one (**18**) (15 mmol, 2.47 g), TBAB (1.5 mmol, 50 mg), and anhydrous K_2CO_3 (15 mmol, 2.08 g) in acetonitrile (25 mL). The crude product was purified by column chromatography over silica gel (S_9: DCM/acetone = 9:1) to yield **21** (4.63 g, 89%, R_f = 0.70 (S_1: chloroform/acetone = 1:1)) as a yellow oil. Formula $C_{23}H_{25}NO_2$, MW 347.46. ^{1}H NMR (300 MHz, $CDCl_3$) δ ppm 2.11–2.24 (m, 2 H (N–CH_2–CH_2-)), 2.30 (s, 3 H (-N-CH_3)), 2.31–2.38 (m, 2 H (O–CH_2–CH_2-)), 2.65–2.81 (m, 3 H (Ar-CH_2-CH_2-)), 3.27 (br. s., 1 H (Ar-CH_2-CH_2-)), 3.59 (t, *J* = 9.62 Hz, 1 H (N–C*H*-)), 4.08–4.18 (m, 2 H (N–CH_2-)), 4.28–4.36 (m, 2 H (O–CH_2-)), 5.86 (t, *J* = 7.31 Hz, 1 H (=C*H*-), 7.03–7.27 (s, 8 H (*Ar*)).

5.1.4. General procedure for the synthesis of N-benzyl-2-{[3-(9H-fluoren-9-ylidene)propyl](methyl)amino}-4-hydroxybutanamide derivatives **22a**–**e**

Under an argon atmosphere, 3-{[3-(9*H*-fluoren-9-ylidene)propyl](methyl)amino}oxolan-2-one (**19**) (1 equiv) was heated with the relevant *N*-benzylamine derivative (2 equiv) in dry THF under reflux for 48 h. After the reaction was complete, the mixture was ice-cooled, and a 1 M solution of HCl (1.5 mL) was added to the mixture. The mixture was then extracted with dichloromethane (3 × 10 mL). The combined organic fractions were dried over Na_2SO_4 and evaporated under vacuum. The crude product was purified by column chromatography.

5.1.4.1. N-Benzyl-2-{[3-(9H-fluoren-9-ylidene)propyl](methyl)amino}-4-hydroxybutanamide (**22a**).

Compound **22a** was prepared using **19** (2.05 mmol, 0.65 g) and *N*-benzylamine (4.10 mmol, 0.44 g) in 10 mL of dry THF. The obtained crude product was purified by column chromatography over silica gel (S_9: CH_2Cl_2/acetone = 9:1) to yield **22a** (330 mg, 38%, R_f = 0.60 (S_1)) as a yellow oil. Formula $C_{28}H_{30}N_2O_2$, MW 426.55. ^{1}H NMR ($CDCl_3$) δ ppm 1.90–2.01 (m, 2 H (CH_2CH_2OH)), 2.32 (s, 3 H (N*Me*)), 2.78–2.85 (m, 2 H (C=CHCH_2)), 2.93–3.10 (m, 2 H (CH_2N)), 3.37 (dd, *J* = 7.82, 4.74 Hz, 1 H (NC*H*)), 3.61–3.71 (m, 1 H (CH_2OH)), 3.86–3.94 (m, 1 H (CH_2OH)), 4.29 (d, *J* = 6.16 Hz, 2 H ($CONHCH_2$)), 6.63 (t, *J* = 7.18 Hz, 1 H (C=C*H*)), 7.17–7.42 (m, 8 H (*fluorene*)), 7.46–7.82 (m, 6 H (*Ar;* CON*H*)). The proton signal from the hydroxyl group was not

identified. ^{13}C NMR ($CDCl_3$) δ ppm 24.81 (-CH_2-CH_2-N), 34.21 (-CH_2-CH_2OH), 41.60 (N−CH_3), 43.81 (−CONH−CH_2-), 57.64 (-CH_2-N), 58.44 (-CH_2-OH), 72.40 (N−CH<), 115.41 (C═CH), 121.21 (2 C, *fluorene*), 124.11 (2 C, *fluorene*), 126.72 (4 C, *Ar*), 127.54 (2 C, *fluorene*), 128.64 (2 C, *fluorene*), 128.74 (*Ar*), 137.91 (*Ar*), 138.40 (2 C, *fluorene*), 141.21 (C═CH), 141.30 (2 C, *fluorene*), 173.21 (1 C, C═O). MS: *m/z* 427 [M+H$^+$].

*5.1.4.2. N-[(2-Chlorophenyl)methyl]-2-{[3-(9H-fluoren-9-ylidene) propyl](methyl)amino}-4-hydroxybutanamide (**22b**).*
Compound **22b** was prepared using **19** (1.75 mmol, 0.56 g) and (2-chlorophenyl)methanamine (3.5 mmol, 0.50 g) in 5 mL of dry THF. The obtained crude product was purified by column chromatography over silica gel (S_9: CH_2Cl_2/acetone = 9:1) to yield **22b** (323 mg, 40%, R_f = 0.64 (S_1)) as a yellow oil. Formula $C_{28}H_{29}ClN_2O_2$, MW 460.19. ^{1}H NMR ($CDCl_3$) δ ppm 1.88−1.97 (m, 2 H (CH_2CH_2OH)), 2.31 (s, 3 H (N*Me*)), 2.76−2.85 (m, 2 H (C═CHCH_2)), 2.94−3.07 (m, 2 H (CH_2N)), 3.33−3.40 (m, 1 H (NC*H*)), 3.60−3.69 (m, 1 H (CH_2OH)), 3.84−3.92 (m, 1 H (CH_2OH)), 4.40 (dd, *J* = 8.85, 6.28 Hz, 2 H (CONHCH_2)), 6.63 (t, *J* = 7.31 Hz, 1 H (C═C*H*)), 7.06−7.17 (m, 2 H (*fluorene*)), 7.19−7.41 (m, 7 H (*fluorene*; *Ar*)), 7.54 (d, *J* = 8.72 Hz, 1 H (*Ar*)), 7.66−7.77 (m, 2 H (*Ar*)), 7.88 (t, *J* = 6.03 Hz, 1 H (CON*H*)). The proton signal from the hydroxyl group was not identified. ^{13}C NMR ($CDCl_3$) δ ppm 24.05 (-CH_2-CH_2-N), 34.31 (-CH_2-CH_2OH), 41.82 (N−CH_3), 42.93 (−CONH−CH_2-), 57.13 (-CH_2-N), 58.04 (-CH_2-OH), 72.61 (N−CH<), 115.44 (C═CH), 121.74 (2 C, *fluorene*), 124.05 (2 C, *fluorene*), 126.64 (*Ar*), 127.40 (2 C, *fluorene*), 128.10 (*Ar*), 128.21 (*Ar*), 128.35 (*Ar*), 128.45 (2 C, *fluorene*), 128.85 (*Ar*), 132.90 (*Ar*−Cl), 138.41 (2 C, *fluorene*), 140.12 (*fluorene*), 140.51 (*fluorene*), 142.41 (*Ar*), 173.10 (C═O). MS: *m/z* 461 [M+H$^+$].

*5.1.4.3. N-[(4-Chlorophenyl)methyl]-2-{[3-(9H-fluoren-9-ylidene) propyl](methyl)amino}-4-hydroxybutanamide (**22c**).* Compound **22c** was prepared using **19** (1.70 mmol, 0.54 g) and (4-chlorophenyl)methanamine (3.4 mmol, 0.48 g) in 5 mL of dry THF. The obtained crude product was purified by column chromatography over silica gel (S_9: CH_2Cl_2/acetone = 9:1) to yield **22c** (335 mg, 43%, R_f = 0.61 (S_1)) as a yellow oil. Formula $C_{28}H_{29}ClN_2O_2$, MW 460.19. ^{1}H NMR ($CDCl_3$) δ ppm 1.88−1.98 (m, 2 H (CH_2CH_2OH)), 2.32 (s, 3 H (N*Me*)), 2.79−2.87 (m, 2 H (C═CHCH_2)), 2.93−3.07 (m, 2 H (CH_2N)), 3.35 (dd, *J* = 7.95, 4.36 Hz, 1 H (NC*H*)), 3.66 (td, *J* = 7.57, 3.85 Hz, 1 H (CH_2OH)), 3.85−3.93 (m, 1 H (CH_2OH)), 4.08−4.21 (m, 2 H (CONHCH_2)), 6.64 (t, *J* = 7.44 Hz, 1 H (C═C*H*)), 6.91 (m, *J* = 8.46 Hz, 2 H (*Ar*)), 7.09 (m, *J* = 8.46 Hz, 2 H (*Ar*)), 7.21−7.43 (m, 5 H (*Ar*)), 7.51 (d, *J* = 7.69 Hz, 1 H (*Ar*)), 7.65−7.83 (m, 3 H (*Ar;* CON*H*)). The proton signal from the hydroxyl group was not identified. ^{13}C NMR ($CDCl_3$) δ ppm 23.85 (-CH_2-CH_2-N), 34.34 (-CH_2-CH_2OH), 41.84 (N−CH_3), 43.92 (−CONH−CH_2-), 57.72 (-CH_2-N), 58.34 (-CH_2-OH), 72.61 (N−CH<), 115.90 (C═CH), 121.41 (2 C, *fluorene*), 124.51 (2 C, *fluorene*), 127.32 (2 C, *fluorene*), 128.34 (2 C, *fluorene*), 128.54 (2 C, *Ar*), 132.84 (*Ar*−Cl), 134.84 (2 C, *Ar*), 136.00 (*Ar*), 138.74 (2 C, *fluorene*), 140.50 (C═CH), 140.41 (2 C, *fluorene*), 173.22 (C═O). MS: *m/z* 461 (M+H$^+$).

*5.1.4.4. 2-{[3-(9H-Fluoren-9-ylidene)propyl](methyl)amino}-N-[(4-fluorophenyl)methyl]-4-hydroxybutanamide (**22d**).* Compound **22d** was prepared using **19** (2.10 mmol, 0.67 g) and (4-fluorophenyl) methanamine (4.2 mmol, 0.53 g) in 8 mL of dry THF. The obtained crude product was purified by column chromatography over silica gel (S_9: CH_2Cl_2/acetone = 9:1) to yield **22d** (299 mg, 32%, R_f = 0.63 (S_1)) as yellow oil. Formula $C_{28}H_{29}FN_2O_2$, MW 444.54. ^{1}H NMR ($CDCl_3$) δ ppm 1.90−2.00 (m, 2 H (CH_2CH_2OH)), 2.32 (s, 3 H (N*Me*)), 2.79−2.87 (m, 2 H (C═CHCH_2)), 2.93−3.03 (m, 2 H (CH_2N)), 3.36 (dd, *J* = 8.08, 4.49 Hz, 1 H (NC*H*)), 3.61−3.69 (m, 1 H (CH_2OH)), 3.85−3.93 (m, 1 H (CH_2OH)), 4.11−4.24 (m, 2 H (CONHCH_2)), 6.64 (t, *J* = 7.31 Hz, 1 H (C═C*H*)), 6.72−6.86 (m, 2 H (*fluorene*)), 6.94−7.02 (m, 2 H (*fluorene*)), 7.21−7.43 (m, 6 H (*fluorene; Ar*)), 7.48−7.54 (m, 1 H (*Ar*)), 7.67−7.75 (m, 2 H (*Ar;* CON*H*)). The proton signal from the hydroxyl group was not identified. ^{13}C NMR ($CDCl_3$) δ ppm 24.12 (-CH_2-CH_2-N), 34.31 (-CH_2-CH_2OH), 41.51 (N−CH_3), 43.12 (−CONH−CH_2-), 57.91 (-CH_2-N), 58.30 (-CH_2-OH), 72.62 (N−CH<), 115.58 (2 C, -CH-C-*F*), 115.92 (C═CH), 121.05 (2 C, *fluorene*), 123.91 (2 C, *fluorene*), 127.51 (2 C, *fluorene*), 128.35 (2 C, *fluorene*), 128.45 (*Ar*), 133.54 (2 C, *Ar*), 138.41 (2 C, *fluorene*), 140.10 (C═CH), 140.21 (2 C, *fluorene*), 162.13 (d, $^1J_{C\text{-}F}$ = 245.24 Hz, *Ar*−F), 173.19 (C═O). MS: *m/z* 445 [M+H$^+$].

*5.1.4.5. 2-{[3-(9H-Fluoren-9-ylidene)propyl](methyl)amino}-4-hydroxy-N-[(4-methylphenyl)methyl]butanamide (**22e**).*
Compound **22e** was prepared using **19** (1.8 mmol, 0.57 g) and *p*-tolylmethanamine (3.6 mmol, 0.44 g) in 7 mL of dry THF. The obtained crude product was purified by column chromatography over silica gel (CH_2Cl_2/acetone = 9:1) to yield **22e** (284 mg, 36%, R_f = 0.65 (S_1)) as a yellow oil. Formula $C_{29}H_{32}N_2O_2$, MW 440.58. ^{1}H NMR ($CDCl_3$) δ ppm ^{1}H NMR ($CDCl_3$) δ ppm 1.91−1.99 (m, 2 H (CH_2CH_2OH)), 2.25 (s, 3 H (Ar*Me*)), 2.32 (s, 3 H (N*Me*)), 2.76−2.85 (m, 2 H (C═CHCH_2)), 2.98 (quin, *J* = 6.92 Hz, 2 H (CH_2N)), 3.36 (dd, *J* = 7.57, 5.00 Hz, 1 H (NC*H*)), 3.63−3.70 (m, 1 H (CH_2OH)), 3.86−3.93 (m, 1 H (CH_2OH)), 4.26 (d, *J* = 6.16 Hz, 2 H (CONHCH_2)), 6.62 (t, *J* = 7.31 Hz, 1 H (C═C*H*)), 6.95−7.03 (m, 4 H (*fluorene*)), 7.20−7.41 (m, 6 H (*fluorene; Ar*)), 7.47−7.52 (m, 1 H (*Ar*)), 7.68−7.80 (m, 2 H (*Ar;* CON*H*)). The proton signal from the hydroxyl group was not identified. ^{13}C NMR ($CDCl_3$) δ ppm 21.15 (Ar-CH_3), 24.81 (-CH_2-CH_2-N), 34.14 (-CH_2-CH_2OH), 41.50 (N−CH_3), 43.41 (−CONH−CH_2-), 57.61 (-CH_2-N), 58.62 (-CH_2-OH), 72.42 (N−CH<), 115.42 (C═CH), 121.02 (2 C, *fluorene*), 124.71 (2 C, *fluorene*), 127.40 (2 C, *fluorene*), 128.12 (2 C, *Ar*), 128.40 (2 C, *fluorene*), 128.61 (2 C, *Ar*), 134.71 (*Ar*), 136.42 (*Ar*), 138.54 (2 C, *fluorene*), 140.13 (C═ CH), 140.24 (2 C, *fluorene*), 173.80 (C═O). MS: *m/z* 441 (M+H$^+$).

*5.1.5. General procedure for the synthesis of N-benzyl-4-hydroxy-2-[methyl(3-{tricyclo[9.4.0.0^{3,8}]pentadeca-1(11),3,5,7,9,12,14-heptaen-2-ylidene}propyl)amino]butanamide derivatives **23a**–**e***

Under an argon atmosphere, 3-[methyl(3-{tricyclo[9.4.0.0^{3,8}] pentadeca-1(11),3,5,7,9,12,14-heptaen-2-ylidene}propyl)amino] oxolan-2-one (**20**) (1 equiv) was heated with the relevant *N*-benzylamine derivative (2 equiv) in dry THF under reflux for 48 h. After the reaction was complete, the mixture was ice-cooled, and a 1 M solution of HCl (1.5 mL) was added to the mixture. The mixture was then extracted with dichloromethane (3 × 10 mL). The combined organic fractions were dried over Na_2SO_4 and evaporated under vacuum. The crude product was purified by column chromatography over silica gel (S_7: DCM/acetone = 7:3).

*5.1.5.1. N-Benzyl-4-hydroxy-2-[methyl(3-{tricyclo[9.4.0.0^{3,8}]pentadeca-1(11),3,5,7,9,12,14-heptaen-2-ylidene}propyl)amino]butanamide (**23a**).* Compound **23a** was prepared using **20** (3 mmol, 0.96 g) and *N*-benzylamine (6 mmol, 0.64 g) in 10 mL of dry THF. Yield **23a** (572 mg, 42%, yellow oil, R_f = 0.44 (S_7)). Formula $C_{30}H_{32}N_2O_2$, MW 452.60. ^{1}H NMR ($CDCl_3$) δ ppm 1.78 (dt, *J* = 10.84, 3.56 Hz, 2 H (-CH_2-CH_2-OH)), 1.92 (s, 3 H (N−CH_3)), 2.08−2.25 (m, 2 H (N−CH_2−CH_2-)), 2.34−2.49 (m, 2 H (N−CH_2-)), 3.07−3.18 (m, 1 H (N−C*H*-)), 3.37−3.62 (m, 2 H (-CH_2-OH)), 4.24−4.37 (m, 2 H (−CONH−CH_2-)), 5.24−5.34 (m, 1 H (C═C*H*-)), 6.65−6.81 (m, 2 H (-C*H* = C*H*-)), 7.10−7.35 (m, 13 H (*Ar*)), 7.73−7.80 (m, 1 H (C*O*−N*H*)). The proton signal from the hydroxyl group was not identified. ^{13}C NMR ($CDCl_3$) δ ppm 22.52 (C═CH−CH_2), 27.01 (-CH_2-CH_2-OH), 41.21 (N−*Me*), 43.82 (CO(NH)CH_2), 55.73 (-CH_2-N), 64.51 (-CH_2-OH), 66.82 (N−C*H*-), 123.93 (C═CH), 124.34 (*Ar*), 125.10 (*Ar*), 125.51 (*Ar*), 126.31 (*Ar*), 127.91 (2 C, *Ar*), 128.20 (*Ar*), 128.42 (*Ar*), 129.41 (*Ar*),

130.31 (2 C, *Ar*), 132.52 (2 C, *Ar*), 134.90 (*Ar*), 135.81 (*Ar*), 136.22 (*Ar*), 137.82 (*Ar*), 138.93 (*Ar*), 143.61 (*Ar*), 144.70 (*Ar*), 144.90 (*C*═C), 171.05 (C═O). MS: *m/z* 453 ($M+H^+$).

*5.1.5.2. N-[(2-Chlorophenyl)methyl]-4-hydroxy-2-[methyl(3-{tricyclo[9.4.0.0^{3,8}]pentadeca-1(11),3,5,7,9,12,14-heptaen-2-ylidene}propyl)amino]butanamide (**23b**).* Compound **23b** was prepared using **20** (0.75 mmol, 239 mg) and (2-chlorophenyl)methanamine (1.5 mmol, 212 mg) in 4 mL of dry THF. Yield **23b** (252 mg, 69%, yellow oil, $R_f = 0.50$ (S_7)). Formula $C_{30}H_{31}ClN_2O_2$, MW 487.04. ^{1}H NMR ($CDCl_3$) δ ppm 1.70–1.87 (m, 2 H (-C*H*$_2$-CH$_2$-OH)), 1.98 (s, 3 H (N–C*H*$_3$)), 2.18–2.36 (m, 2 H (N–CH$_2$–C*H*$_2$-)), 2.37–2.54 (m, 2 H (N–C*H*$_2$-)), 3.10–3.23 (m, 1 H (N–C*H*-)), 3.39–3.59 (m, 1 H (-C*H*$_2$-OH)), 3.71–3.82 (m, 1 H (-C*H*$_2$-OH)), 4.23–4.33 (m, 1 H (–NH–C*H*$_2$-)), 4.44 (dd, $J = 6.28$, 4.23 Hz, 1 H (–NH–C*H*$_2$-)), 5.42–5.53 (m, 1 H (=C*H*-)), 6.66–6.85 (m, 2 H (-C*H* = C*H*-)), 7.04–7.41 (m, 12 H (*Ar*)), 7.83 (dd, $J = 12.70$, 6.28 Hz, 1 H (C*O*–N*H*)). The proton signal from the hydroxyl group was not identified. ^{13}C NMR ($CDCl_3$) δ ppm 23.71 (C═CH–*C*H$_2$), 26.11 (-*C*H$_2$-CH$_2$-OH), 40.05 (N–*Me*), 42.72 (CO(NH)*C*H$_2$), 54.90 (-*C*H$_2$-N), 63.41 (-*C*H$_2$-OH), 69.72 (N–*C*H-), 125.90 (C═*C*H), 126.10 (2 C, *Ar*), 127.41 (4 C, *Ar*), 128.02 (2 C, *Ar*), 128.40 (*Ar*), 129.30 (2 C, *Ar*), 131.15 (*Ar*), 131.40 (2 C, *Ar*), 133.91 (*Ar*), 134.82 (*Ar*), 135.13 (*Ar*), 136.71 (*Ar*), 137.71 (*Ar*), 142.51 (*Ar*), 143.72 (*C*═CH), 171.01 (C═O). MS: *m/z* 487 ($M+H^+$).

*5.1.5.3. N-[(4-Chlorophenyl)methyl]-4-hydroxy-2-[methyl(3-{tricyclo[9.4.0.0^{3,8}]pentadeca-1(11),3,5,7,9,12,14-heptaen-2-ylidene}propyl)amino]butanamide (**23c**).* Compound **23c** was prepared using **20** (0.75 mmol, 239 mg) and (4-chlorophenyl)methanamine (1.5 mmol, 212 mg) in 4 mL of dry THF. Yield **23c** (248 mg, 68%, yellow oil, $R_f = 0.48$ (S_7)). Formula $C_{30}H_{31}ClN_2O_2$, MW 487.04. ^{1}H NMR ($CDCl_3$) δ ppm 1.67–1.80 (m, 2 H (-C*H*$_2$-CH$_2$-OH)), 1.84 (s, 2 H (N–C*H*$_3$)), 1.89 (s, 1 H (N–C*H*$_3$)), 2.06–2.16 (m, 1 H (N–CH$_2$–C*H*$_2$-)), 2.18–2.30 (m, 1 H (N–CH$_2$–C*H*$_2$-), 2.30–2.36 (m, 1 H (N–C*H*$_2$-)), 2.37–2.49 (m, 1 H (N–C*H*$_2$-)), 3.07–3.20 (m, 1 H (N–C*H*-)), 3.41–3.57 (m, 1 H (-C*H*$_2$-OH)), 3.72–3.82 (m, 1 H (-C*H*$_2$-OH)), 4.07–4.42 (m, 2 H (–NH–C*H*$_2$-)), 5.17–5.28 (m, 1 H (=C*H*-)), 6.76–6.89 (m, 2 H (-C*H* = C*H*-)), 6.99 (d, $J = 8.72$ Hz, 1 H (*Ar*)), 7.06–7.45 (m, 11 H (*Ar*)), 7.73–7.89 (m, 1 H (C*O*–N*H*)). The proton signal from the hydroxyl group was not identified. ^{13}C NMR ($CDCl_3$) δ ppm 25.90 (C═CH–*C*H$_2$), 27.11 (-*C*H$_2$-CH$_2$-OH), 39.02 (N–*Me*), 43.80 (CO(NH)*C*H$_2$), 55.10 (-*C*H$_2$-N), 62.34 (-*C*H$_2$-OH), 68.65 (N–*C*H-), 126.80 (C═*C*H), 127.12 (2 C, *Ar*), 127.40 (4 C, *Ar*), 128.02 (2 C, *Ar*), 128.20 (*Ar*), 128.61 (2 C, *Ar*), 129.22 (2 C, *Ar*), 131.23 (*Ar*), 134.81 (*Ar*), 135.22 (*Ar*), 136.83 (*Ar*), 137.10 (2 C, *Ar*), 142.31 (*Ar*), 142.70 (*C*═CH), 171.45 (C═O). MS: *m/z* 487 ($M+H^+$).

*5.1.5.4. N-[(4-Fluorophenyl)methyl]-4-hydroxy-2-[methyl(3-{tricyclo[9.4.0.0^{3,8}]pentadeca-1(11),3,5,7,9,12,14-heptaen-2-ylidene}propyl)amino]butanamide (**23d**).* Compound **23d** was prepared using **20** (0.50 mmol, 160 mg) and (4-fluorophenyl)methanamine (1 mmol, 125 mg) in 2 mL of dry THF. Yield **23d** (116 mg, 49%, yellow oil, $R_f = 0.33$ (S_7)). Formula $C_{30}H_{31}FN_2O_2$, MW 470.59. ^{1}H NMR ($CDCl_3$) δ ppm 1.73–1.79 (m, 2 H (-C*H*$_2$-CH$_2$-OH)), 1.84 (s, 3 H (N–C*H*$_3$)), 2.28–2.39 (m, 3 H (N–C*H*$_2$–C*H*$_2$-), 2.42–2.49 (m, 1 H (N–CH$_2$–C*H*$_2$-), 3.10 (dd, $J = 8.85$, 3.21 Hz, 1 H (N–C*H*-)), 3.41–3.61 (m, 2 H (N–C*H*$_2$-) (-C*H*$_2$-OH)), 4.20–4.32 (m, 2 H (–CONH–C*H*$_2$-)), 5.19–5.26 (m, 1 H (C═C*H*-)), 6.70–6.80 (m, 2 H (-C*H* = C*H*-)), 7.15–7.40 (m, 12 H (*Ar*)), 7.82 (br. s., 1 H (C*O*–N*H*)). The proton signal from the hydroxyl group was not identified. ^{13}C NMR ($CDCl_3$) δ ppm 26.43 (C═CH–*C*H$_2$), 27.88 (-*C*H$_2$-CH$_2$-OH), 38.36 (N–*Me*), 42.34 (CO(NH)*C*H$_2$), 54.84 (-*C*H$_2$-N), 61.77 (-*C*H$_2$-OH), 67.65 (N–*C*H-), 115.08 (C═*C*H), 115.54 (2 C, -*C*H-C-F), 127.02 (*Ar*), 127.12 (2 C, *Ar*), 128.81 (2 C, *Ar*), 129.12 (2 C, *Ar*), 131.32 (3 C, *Ar*), 133.71 (*Ar*), 134.24 (*Ar*), 134.90 (*Ar*), 136.91 (*Ar*), 137.00 (*Ar*), 142.31 (*Ar*), 143.31 (*Ar*), 143.81 (*C* = CH), 161.92 (d, $^1J_{C\text{-}F} = 245.24$ Hz, *C*–F), 174.21 (C═O). MS: *m/z* 471 ($M+H^+$).

*5.1.5.5. 4-Hydroxy-2-[methyl(3-{tricyclo[9.4.0.0^{3,8}]pentadeca-1(11),3,5,7,9,12,14-heptaen-2-ylidene}propyl)amino]-N-[(4-methylphenyl)methyl]butanamide (**23e**).* Compound **23e** was prepared using **20** (0.50 mmol, 160 mg) and *p*-tolylmethanamine (1 mmol, 121 mg) in 2 mL of dry THF. Yield **23e** (112 mg, 48%, yellow oil, $R_f = 0.42$ (S_7)). Formula $C_{31}H_{34}N_2O_2$, MW 466.62. ^{1}H NMR ($CDCl_3$) δ ppm 1.73–1.83 (m, 2 H (-C*H*$_2$-CH$_2$-OH)), 1.93 (d, $J = 11.03$ Hz, 3 H (N–C*H*$_3$)), 2.10–2.30 (m, 2 H (N–CH$_2$–C*H*$_2$-), 2.32 (d, $J = 6.92$ Hz, 3 H (Ar-C*H*$_3$)), 2.34–2.50 (m, 2 H (N–C*H*$_2$-)), 3.07–3.22 (m, 1 H (N–C*H*-)), 3.37–3.59 (m, 1 H (-C*H*$_2$-OH)) 3.74–3.82 (m, 1 H (-C*H*$_2$-OH)) 4.04 (dd, $J = 14.62$, 5.90 Hz, 1 H (–NH–C*H*$_2$-)), 4.21–4.34 (m, 1 H (–CONH–C*H*$_2$-)), 5.23–5.35 (m, 1 H (C═C*H*-)), 6.71–6.89 (m, 2 H (-C*H* = C*H*-)), 6.98–7.38 (m, 12 H (*Ar*)), 7.73 (d, $J = 5.39$ Hz, 1 H (C*O*–N*H*)). The proton signal from the hydroxyl group was not identified. ^{13}C NMR ($CDCl_3$) δ ppm 21.12 (Ar-*Me*), 26.62 (C═CH–*C*H$_2$), 27.64 (-*C*H$_2$-CH$_2$-OH), 38.32 (N–*Me*), 42.94 (CO(NH)*C*H$_2$), 54.71 (-*C*H$_2$-N), 61.81 (-*C*H$_2$-OH), 67.70 (N–*C*H-), 126.91 (*Ar*), 127.10 (2 C, *Ar*), 127.51 (2 C, *Ar*), 128.00 (*Ar*), 128.31 (4 C, *Ar*), 129.11 (*Ar*), 131.02 (*Ar*), 131.10 (2 C, *Ar*), 133.70 (*Ar*), 134.91 (*Ar*), 135.21 (*Ar*), 136.91 (*Ar*), 137.02 (2 C, *Ar*), 142.40 (*Ar*), 143.61 (*C* = CH), 171.90 (C═O). MS: *m/z* 467 ($M+H^+$).

*5.1.6. General procedure for the synthesis of N-benzyl-4-hydroxy-2-[methyl(3-{tricyclo[9.4.0.0^{3,8}]pentadeca-1(11),3,5,7,12,14-hexaen-2-ylidene}propyl)amino]butanamide derivatives **24a–e***

Under an argon atmosphere, 3-[methyl(3-{tricyclo[9.4.0.0^{3,8}]pentadeca-1(11),3,5,7,12,14-hexaen-2-ylidene}propyl)amino]oxolan-2-one (**21**) (1 equiv) was heated with the relevant *N*-benzylamine derivative (2 equiv) in dry THF under reflux for 48 h. After the reaction was completed, the mixture was ice-cooled, and a 1 M solution of HCl (1.5 mL) was added to the mixture. The mixture was then extracted with dichloromethane (3 × 10 mL). The combined organic fractions were dried over Na_2SO_4 and evaporated under vacuum. The crude product was purified by column chromatography over silica gel (S_7: DCM/acetone = 7:3).

*5.1.6.1. N-Benzyl-4-hydroxy-2-[methyl(3-{tricyclo[9.4.0.0^{3,8}]pentadeca-1(11),3,5,7,12,14-hexaen-2-ylidene}propyl)amino]butanamide (**24a**).* Compound **24a** was prepared using **21** (0.85 mmol, 271 mg) and *N*-benzylamine (1.7 mmol, 182 mg) in 4 mL of dry THF. Yield **24a** (351 mg, 91%, yellow oil, $R_f = 0.31$ (S_7)). Formula $C_{30}H_{34}N_2O_2$, MW 454.29. ^{1}H NMR ($CDCl_3$) δ ppm 1.80–1.91 (m, 2 H (-C*H*$_2$-CH$_2$-OH)), 2.08 (s, 3 H (N–C*H*$_3$)), 2.20–2.34 (m, 2 H (Ar-C*H*$_2$-CH$_2$-Ar)), 2.42–2.57 (m, 2 H (Ar–CH$_2$–C*H*$_2$-Ar)), 2.66–2.81 (m, 1 H (N–CH$_2$–C*H*$_2$-)), 2.95 (d, $J = 12.31$ Hz, 1 H (N–CH$_2$–C*H*$_2$-)), 3.09–3.42 (m, 2 H (N–C*H*$_2$-)), 3.51–3.61 (m, 1 H (N–C*H*-)), 3.77–3.88 (m, 1 H (-C*H*$_2$-OH)), 4.13–4.27 (m, 1 H (-C*H*$_2$-OH)), 4.28–4.49 (m, 2 H (–NH–C*H*$_2$-)), 5.68–5.83 (m, 1 H (=C*H*-)), 6.97–7.34 (m, 13 H (*Ar*)), 7.91 (br. s., 1 H (C*O*–N*H*)). The proton signal from the hydroxyl group was not identified. ^{13}C NMR ($CDCl_3$) δ ppm 27.90 (C═CH–*C*H$_2$), 31.91 (2 C, Ar-*C*H$_2$-*C*H$_2$-Ar), 33.71 (-*C*H$_2$-CH$_2$-OH), 41.31 (N–*Me*), 43.20 (CO(NH)*C*H$_2$), 57.31 (-*C*H$_2$-OH), 58.41 (-*C*H$_2$-N), 67.51 (N–*C*H-), 125.80 (C═*C*H), 126.11 (*Ar*), 127.61 (2 C, *Ar*), 128.42 (4 C, *Ar*), 128.64 (4 C, *Ar*), 130.20 (*Ar*), 133.54 (2 C, *Ar*), 135.32 (2 C, *Ar*), 136.94 (2 C, *Ar*), 139.83 (*C* = CH), 174.12 (C═O). MS: *m/z* 455 ($M+H^+$).

*5.1.6.2. N-[(2-Chlorophenyl)methyl]-4-hydroxy-2-[methyl(3-{tricyclo[9.4.0.0^{3,8}]pentadeca-1(11),3,5,7,12,14-hexaen-2-ylidene}propyl)amino]butanamide (**24b**).* Compound **24b** was prepared using **21** (0.75 mmol, 239 mg) and (2-chlorophenyl)methanamine (1.5 mmol, 212 mg) in 5 mL of dry THF. Yield **24b** (304 mg, 83%,

yellow oil, $R_f = 0.44$ (S_7)). Formula $C_{30}H_{33}ClN_2O_2$, MW 489.06. ^{1}H NMR ($CDCl_3$) δ ppm 1.73–1.92 (m, 2 H (-C*H*$_2$-CH$_2$-OH)), 2.11 (s, 3 H (N–C*H*$_3$)), 2.23–2.39 (m, 2 H (Ar-C*H*$_2$-CH$_2$-Ar)), 2.52 (d, $J = 6.92$ Hz, 2 H (Ar–CH$_2$–C*H*$_2$-Ar)), 2.68–2.84 (m, 1 H (N–CH$_2$–C*H*$_2$-)), 2.85–3.05 (m, 1 H (N–CH$_2$–C*H*$_2$-)), 3.13–3.44 (m, 3 H ((N–C*H*-; N–C*H*$_2$-)), 3.49–3.61 (m, 1 H (-C*H*$_2$-OH)), 3.74–3.86 (m, 1 H (-C*H*$_2$-OH)), 4.32–4.54 (m, 2 H (–NH–C*H*$_2$-)), 5.71–5.85 (m, 1 H (=C*H*-)), 7.05–7.37 (m, 12 H (*Ar*)), 7.95 (br. s., 1 H (CO–N*H*)). The proton signal from the hydroxyl group was not identified. ^{13}C NMR ($CDCl_3$) δ ppm 28.01 (C=CH–*C*H$_2$), 30.92 (2 C, Ar-*C*H$_2$-*C*H$_2$-Ar), 33.71 (-*C*H$_2$-CH$_2$-OH), 41.31 (N–*Me*), 43.62 (CO(NH)*C*H$_2$), 57.62 (-*C*H$_2$-OH), 61.52 (-*C*H$_2$-N), 67.21 (N–*C*H-), 125.82 (C=*C*H), 126.11 (*Ar*), 127.01 (*Ar*), 127.21 (*Ar*), 127.61 (*Ar*), 128.01 (2 C, *Ar*), 128.42 (*Ar*), 128.92 (2 C, *Ar*), 129.51 (*Ar*), 130.13 (2 C, *Ar*), 133.53 (2 C, *Ar*), 135.41 (*Ar*), 136.91 (*Ar*), 139.31 (2 C, *Ar*), 139.80 (*C* = CH), 174.20 (C=O). MS: *m/z* 489 [M+H$^+$].

*5.1.6.3. N-[(4-Chlorophenyl)methyl]-4-hydroxy-2-[methyl(3-{tricyclo[9.4.0.0^{3,8}]pentadeca-1(11),3,5,7,12,14-hexaen-2-ylidene}propyl)amino]butanamide (**24c**).* Compound **24c** was prepared using **21** (0.75 mmol, 239 mg) and (4-chlorophenyl)methanamine (1.5 mmol, 212 mg) in 5 mL of dry THF. Yield **24c** (275 mg, 75%, yellow oil, $R_f = 0.40$ (S_7)). Formula $C_{30}H_{33}ClN_2O_2$, MW 489.06. ^{1}H NMR ($CDCl_3$) δ ppm 1.76–1.92 (m, 2 H (-C*H*$_2$-CH$_2$-OH)), 2.06 (br. s., 3 H (N–C*H*$_3$)), 2.20–2.39 (m, 2 H (Ar-C*H*$_2$-CH$_2$-Ar)), 2.39–2.60 (m, 2 H (Ar–CH$_2$–C*H*$_2$-Ar)), 2.65–2.82 (m, 1 H (N–CH$_2$–C*H*$_2$-)), 2.95 (d, $J = 13.08$ Hz, 1 H (N–CH$_2$–C*H*$_2$-)), 3.07–3.42 (m, 2 H (N–C*H*$_2$-)), 3.48–3.62 (m, 1 H (-C*H*$_2$-OH)), 3.74–3.88 (m, 1 H (-C*H*$_2$-OH)), 4.06–4.20 (m, 1 H (N–C*H*-)), 4.20–4.38 (m, 2 H (–NH–C*H*$_2$-)), 5.65–5.81 (m, 1 H (=C*H*-)), 6.90–7.30 (m, 12 H (*Ar*)), 7.88 (br. s., 1 H (CO–N*H*)). The proton signal from the hydroxyl group was not identified. ^{13}C NMR ($CDCl_3$) δ ppm 27.81 (C=CH–*C*H$_2$), 31.90 (2 C, Ar-*C*H$_2$-*C*H$_2$-Ar), 33.70 (-*C*H$_2$-CH$_2$-OH), 42.51 (N–*Me*), 43.92 (CO(NH)*C*H$_2$), 57.42 (-*C*H$_2$-OH), 58.32 (-*C*H$_2$-N), 67.52 (N–*C*H-), 125.52 (C=*C*H), 126.12 (2 C, *Ar*), 127.20 (2 C, *Ar*), 128.11 (*Ar*), 128.41 (2 C, *Ar*), 128.91 (2 C, *Ar*), 129.00 (2 C, *Ar*), 130.21 (4 C, *Ar*), 136.70 (*Ar*), 136.93 (2 C, *Ar*), 139.73 (*C* = CH), 174.20 (C=O). MS: *m/z* 489 [M+H$^+$].

*5.1.6.4. N-[(4-Fluorophenyl)methyl]-4-hydroxy-2-[methyl(3-{tricyclo[9.4.0.0^{3,8}]pentadeca-1(11),3,5,7,12,14-hexaen-2-ylidene}propyl)amino]butanamide (**24d**).* Compound **24d** was prepared using **21** (0.55 mmol, 176 mg) and (4-fluorophenyl)methanamine (1.1 mmol, 138 mg) in 5 mL of dry THF. Yield **24d** (214 mg, 82%, yellow oil, $R_f = 0.42$ (S_7)). Formula $C_{30}H_{33}FN_2O_2$, MW 472.60. ^{1}H NMR ($CDCl_3$) δ ppm 1.77–1.90 (m, 2 H (-C*H*$_2$-CH$_2$-OH)), 2.06 (s, 3 H (N–C*H*$_3$)) 2.20–2.35 (m, 2 H (Ar-C*H*$_2$-CH$_2$-Ar)), 2.48 (dd, $J = 9.62$, 5.51 Hz, 2 H (Ar–CH$_2$–C*H*$_2$-Ar)), 2.68–2.81 (m, 1 H (N–CH$_2$–C*H*$_2$-)), 2.87–3.02 (m, 1 H (N–CH$_2$–C*H*$_2$-)), 3.12–3.37 (m, 3 H (N–C*H*-;N–C*H*$_2$-)), 3.50–3.60 (m, 1 H (-C*H*$_2$-OH)), 3.76–3.87 (m, 1 H (-C*H*$_2$-OH)), 4.21–4.37 (m, 2 H (–NH–C*H*$_2$-)), 5.67–5.80 (m, 1 H (=C*H*-) 6.86–7.26 (m, 12 H (*Ar*)), 7.92 (br. s., 1 H (CO–N*H*)). The proton signal from the hydroxyl group was not identified. ^{13}C NMR ($CDCl_3$) δ ppm 27.85 (C=CH–*C*H$_2$), 31.96 (2 C, Ar-*C*H$_2$-*C*H$_2$-Ar), 33.69 (-*C*H$_2$-CH$_2$-OH), 42.47 (N–*Me*), 43.92 (CO(NH)*C*H$_2$), 57.81 (-*C*H$_2$-OH), 58.72 (-*C*H$_2$-N), 67.55 (N–*C*H-), 115.29 (C=*C*H), 115.58 (2 C, *C*H–C–F), 125.77 (*Ar*), 126.13 (*Ar*), 127.30 (2 C, *Ar*), 127.61 (*Ar*), 128.11 (2 C, *Ar*), 128.43 (2 C, *Ar*), 129.24 (2 C, *Ar*), 130.20 (*Ar*), 133.97 (*Ar*), 134.03 (*Ar*), 136.91 (*Ar*), 139.70 (*C* = CH), 162.05 (d, $^1J_{C\text{-}F} = 245.25$ Hz, *C*–F), 174.15 (C=O). MS: *m/z* 473 [M+H$^+$].

*5.1.6.5. 4-Hydroxy-2-[methyl(3-{tricyclo[9.4.0.0^{3,8}]pentadeca-1(11),3,5,7,12,14-hexaen-2-ylidene}propyl)amino]-N-[(4-methylphenyl)methyl]butanamide (**24e**).* Compound **24e** was prepared using **21** (0.75 mmol, 239 mg) and *p*-tolylmethanamine (1.5 mmol, 182 mg) in 5 mL of dry THF. Yield **24e** (267 mg, 76%, yellow oil, $R_f = 0.41$ (S_7)). Formula $C_{31}H_{36}N_2O_2$, MW 468.64. ^{1}H NMR ($CDCl_3$) δ ppm ^{1}H NMR ($CDCl_3$) δ ppm 1.77–1.92 (m, 2 H (-C*H*$_2$-CH$_2$-OH)), 2.10 (s, 3 H (N–C*H*$_3$)), 2.19–2.41 (m, 5 H (Ar-C*H*$_2$-CH$_2$-Ar, Ar-C*H*$_3$)), 2.43–2.61 (m, 2 H (Ar–CH$_2$–C*H*$_2$-Ar)), 2.68–2.81 (m, 1 H (N–CH$_2$–C*H*$_2$-)), 2.88–3.02 (m, 1 H (N–CH$_2$–C*H*$_2$-)), 3.13–3.41 (m, 3 H (N–C*H*-; N–C*H*$_2$-)), 3.55 (ddd, $J = 11.61$, 7.25, 4.23 Hz, 1 H (-C*H*$_2$-OH)), 3.83 (dd, $J = 10.39$, 4.74 Hz, 1 H (-C*H*$_2$-OH)), 4.30 (dd, $J = 16.03$, 6.54 Hz, 2 H (–NH–C*H*$_2$-)), 5.71–5.79 (m, 1 H (=C*H*-)), 6.85–7.25 (m, 12 H (*Ar*)), 7.83 (br. s., 1 H (CO–N*H*)). The proton signal from the hydroxyl group was not identified. ^{13}C NMR ($CDCl_3$) δ ppm 20.91 (Ar-*Me*), 21.10 (C=CH–*C*H$_2$), 32.01 (2 C, Ar-*C*H$_2$-*C*H$_2$-Ar), 33.27 (-*C*H$_2$-CH$_2$-OH), 41.45 (N–*Me*), 43.00 (CO(NH)*C*H$_2$), 57.61 (-*C*H$_2$-OH), 58.61 (-*C*H$_2$-N), 67.42 (N–*C*H-), 125.82 (C=*C*H), 126.13 (*Ar*), 127.23 (*Ar*), 127.63 (2 C, *Ar*), 128.00 (2 C, *Ar*), 128.41 (2 C, *Ar*), 129.32 (4 C, *Ar*), 130.20 (2 C, *Ar*), 135.05 (2 C, *Ar*), 136.91 (2 C, *Ar*), 139.70 (*C* = CH), 173.90 (C=O). MS: *m/z* 469 [M+H$^+$].

*5.1.7. General procedure for the synthesis of N-benzyl-4-(1,3-dioxo-2,3-dihydro-1H-isoindol-2-yl)-2-[methyl(3-{tricyclo[9.4.0.0^{3,8}]pentadeca-1(11),3,5,7,12,14-hexaen-2-ylidene}propyl)amino]butanamide derivatives **26a–e***

Anhydrous K_2CO_3 (2.5 equiv) and KI (1 equiv) were added to a solution of methyl(3-{tricyclo[9.4.0.0^{3,8}]pentadeca-1(11),3,5,7,12,14-hexaen-2-ylidene}propyl)amine (**17**) (1 equiv) in acetonitrile. Then, the relevant *N*-benzyl-2-bromo-4-(1,3-dioxoisoindolin-2-yl)butanamide derivative (**25a**–**e**) (1.76 mmol, 1 equiv) was added, and the reaction mixture was stirred and under reflux for 24 h. After the reaction was complete, the precipitate was filtered, the filtrate was concentrated under vacuum, and the product was purified by column chromatography over silica gel (S_5: PE/EtOAc = 1:1).

*5.1.7.1. N-Benzyl-4-(1,3-dioxo-2,3-dihydro-1H-isoindol-2-yl)-2-[methyl(3-{tricyclo[9.4.0.0^{3,8}]pentadeca-1(11),3,5,7,12,14-hexaen-2-ylidene}propyl)amino]butanamide (**26a**).* Compound **26a** was prepared using **25a** (1.5 mmol, 0.60 g), amine **17** (1.5 mmol, 0.40 g), KI (1.5 mmol, 0.25 g), anhydrous K_2CO_3 (3 mmol, 0.41 g), and acetonitrile (15 mL). Yield **26a** (461 mg, 52%, yellow oil, $R_f = 0.51$ (S_5)). Formula $C_{38}H_{37}N_3O_3$, MW 583.72. ^{1}H NMR ($CDCl_3$) δ ppm 1.81–1.95 (m, 1 H (NCHC*H*$_2$)), 2.08 (s, 3 H (*Me*)), 2.12–2.33 (m, 3 H (NCHC*H*$_2$; =CHC*H*$_2$)), 2.41–2.57 (m, 2 H (C*H*$_2$N)), 2.60–2.78 (m, 1 H (Ar-C*H*$_2$-)), 2.80–3.02 (m, 1 H (Ar-C*H*$_2$-)), 3.08–3.44 (m, 3 H (Ar-C*H*$_2$-; NC*H*)), 3.78 (dt, $J = 13.98$, 7.12 Hz, 1 H (C*H*$_2$N)), 3.86–4.03 (m, 1 H (C*H*$_2$N)), 4.20–4.48 (m, 2 H (C*H*$_2$NH)), 5.63–5.77 (m, 1 H (C = C*H*)), 6.96–7.21 (m, 9 H (*Ar*)), 7.21–7.34 (m, 4 H (*Ar*)), 7.36–7.52 (m, 1 H (CON*H*)), 7.65–7.75 (m, 2 H (*phthalimide*)), 7.79–7.88 (m, 2 H (*phthalimide*)).

*5.1.7.2. N-[(2-Chlorophenyl)methyl]-4-(1,3-dioxo-2,3-dihydro-1H-isoindol-2-yl)-2-[methyl(3-{tricyclo[9.4.0.0^{3,8}]pentadeca-1(11),3,5,7,12,14-hexaen-2-ylidene}propyl)amino]butanamide (**26b**).* Compound **26b** was prepared using **25b** (1.5 mmol, 0.65 g), amine **17** (1.5 mmol, 0.40 g), KI (1.5 mmol, 0.25 g), anhydrous K_2CO_3 (3 mmol, 0.41 g), and acetonitrile (15 mL). Yield **26b** (441 mg, 47%, yellow oil, $R_f = 0.58$ (S_5)). Formula $C_{38}H_{36}N_3ClO_3$, MW 618.16. ^{1}H NMR ($CDCl_3$) δ ppm 1.80–1.95 (m, 1 H (NCHC*H*$_2$)), 2.10 (s, 3 H (*Me*)), 2.15–2.34 (m, 3 H (NCHC*H*$_2$; =CHC*H*$_2$)), 2.44–2.55 (m, 2 H (C*H*$_2$N)), 2.62–2.79 (m, 1 H (ArC*H*$_2$)), 2.83–2.99 (m, 1 H (ArC*H*$_2$)), 3.13–3.18 (m, 1 H (NC*H*)), 3.20–3.46 (m, 2 H (ArC*H*$_2$)), 3.69–3.82 (m, 1 H (C*H*$_2$N)), 3.83–4.00 (m, 1 H (C*H*$_2$N)), 4.42 (br. s., 2 H (C*H*$_2$NH)), 5.73 (t, $J = 7.31$ Hz, 1 H (C = C*H*)), 6.95–7.23 (m, 8 H (*Ar*)), 7.23–7.34 (m, 2 H (*Ar*)), 7.42–7.63 (m, 3 H (*Ar;* CON*H*)), 7.64–7.73 (m, 2 H (*phthalimide*)), 7.78–7.89 (m, 2 H (*phthalimide*)).

*5.1.7.3. N-[(4-Chlorophenyl)methyl]-4-(1,3-dioxo-2,3-dihydro-1H-isoindol-2-yl)-2-[methyl(3-{tricyclo[9.4.0.0^{3},^{8}]pentadeca-1(11),3,5,7,12,14-hexaen-2-ylidene}propyl)amino]butanamide (**26c**).* Compound **26c** was prepared using **25c** (1.5 mmol, 0.65 g), amine **17** (1.5 mmol, 0.40 g), KI (1.5 mmol, 0.25 g), anhydrous K_2CO_3 (3 mmol, 0.41 g), and acetonitrile (15 mL). Yield **26c** (601 mg, 64%, yellow oil, $R_f = 0.54$ (S_5)). Formula $C_{38}H_{36}N_3ClO_3$, MW 618.16. ^{1}H NMR ($CDCl_3$) δ ppm 1.79–1.96 (m, 1 H (NCHCH_2)), 2.05 (s, 3 H (*Me*)), 2.08–2.35 (m, 3 H (NCHCH_2; =CHCH_2)), 2.37–2.57 (m, 2 H (CH_2N)), 2.61–2.78 (m, 1 H (ArCH_2)), 2.81–3.00 (m, 1 H (ArCH_2)), 3.04–3.40 (m, 3 H (ArCH_2; NC*H*)), 3.67–3.83 (m, 1 H (CH_2N)), 3.84–4.00 (m, 1 H (CH_2N)), 4.06–4.41 (m, 2 H (CH_2NH)), 5.60–5.78 (m, 1 H (C = C*H*)), 6.93–7.33 (m, 12 H (*Ar*)), 7.41–7.57 (m, 1 H (CON*H*)), 7.63–7.76 (m, 2 H (*phthalimide*)), 7.78–7.89 (m, 2 H (*phthalimide*)).

*5.1.7.4. N-[(4-Fluorophenyl)methyl]-4-(1,3-dioxo-2,3-dihydro-1H-isoindol-2-yl)-2-[methyl(3-{tricyclo[9.4.0.0^{3},^{8}]pentadeca-1(11),3,5,7,12,14-hexaen-2-ylidene}propyl)amino]butanamide (**26d**).* Compound **26d** was prepared using **25d** (1.75 mmol, 0.73 g), amine **17** (1.75 mmol, 0.46 g), KI (1.75 mmol, 0.29 g), anhydrous K_2CO_3 (3.5 mmol, 0.48 g), and acetonitrile (15 mL). Yield **26d** (429 mg, 47%, yellow oil, $R_f = 0.50$ (S_5)). Formula $C_{38}H_{36}N_3FO_3$, MW 601.71. ^{1}H NMR ($CDCl_3$) δ ppm 1.80–1.96 (m, 1 H (NCHCH_2)), 2.05 (s, 3 H (*Me*)), 2.10–2.32 (m, 3 H (NCHCH_2; =CHCH_2)), 2.36–2.54 (m, 2 H (CH_2N)), 2.61–2.78 (m, 1 H (ArCH_2)), 2.94 (dd, J = 13.72, 8.59 Hz, 1 H (ArCH_2)), 3.14 (d, J = 3.59 Hz, 1 H (NC*H*)), 3.15–3.43 (m, 2 H (ArCH_2)), 3.77 (dt, J = 13.91, 7.02 Hz, 1 H (CH_2N)), 3.93 (dd, J = 16.16, 7.18 Hz, 1 H (CH_2N)), 4.25 (dd, J = 13.72, 5.26 Hz, 2 H (CH_2NH)), 5.60–5.78 (m, 1 H (C = C*H*)), 6.83–7.23 (m, 12 H (*Ar*)), 7.38–7.53 (m, 1 H (CON*H*)), 7.62–7.73 (m, 2 H (*phthalimide*)), 7.76–7.88 (m, 2 H (*phthalimide*)).

*5.1.7.5. 4-(1,3-Dioxo-2,3-dihydro-1H-isoindol-2-yl)-2-[methyl(3-{tricyclo[9.4.0.0^{3},^{8}]pentadeca-1(11),3,5,7,12,14-hexaen-2-ylidene}propyl)amino]-N-[(4-methylphenyl)methyl]butanamide (**26e**).* Compound **26e** was prepared using **25e** (1.65 mmol, 0.69 g), amine **17** (1.65 mmol, 0.43 g), KI (1.65 mmol, 0.27 g), anhydrous K_2CO_3 (3.3 mmol, 0.46 g), and acetonitrile (15 mL). Yield **26e** (439 mg, 45%, yellow oil, $R_f = 0.59$ (S_5)). Formula $C_{39}H_{39}N_3O_3$, MW 597.75. ^{1}H NMR ($CDCl_3$) δ ppm 1.80–1.94 (m, 1 H (NCHCH_2)), 2.08 (s, 3 H (*Me*)), 2.10–2.25 (m, 3 H (NCHCH_2; =CHCH_2)), 2.31 (s, 3 H (*Me*)), 2.39–2.54 (m, 2 H (CH_2N)), 2.60–2.75 (m, 1 H (ArCH_2)), 2.82–3.00 (m, 1 H (ArCH_2)), 3.15 (dd, J = 8.46, 4.10 Hz, 1 H (NC*H*)), 3.17–3.42 (m, 2 H (ArCH_2)), 3.70–3.84 (m, 1 H (CH_2N)), 3.85–4.01 (m, 1 H (CH_2N)), 4.20–4.33 (m, 2 H (CH_2NH)), 5.64–5.76 (m, 1 H (C = C*H*)), 6.91–7.23 (m, 12 H (*Ar*)), 7.37 (br. s., 1 H (CON*H*)), 7.64–7.76 (m, 2 H (*phthalimide*)), 7.76–7.89 (m, 2 H (*phthalimide*)).

*5.1.8. General procedure for the synthesis of 4-amino-N-benzyl-2-[methyl(3-{tricyclo[9.4.0.0^{3},^{8}]pentadeca-1(11),3,5,7,12,14-hexaen-2-ylidene}propyl)amino]butanamide derivatives **27(a–e)***

Two millimoles of hydrazine hydrate (2 equiv) was added to a suspension of 1 mmol of the relevant 2-substituted 4-phthalimidobutanoic acid derivative **26(a–e)** (1 equiv) in ethanol (10 mL). The reaction was carried out at 60 °C for 2 h then cooled to room temperature, with continued stirring for an additional 5 h. Next, the precipitate was filtered and washed with methylene chloride (5 mL). The filtrate was evaporated, and the product was extracted with DCM (2 × 10 mL). The combined organic fractions were dried over Na_2SO_4, and the obtained product was purified by column chromatography over silica gel (started with S_5: PE/EtOAc = 1:1 and changed eluent to S_{10}: 25% NH_3/methanol/DCM/petroleum ether = 9:45:120:18).

*5.1.8.1. 4-Amino-N-benzyl-2-[methyl(3-{tricyclo[9.4.0.0^{3},^{8}]pentadeca-1(11),3,5,7,12,14-hexaen-2-ylidene}propyl)amino]butanamide (**27a**).* Compound **27a** was prepared using **26a** (0.75 mmol, 0.44 g) and hydrazine hydrate (1.5 mmol, 75 mg) in ethanol (10 mL). Yield **27a** (280 mg, 82%, yellow oil, $R_f = 0.95$ (S_{10})). Formula $C_{30}H_{35}N_3O$, MW 453.62. ^{1}H NMR ($CDCl_3$) δ ppm 1.69–1.89 (m, 2 H (NCHCH_2)), 2.07 (s, 3 H (*Me*)), 2.19–2.31 (m, 2 H (=CHCH_2)), 2.41–2.59 (m, 2 H (CH_2NH$_2$)), 2.84–2.98 (m, 2 H (ArCH_2)), 3.08–3.37 (m, 3 H (ArCH_2; NC*H*)), 3.97 (br. s., 2 H (ArCH_2)), 4.28 (dd, J = 12.31, 4.87 Hz, 2 H (CH_2NH)), 5.74 (br. s., 1 H (C = C*H*)), 6.95–7.34 (m, 13 H (*Ar*)), 7.53–7.74 (m, 1 H (CON*H*)). ^{13}C NMR ($CDCl_3$) δ ppm 26.81 (=CH–CH_2), 31.00 (*N*–CH–CH_2), 32.61 (2 C, Ar-CH_2-CH_2-Ar), 42.91 (CH_2–NH$_2$), 43.71 (N–*Me*), 44.71 (CO(NH)CH_2), 57.80 (CH_2N), 73.12 (N–C*H*), 115.55 (=C*H*), 124.70 (*Ar*), 125.11 (*Ar*), 126.10 (2 C, *Ar*), 126.33 (*Ar*), 126.37 (*Ar*), 126.52 (*Ar*), 128.00 (*Ar*), 128.11 (*Ar*), 128.21 (*Ar*), 128.41 (*Ar*), 129.20 (2 C, *Ar*), 135.83 (2 C, *Ar*), 137.24 (2 C, *Ar*), 138.21 (*Ar*), 138.70 (*C*=CH), 172.70 (C=O). MS: *m/z* 454 [M+H$^+$].

*5.1.8.2. 4-Amino-N-[(2-chlorophenyl)methyl]-2-[methyl(3-{tricyclo[9.4.0.0^{3},^{8}]pentadeca-1(11),3,5,7,12,14-hexaen-2-ylidene}propyl)amino]butanamide (**27b**).* Compound **27b** was prepared using **26b** (0.7 mmol, 0.43 g) and hydrazine hydrate (1.4 mmol, 70 mg) in ethanol (7 mL). Yield **27b** (221 mg, 65%, yellow oil, $R_f = 0.89$ (S_{10})). Formula $C_{30}H_{34}ClN_3O$, MW 488.31. ^{1}H NMR ($CDCl_3$) δ ppm 1.73–1.91 (m, 2 H (NCHCH_2)), 2.08 (s, 3 H (*Me*)), 2.19–2.33 (m, 2 H (=CHCH_2)), 2.42–2.58 (m, 2 H (CH_2NH$_2$)), 2.66–2.80 (m, 1 H (CH_2N)), 2.80–3.03 (m, 3 H (ArCH_2; CH_2N)), 3.09–3.24 (m, 2 H (ArCH_2; NC*H*)), 3.24–3.40 (m, 1 H (ArCH_2)), 4.22–4.53 (m, 4 H (CH_2NH; -NH$_2$)), 5.77 (t, J = 6.67 Hz, 1 H (C = C*H*)), 7.02–7.42 (m, 12 H (*Ar*)), 7.76 (br. s., 1 H (CON*H*)). ^{13}C NMR ($CDCl_3$) δ ppm 27.02 (=CH–CH_2), 31.00 (N–CH–CH_2), 32.63 (2 C, Ar-CH_2-CH_2-Ar), 40.14 (CH_2–NH$_2$), 43.44 (N–*Me*), 44.33 (CO(NH)CH_2), 57.61 (CH_2N), 73.00 (N–C*H*), 115.81 (=C*H*), 124.71 (*Ar*), 125.05 (*Ar*), 126.05 (*Ar*), 126.10 (*Ar*), 126.50 (*Ar*), 127.02 (*Ar*), 127.10 (*Ar*), 127.31 (2 C, *Ar*), 127.41 (*Ar*), 127.72 (*Ar*), 128.42 (*Ar*), 129.12 (2 C, *Ar*), 132.42 (C–Cl), 134.42 (2 C, *Ar*), 135.83 (*Ar*), 138.11 (*C*=CH), 172.81 (C=O). MS: *m/z* 488 [M+H$^+$].

*5.1.8.3. 4-Amino-N-[(4-chlorophenyl)methyl]-2-[methyl(3-{tricyclo[9.4.0.0^{3},^{8}]pentadeca-1(11),3,5,7,12,14-hexaen-2-ylidene}propyl)amino]butanamide (**27c**).* Compound **27c** was prepared using **26c** (0.86 mmol, 0.53 g) and hydrazine hydrate (1.68 mmol, 84 mg) in ethanol (10 mL). Yield **27c** (306 mg, 73%, yellow oil, $R_f = 0.94$ (S_{10})). Formula $C_{30}H_{34}ClN_3O$, MW 488.31. ^{1}H NMR ($CDCl_3$) δ ppm 1.90 (s, 2 H (NCHCH_2)), 2.05 (s, 3 H (*Me*)), 2.16–2.35 (m, 2 H (=CHCH_2)), 2.48 (br. s., 2 H (CH_2N)), 2.63–3.02 (m, 4 H (ArCH_2; CH_2NH$_2$)), 3.05–3.24 (m, 2 H (ArCH_2; NC*H*)), 3.24–3.43 (m, 1 H (ArCH_2)), 4.08–4.34 (m, 2 H (CH_2NH)), 5.73 (br. s., 1 H (C = C*H*)), 6.89–7.24 (m, 12 H (*Ar*)), 7.65 (br. s., 1 H (CON*H*)). ^{13}C NMR ($CDCl_3$) δ ppm 26.70 (=CH–CH_2), 31.90 (N–CH–CH_2), 32.60 (2 C, Ar-CH_2-CH_2-Ar), 41.31 (CH_2–NH$_2$), 43.71 (N–*Me*), 44.62 (CO(NH)CH_2), 57.92 (CH_2N), 73.33 (N–C*H*), 115.60 (=C*H*), 124.71 (*Ar*), 125.02 (2 C, *Ar*), 126.25 (*Ar*), 126.50 (*Ar*), 127.02 (*Ar*), 127.10 (*Ar*), 127.33 (*Ar*), 127.60 (*Ar*), 127.81 (2 C, *Ar*), 129.12 (*Ar*), 132.00 (C–Cl), 135.61 (2 C, *Ar*), 135.80 (2 C, *Ar*), 138.21 (*Ar*), 138.62 (*C*=CH), 172.72 (C=O). MS: *m/z* 488 [M+H$^+$].

*5.1.8.4. 4-Amino-N-[(4-fluorophenyl)methyl]-2-[methyl(3-{tricyclo[9.4.0.0^{3},^{8}]pentadeca-1(11),3,5,7,12,14-hexaen-2-ylidene}propyl)amino]butanamide (**27d**).* Compound **27d** was prepared using **26d** (0.69 mmol, 0.42 g) and hydrazine hydrate (1.43 mmol, 72 mg) in ethanol (7 mL). Yield **27d** (300 mg, 91%, yellow oil, $R_f = 0.90$ (S_{10})). Formula $C_{30}H_{34}FN_3O$, MW 471.61. ^{1}H NMR ($CDCl_3$) δ ppm 1.71–1.94 (m, 2 H (NCHCH_2)), 2.03 (s, 3 H (*Me*)), 2.14–2.34 (m, 2 H (=CHCH_2)), 2.46 (br. s., 2 H (CH_2NH$_2$)), 2.64–2.79 (m, 1 H (CH_2N)), 2.91 (br. s., 2 H (ArCH_2)), 3.04–3.14 (m, 2 H (CH_2N; NC*H*)), 3.18 (dd, J = 8.34,

4.23 Hz, 1 H (*Ar*C*H*$_2$)), 3.21−3.39 (m, 1 H (*Ar*C*H*$_2$)), 4.21 (dd, *J* = 13.98, 5.00 Hz, 2 H (C*H*$_2$NH)), 4.83 (br. s., 1 H (C = C*H*)), 5.65−5.79 (m, 2 H (*Ar*)), 6.81−6.97 (m, 2 H (*Ar*)), 6.97−7.24 (m, 8 H (*Ar*)), 7.78 (br. s., 1 H (CON*H*)). ^{13}C NMR ($CDCl_3$) *δ* ppm 27.90 (=CH−*C*H$_2$), 31.00 (N−CH−*C*H$_2$), 31.97 (2 C, Ar-*C*H$_2$-*C*H$_2$-Ar), 42.32 (*C*H$_2$−NH$_2$), 43.63 (N−*Me*), 44.05 (CO(NH)*C*H$_2$), 57.62 (*C*H$_2$N), 73.12 (N−*C*H), 115.25 (−CH−C-F), 115.53 (−CH−C-F), 115.89 (=*C*H), 124.2 (*Ar*), 125.00 (2 C, *Ar*), 126.31 (*Ar*), 126.61 (*Ar*), 127.02 (*Ar*), 127.43 (2 C, *Ar*), 128.12 (*Ar*), 128.31 (*Ar*), 129.22 (*Ar*), 133.00 (*Ar*), 133.21 (*Ar*), 135.81 (*Ar*), 138.22 (*Ar*), 138.63 (*C*=CH), 161.99 (d, $^{1}J_{C\text{-}F}$ = 245.24 Hz, *C*−F), 173.36 (C=O). MS: *m/z* 472 [M+H$^+$].

*5.1.8.5. 4-Amino-2-[methyl(3-{tricyclo[9.4.0.0^{3,8}]pentadeca-1(11),3,5,7,12,14-hexaen-2-ylidene}propyl)amino]-N-[(4-methylphenyl)methyl]butanamide (**27e**).* Compound **27e** was prepared using **26e** (0.69 mmol, 0.41 g) and hydrazine hydrate (1.4 mmol, 70 mg) in ethanol (10 mL). Yield **27e** (253 mg, 79%, yellow oil, R_f = 0.92 (S_{10})). Formula $C_{31}H_{37}N_3O$, MW 467.64. ^{1}H NMR ($CDCl_3$) *δ* ppm 1.63−1.93 (m, 2 H (NCHC*H*$_2$)), 2.08 (s, 3 H (*Me*)), 2.17−2.37 (m, 2 H (=CHC*H*$_2$)), 2.50 (t, *J* = 6.28 Hz, 2 H (C*H*$_2$NH$_2$)), 2.61−2.83 (m, 4 H (C*H*$_2$Ar; *Me*)), 2.90−3.05 (m, 3 H (*Ar*C*H*$_2$; C*H*$_2$N)), 3.11 (dd, *J* = 8.34, 4.49 Hz, 1 H (NC*H*)), 3.17−3.37 (m, 2 H (*Ar*C*H*$_2$)), 4.25 (br. s., 2 H (C*H*$_2$NH)), 5.76 (t, *J* = 6.92 Hz, 1 H (C = C*H*)), 6.92−7.27 (m, 12 H (*Ar*)), 7.47−7.66 (m, 1 H (CON*H*)). ^{13}C NMR ($CDCl_3$) *δ* ppm 20.10 (Ar-*Me*), 26.91 (=CH−*C*H$_2$), 31.02 (N−CH−*C*H$_2$), 32.61 (2 C, Ar-*C*H$_2$-*C*H$_2$-Ar), 41.81 (*C*H$_2$−NH$_2$), 43.91 (N−*Me*), 44.12 (CO(NH)*C*H$_2$), 57.63 (*C*H$_2$N), 73.02 (N−*C*H), 115.63 (=*C*H), 124.74 (*Ar*), 125.03 (*Ar*), 126.02 (*Ar*), 126.20 (*Ar*), 126.51 (2 C, *Ar*), 126.92 (2 C, *Ar*), 127.05 (*Ar*), 127.44 (2 C, *Ar*), 128.22 (2 C, *Ar*), 129.03 (*Ar*), 134.11 (2 C, *Ar*), 135.81 (*C*$_{Ar}$-Me), 138.21 (*Ar*), 138.72 (*C*=CH), 172.61 (C=O). MS: *m/z* 468 [M+H$^+$].

*5.1.9. General procedure for the synthesis of N-benzyl-4-acetamido-2-[methyl(3-{tricyclo[9.4.0.0^{3,8}]pentadeca-1(11),3,5,7,12,14-hexaen-2-ylidene}propyl)amino]butanamide derivatives **28(a−e)***

A mixture of acetic acid (2 equiv) and DCC (2 equiv) in 5 mL of DCM stirred at 0 °C for 10 min. Then, the relevant 4-amino-*N*-benzyl-2-[methyl(3-{tricyclo[9.4.0.0^{3,8}]pentadeca-1(11),3,5,7,12,14-hexaen-2-ylidene}propyl)amino]butanamide derivative **27(a−e)** (1 equiv) and DMAP (2 equiv) were added to the reaction mixture, and stirring continued for 20 h at room temperature. The obtained DCU was filtered, the filtrate was evaporated, and the product was purified by column chromatography over silica gel (S_1: chloroform/acetone = 1:1).

*5.1.9.1. N-Benzyl-4-acetamido-2-[methyl(3-{tricyclo[9.4.0.0^{3,8}]pentadeca-1(11),3,5,7,12,14-hexaen-2-ylidene}propyl)amino]butanamide (**28a**).* Compound **28a** was prepared using acetic acid (0.60 mmol, 36 mg), DCC (0.60 mmol, 0.12 g), **27a** (0.60 mmol, 0.27 g) and DMAP (0.30 mmol, 37 mg) in DCM (8 mL). Yield **28a** (280 mg, 95%, yellow oil, R_f = 0.41 (S_1)). Formula $C_{32}H_{37}N_3O_2$, MW 495.66. ^{1}H NMR ($CDCl_3$) *δ* ppm 1.72−1.90 (m, 2 H (NCHC*H*$_2$)), 1.93 (s, 3 H (*Me*)), 2.06 (s, 3 H (*Me*)), 2.26 (dd, *J* = 5.51, 12.18 Hz, 2 H (=CHC*H*$_2$)), 2.48 (br. s., 2 H (C*H*$_2$N)), 2.65−2.79 (m, 1 H (C*H*$_2$NH)), 2.87−3.01 (m, 1 H (C*H*$_2$NH)), 3.06 (dd, *J* = 3.85, 7.95 Hz, 1 H (NC*H*)), 3.11−3.27 (m, 2 H (*Ar*C*H*$_2$)), 3.27−3.52 (m, 2 H (*Ar*C*H*$_2$)), 4.31 (dd, *J* = 6.03, 13.98 Hz, 2 H (C*H*$_2$NH)), 5.64−5.85 (m, 1 H (C = C*H*)), 6.95−7.35 (m, 13 H (*Ar*)), 7.79 (br. s., 2 H (CON*H*)). ^{13}C NMR ($CDCl_3$) *δ* ppm 23.25 (NH(CO)*Me*), 27.94 (=CH−*C*H$_2$), 31.99 (N−CH−*C*H$_2$), 33.71 (2 C, Ar-*C*H$_2$-*C*H$_2$-Ar), 43.13 (*C*H$_2$−NH), 43.71 (N−*Me*), 44.51 (CO(NH)*C*H$_2$), 57.31 (*C*H$_2$N), 73.71 (N−*C*H), 115.31 (=*C*H), 125.81 (*Ar*), 126.12 (2 C, *Ar*), 127.21 (*Ar*), 127.42 (*Ar*), 127.51 (*Ar*), 127.61 (*Ar*), 128.01 (*Ar*), 128.10 (*Ar*), 128.51 (*Ar*), 128.64 (*Ar*), 130.16 (2 C, *Ar*), 136.92 (2 C, *Ar*), 138.25 (2 C, *Ar*), 139.31 (*Ar*), 139.78 (*C*=CH), 170.38 (C=O), 173.77 (C=O). MS: *m/z* 454 [M+H$^+$].

*5.1.9.2. N-[(2-Chlorophenyl)methyl]-4-acetamido-2-[methyl(3-{tricyclo[9.4.0.0^{3,8}]pentadeca-1(11),3,5,7,12,14-hexaen-2-ylidene}propyl)amino]butanamide (**28b**).* Compound **28b** was prepared using acetic acid (0.43 mmol, 26 mg), DCC (0.43 mmol, 89 mg), **27b** (0.43 mmol, 0.21 g) and DMAP (0.22 mmol, 27 mg) in DCM (7 mL). Yield **28b** (221 mg, 97%, yellow oil, R_f = 0.47 (S_1)). Formula $C_{32}H_{36}N_3ClO_2$, MW 530.10. ^{1}H NMR ($CDCl_3$) *δ* ppm 1.71−1.86 (m, 2 H (NCHC*H*$_2$)), 1.91 (s, 3 H (*Me*)), 2.08 (s, 3 H (*Me*)), 2.18−2.32 (m, 2 H (=CHC*H*$_2$)), 2.41−2.57 (m, 2 H (C*H*$_2$N)), 2.66−2.84 (m, 1 H (C*H*$_2$NH)), 2.84−2.99 (m, 1 H (C*H*$_2$NH)), 3.06 (dd, *J* = 3.46, 8.34 Hz, 1 H (NC*H*)), 3.08−3.25 (m, 2 H (*Ar*C*H*$_2$)), 3.27−3.47 (m, 2 H (*Ar*C*H*$_2$)), 4.30−4.53 (m, 2 H (C*H*$_2$NH)), 5.77 (t, *J* = 7.18 Hz, 1 H (C = C*H*)), 6.89−7.14 (m, 6 H (*Ar*)), 7.14−7.26 (m, 6 H (*Ar*)), 7.31 (d, *J* = 6.16 Hz, 1 H (CON*H*)), 7.74−7.88 (m, 1 H (CON*H*)). ^{13}C NMR ($CDCl_3$) *δ* ppm 23.25 (NH(CO)*Me*), 28.03 (=CH−*C*H$_2$), 32.00 (N−CH−*C*H$_2$), 33.74 (2 C, Ar-*C*H$_2$-*C*H$_2$-Ar), 41.22 (*C*H$_2$−NH), 43.51 (N−*Me*), 44.11 (CO(NH)*C*H$_2$), 57.00 (*C*H$_2$N), 72.91 (N−*C*H), 115.13 (=*C*H), 125.81 (*Ar*), 126.10 (*Ar*), 126.97 (*Ar*), 127.19 (*Ar*), 127.60 (*Ar*), 128.03 (*Ar*), 128.09 (*Ar*), 128.40 (*Ar*), 128.55 (2 C, *Ar*), 128.85 (2 C, *Ar*), 129.54 (*Ar*), 130.06 (*Ar*), 133.51 (*C*−Cl), 135.49 (*Ar*), 136.88 (2 C, *Ar*), 139.27 (*C*=CH), 170.34 (C=O), 173.90 (C=O). MS: *m/z* 488 [M+H$^+$].

*5.1.9.3. N-[(4-Chlorophenyl)methyl]-4-acetamido-2-[methyl(3-{tricyclo[9.4.0.0^{3,8}]pentadeca-1(11),3,5,7,12,14-hexaen-2-ylidene}propyl)amino]butanamide (**28c**).* Compound **28c** was prepared using acetic acid (0.60 mmol, 36 mg), DCC (0.60 mmol, 0.12 g), **27c** (0.60 mmol, 0.29 g) and DMAP (0.30 mmol, 37 mg) in DCM (8 mL). Yield **28c** (280 mg, 89%, yellow oil, R_f = 0.41 (S_1)). Formula $C_{32}H_{36}N_3ClO_2$, MW 530.10. ^{1}H NMR ($CDCl_3$) *δ* ppm 1.73−1.86 (m, 2 H (NCHC*H*$_2$)), 1.92 (s, 3 H (*Me*), 2.04 (s, 3 H (*Me*)), 2.15−2.34 (m, 2 H (=CHC*H*$_2$)), 2.39−2.53 (m, 2 H (C*H*$_2$N)), 2.64−2.79 (m, 1 H (C*H*$_2$NH)), 2.85−2.99 (m, 1 H (C*H*$_2$NH)), 3.05 (dd, *J* = 3.98, 7.82 Hz, 1 H (NC*H*)), 3.09−3.25 (m, 2 H (*Ar*C*H*$_2$)), 3.27−3.46 (m, 2 H (*Ar*C*H*$_2$)), 4.23 (dd, *J* = 5.90, 14.36 Hz, 2 H (C*H*$_2$NH)), 5.66−5.77 (m, 1 H (C = C*H*)), 6.89−7.27 (m, 13 H (CON*H*; *Ar*)), 7.70−7.92 (m, 1 H (CON*H*)). ^{13}C NMR ($CDCl_3$) *δ* ppm 23.24 (NH(CO)*Me*), 27.88 (=CH−*C*H$_2$), 31.99 (N−CH−*C*H$_2$), 33.71 (2 C, Ar-*C*H$_2$-*C*H$_2$-Ar), 42.43 (*C*H$_2$−NH), 43.81 (N−*Me*), 44.10 (CO(NH)*C*H$_2$), 57.01 (*C*H$_2$N), 73.10 (N−*C*H), 115.61 (=*C*H), 125.79 (*Ar*), 126.12 (*Ar*), 127.31 (*Ar*), 127.61 (2 C, *Ar*), 128.00 (2 C, *Ar*), 128.19 (*Ar*), 128.43 (*Ar*), 128.72 (*Ar*), 128.89 (2 C, *Ar*), 130.17 (2 C, *Ar*), 133.09 (*C*−Cl), 136.84 (*Ar*), 136.89 (*Ar*), 139.35 (*Ar*), 139.71 (*C*=CH), 170.36 (C=O), 173.81 (C=O). MS: *m/z* 488 [M+H$^+$].

*5.1.9.4. N-[(4-Fluorophenyl)methyl]-4-acetamido-2-[methyl(3-{tricyclo[9.4.0.0^{3,8}]pentadeca-1(11),3,5,7,12,14-hexaen-2-ylidene}propyl)amino]butanamide (**28d**).* Compound **28d** was prepared using acetic acid (0.6 mmol, 36 mg), DCC (0.6 mmol, 0.12 g), **27d** (0.6 mmol, 0.28 g) and DMAP (0.3 mmol, 37 mg) in DCM (8 mL). Yield **28d** (256 mg, 84%, yellow oil, R_f = 0.38 (S_1)). Formula $C_{32}H_{36}N_3FO_2$, MW 513.65. ^{1}H NMR ($CDCl_3$) *δ* ppm 1.70−1.88 (m, 2 H (NCHC*H*$_2$)), 1.93 (s, 3 H (*Me*)), 2.05 (s, 3 H (*Me*)), 2.13−2.34 (m, 2 H (=CHC*H*$_2$)), 2.48 (br. s., 2 H (C*H*$_2$N)), 2.65−2.80 (m, 1 H (C*H*$_2$NH)), 2.86−2.99 (m, 1 H (C*H*$_2$NH)), 3.05 (dd, *J* = 3.21, 8.34 Hz, 1 H (NC*H*)), 3.10−3.27 (m, 2 H (*Ar*C*H*$_2$)), 3.27−3.63 (m, 2 H (*Ar*C*H*$_2$)), 4.25 (dd, *J* = 5.13, 13.85 Hz, 2 H (C*H*$_2$NH)), 5.64−5.79 (m, 1 H (C = C*H*)), 6.85−7.22 (m, 13 H (CON*H; Ar*)), 7.79 (br. s., 1 H (CON*H*)). ^{13}C NMR ($CDCl_3$) *δ* ppm 23.27 (NH(CO)*Me*), 27.81 (=CH−*C*H$_2$), 31.96 (N−CH−*C*H$_2$), 33.69 (2 C, Ar-*C*H$_2$-*C*H$_2$-Ar), 42.42 (*C*H$_2$−NH), 43.51 (N−*Me*), 44.41 (CO(NH)*C*H$_2$), 57.71 (*C*H$_2$N), 73.10 (N−*C*H), 115.30 (=*C*H), 115.41 (2 C, −CH−C-F), 115.59 (2 C, *C*H−C−F), 125.79 (*Ar*), 126.12 (*Ar*), 127.43 (*Ar*), 127.61 (*Ar*), 128.02 (*Ar*), 128.43 (*Ar*), 129.15 (*Ar*), 129.26 (*Ar*), 130.21 (*Ar*), 134.01 (*Ar*), 134.10 (*Ar*), 136.91 (*Ar*), 139.31 (*Ar*), 139.70 (*C*=CH), 162.05 (d, $^{1}J_{C\text{-}F}$ = 246.00 Hz, *C*−F), 170.37 (C=O), 173.72 (C=O). MS: *m/z* 472 [M+H$^+$].

*5.1.9.5. 4-Acetamido-2-[methyl(3-{tricyclo[9.4.0.0^{3,8}]pentadeca-1(11),3,5,7,12,14-hexaen-2-ylidene}propyl)amino]-N-[(4-methylphenyl)methyl]butanamide (**28e**).* Compound **28e** was prepared using acetic acid (0.51 mmol, 31 mg), DCC (0.51 mmol, 0.11 g), **27e** (0.51 mmol, 0.24 g) and DMAP (0.26 mmol, 31 mg) in DCM (7 mL). Yield **28e** (212 mg, 81%, yellow oil, $R_f = 0.42$ (S_1)). Formula $C_{33}H_{39}N_3O_2$, MW 509.68. ^{1}H NMR ($CDCl_3$) δ ppm 1.72–1.88 (m, 2 H (NCHC*H*$_2$)), 1.94 (s, 3 H (*Me*)), 2.06 (s, 3 H (*Me*)), 2.19–2.29 (m, 2 H (=CHC*H*$_2$)), 2.32 (s, 3 H), 2.39–2.55 (m, 2 H (C*H*$_2$N)), 2.72 (br. s., 1 H (C*H*$_2$NH)), 2.85–3.01 (m, 1 H (C*H*$_2$NH)), 3.05 (dd, $J = 3.21$, 8.34 Hz, 1 H (NC*H*)), 3.19 (br. s., 2 H (*Ar*C*H*$_2$)), 3.30–3.56 (m, 2 H (*Ar*C*H*$_2$)), 4.27 (dd, $J = 5.13$, 12.82 Hz, 2 H (C*H*$_2$NH)), 5.74 (br. s., 1 H (C = C*H*)), 6.89–7.29 (m, 13 H (CONH*; Ar*)), 7.64–7.81 (m, 1 H (CONH*)). ^{13}C NMR ($CDCl_3$) δ ppm 21.10 (Ar-*Me*), 23.27 (NH(CO)*Me*), 27.92 (=CH–*C*H$_2$), 31.99 (N–CH–*C*H$_2$), 33.71 (2 C, Ar-*C*H$_2$-*C*H$_2$-Ar), 42.93 (*C*H$_2$–NH), 43.61 (N–*Me*), 44.11 (CO(NH)*C*H$_2$), 57.41 (*C*H$_2$N), 72.90 (N–*C*H), 115.51 (=*C*H), 125.79 (*Ar*), 126.09 (*Ar*), 127.21 (*Ar*), 127.54 (*Ar*), 127.61 (2 C, *Ar*), 128.05 (*Ar*), 128.15 (*Ar*), 128.51 (2 C, *Ar*), 129.31 (2 C, *Ar*), 130.12 (*Ar*), 135.18 (2 C, *Ar*), 136.94 (*C$_{Ar}$*-Me), 139.78 (2 C, *Ar*), 139.81 (*C*=CH), 170.35 (C=O), 173.69 (C=O). MS: *m/z* 468 [M+H$^+$].

5.2. Molecular modeling

5.2.1. Docking studies

We used models of human GABA transporters that were selected in our previous work [43]. They were built with the SWISS-MODEL server based on the 4XP9 (GAT-1, GAT-2, GAT-3) or 4XP4 (BGT-1) template from the PDB. We used sequence alignment generated automatically by SWISS-MODEL. *N*- and C-termini were omitted because of their low homology. Sodium and chloride ions were transferred directly from the templates.

The ligand 3D structures were created in the Maestro program. Ionization states were predicted under physiological conditions (pH 7.4) using the Marvin program. Ligands were optimized in the LigPrep module. All possible stereoisomers for each ligand were generated. Models were prepared in Protein Preparation Wizard using default settings.

To better fit the models to the examined compounds, the most active representatives were initially docked into the models of each type of GABA transporter using the induced fit docking protocol available in the Schrödinger Suite. The box center was defined by residues PHE294, TYR140, TYR452, and ARG69 in GAT-1 and by the corresponding amino acids in BGT-1, GAT-2, and GAT-3. The box size was 10 Å × 10 Å × 10 Å. The obtained complexes were then visually inspected in terms of the created interactions, frequency and score of the poses as well as their coherency between the particular types of GABA transporters. The compliance with previous observations of the binding mode for other 4-aminobutanamide and 4-hydroxybutanamide derivatives was also taken into account [43]. After selecting the best optimized models, all studied compounds were docked into the models using the GLIDE program, and the final models were selected based on ligand pose coherency. The grid center in Glide docking was set as the centroid of the ligand from the complex, and the inner box size was 10 Å × 10 Å × 10 Å. The OPLS2005 force field was applied during grid generation as well as GLIDE and IFD docking. The binding modes were visualized in the PyMOL program.

5.2.2. Molecular dynamics

MD simulations were performed in NAMD using the CHARMM36 m force field. Before simulations, all models were positioned in the membrane using the OPM server, and input files for NAMD were prepared with the CHARMM-GUI online server. The protein-ligand complexes were embedded in a POPC membrane and solvated with TIP3P water molecules. The system size was 100 Å × 100 Å. A water pore for each complex was generated. Sodium and chloride ions (0.15 M NaCl) were added to provide standard physiological ionic strength. The system was equilibrated *via* a six-step protocol recommended by CHARMM-GUI for the NAMD program. MD simulations were run at 303.15 K with a timestep of 2 fs and a total duration of 10 ns. The interval for both the energy and trajectory recordings were 10 ps. The results were analyzed with the VMD program.

5.3. Hepatotoxicity and cytotoxicity

Hepatotoxicity and cytotoxicity were estimated according to previously described protocols [77] using the *hepatoma* HepG2 (ATCC HB-8065™) and human embryonic kidney HEK–293 (ATCC® CRL¬1573) cell lines, respectively. In brief, cells were seeded in 96-well plates at a concentration of 0.7×10^4 and cultured at 37 °C in an atmosphere containing 5% CO_2. Next, the compounds were added and investigated in quadruplicate at concentrations ranging from 0.1 to 100 μM for 72 h. The antiproliferative drug doxorubicin was used as the reference. The CellTiter 96® AQueous Non-Radioactive Cell Proliferation Assay (MTS) purchased from Promega (Madison, WI, USA) was used for the determination of cell viability. The absorbance at 492 nm was measured using a microplate reader (PerkinElmer).

5.4. In vitro activity

5.4.1. [^{3}H] GABA uptake assay

The inhibitory activities of the synthesized compounds were determined in a [^{3}H]GABA uptake assay as described [26], and all compounds were tested at a screening concentration of 100 μM.

5.4.2. MS Binding Assays

MS Binding Assays for mGAT1 were performed as described earlier [53]. Inhibition of mGAT1 binding by the synthesized compounds was determined in MS Binding Assays at a screening concentration of 100 μM.

5.5. In vivo evaluation

5.5.1. Animals and housing conditions

Adult male Albino Swiss (CD-1) mice weighing between 18 g and 22 g were used in all *in vivo* experiments, except for the tail suspension test in which C57BL/6J mice of the same age and body weight were used (Animalab, Poland). The animals were kept in groups of 10 mice in cages at room temperature (22 ± 2 °C) under a light/dark (12:12) cycle and had free access to food and water before the experiments. The ambient temperature of the room and humidity were kept consistent throughout all the tests. For the experiments, the animals were selected randomly. Each group consisted of 6–12 animals/dose, and each mouse was used only once. The experiments were performed between 8 a.m. and 3 p.m. Immediately after each assay, the animals were euthanized by cervical dislocation. All procedures were approved by the Local Ethics Committee of Jagiellonian University in Cracow (ZI/595/2011). To avoid potential bias in data recording, the investigators who were involved in behavioral tests were blinded to the experimental groups.

5.5.2. Test compounds

For the *in vivo* tests. Compounds **23a** and **24e** were suspended in 1% Tween 80 solution (Polskie Odczynniki Chemiczne, Poland). Control mice received 1% Tween 80 solution. Both vehicle and test compounds were injected intraperitoneally (*i.p.*) 60 min before the

experiments. In tests assessing anticonvulsant activity, 100 mg/kg was the starting dose. In the other behavioral assays, 30 mg/kg was the highest (and starting) dose. These doses were selected based on our previous preliminary experiments as well as earlier studies that assessed pharmacological properties of other GAT inhibitors [46].

5.5.3. Anticonvulsant activity

Two mouse models of electrically induced seizures *(i.e.*, electroconvulsive threshold test and maximal electroshock seizure test) and two models of chemically induced seizures (*i.e.,* pentylenetetrazole seizures and pilocarpine-induced seizures) were used to assess whether compounds **23a** and **24e** could protect mice from seizures.

5.5.3.1. Electroconvulsive threshold test. In the electroconvulsive threshold test (ECT test), the anticonvulsant efficacy of the test compounds at a dose of 100 mg/kg was evaluated at their previously established time of peak drug effect (60 min after *i.p.* Injection) according to a procedure recently described [28]. Electroconvulsions were produced by an alternating current (duration of the stimulus: 0.2 s; 50 Hz) delivered via standard auricular electrodes by an electroshock generator (Hugo Sachs rodent shocker, Germany). Tonic hind limb extension (i.e., the hind limbs outstretched 180° to the plane of the body axis) was an indicator of seizure episodes. For evaluation of the ECT, at least four groups of animals per dose were used (each group consisted of 8 animals). These mice were challenged with electroshocks of various intensities to yield 10–30%, 30–50%, 50–70% and 70–90% of animals with seizures. Then, a median current strength value (CS_{50}, in mA), defined as the current intensity required to induce tonic hind limb extension in 50% of the challenged mice, was estimated by means of the log-probit method [78].

5.5.3.2. Maximal electroshock seizure test. The maximal electroshock test (MES test) was performed as previously described [28]. Briefly, the vehicle-treated mice and drug-treated mice received a stimulus of sufficient intensity (25 mA) delivered by an electroshock generator (Hugo Sachs rodent shocker, Germany) to induce maximal seizures (tonic extension) of hind limbs. Electroconvulsions were produced with the use of auricular electrodes, and the stimulus duration was 0.2 s. The endpoint was the tonic extension of the hind limbs.

5.5.3.3. Pentylenetetrazole-induced seizures test. This study was performed based on the method previously described by Kowalczyk et al. [46]. Mice were administered a test compound or vehicle, and 60 min later, they were subcutaneously (*s.c.*) injected with pentylenetetrazole at a dose of 100 mg/kg to induce seizures. Then, the animals were individually placed under glass cylinders for 30 min for the purpose of observation. Measured parameters were latency to the first seizure episode and the number of seizure episodes during the 30-min observation period.

5.5.3.4. Pilocarpine-induced seizures test. The study was performed based on the method previously described by Kowalczyk et al. [46]. Mice were administered a test compound or vehicle. Sixty minutes later, pilocarpine (Sigma Aldrich, Poland) was intraperitoneally (*i.p.*) injected at a dose of 400 mg/kg in order to induce seizures. To reduce the effects resulting from peripheral parasympathetic stimulation, 45 min before pilocarpine administration, the mice were injected (*i.p.*) with scopolamine hydrobromide (Sopharma, Poland) at a dose of 1 mg/kg. After the administration of pilocarpine, the mice were individually placed under glass cylinders for a 60-min observation period. Latency to status epilepticus was measured in each group.

5.5.4. Pain tests

5.5.4.1. Hot plate test. This study was conducted based on the method previously described by Eddy and Leimbach [79]. The device used in the hot plate test (hot/cold plate, Bioseb, France) is a heated metal plate surrounded by Plexiglas walls and covered by a glass lid to prevent the mice from escaping from the plate. The animals were individually placed on the center of the plate (heated to a constant temperature of 55 °C) for a maximum period of 1 min (to prevent tissue damage). The measured parameter was the latency to the occurrence of nociceptive reaction (*i.e.,* hind paw licking or jumping).

5.5.4.2. Formalin test. The formalin test was performed based on the method previously described by Laughlin et al. [80]. In rodents, the injection of diluted formalin solution evokes a biphasic nocifensive behavioral response (licking or biting the injected paw). The first (acute, neurogenic) phase of the test lasts for 5 min, while the second (late, inflammatory) phase occurs between 15 and 30 min after formalin injection. In this assay, 20 μl of 5% formalin solution was injected into the dorsal surface of the right hind paw of each mouse. Then, the mice were placed separately into glass beakers and observed for the next 30 min. The total time spent licking or biting the formalin-injected paw was measured during the first 5 min of the test and then between 15 and 30 min of the test in both drug-treated and vehicle-treated mice.

5.5.5. Antidepressant-like activity

5.5.5.1. Forced swim test. The forced swim test was performed based on the method previously described by Porsolt et al. [81]. The mice were dropped individually into glass cylinders (height 25 cm, diameter 10 cm) filled with water to a height of 10 cm (maintained at 23–25 °C). In this assay, after an initial 2-min period of vigorous activity, each mouse assumes an immobile posture. The duration of immobility in the experimental groups was recorded during the final 4 min of the total 6-min testing period. Mice were judged to be immobile when they remained floating passively in the water, making only small movements to keep their heads above the water surface.

5.5.5.2. Tail suspension test. The tail suspension test was performed based on the method previously described by Steru et al. [82]. C57BL/6J mice were *i.p.* administered the test compound or vehicle. Each mouse was suspended for 6 min by the tail (2 cm from the end of the tail) using adhesive tape, 75 cm above the surface of the table. The experiment lasted 6 min, and the total duration of immobility (in seconds) was measured. Immobility was defined as the absence of any limb or body movements, except for those caused by respiration.

5.5.6. Anxiolytic-like activity

5.5.6.1. Four-plate test. A four-plate test was performed based on the method previously described by Aron et al. [83]. The four-plate test device (Bioseb, France) consists of a rectangular chamber (18 cm × 26 cm × 16 cm) covered by a PVC-constructed lid. The bottom of the apparatus contains four metal plates (each with dimensions of 8 cm × 11 cm), each separated by a 4 mm-long gap between them. The bottom of the chamber is connected to the electric impulse generator. Mice were individually placed in the device. The first 15 s was the habituation period, while during the next 60 s, the test was carried out. Each time a mouse moved from one metal plate to another, an electric impulse (0.8 mA, duration of 0.5 s) was applied. The parameter measured in the four-plate test was the number of "punished" crossings made by the mouse when moving from one plate to another.

5.5.6.2. Elevated plus maze. The elevated plus maze test was performed based on the method previously described by Walf and Frye [84]. The elevated plus maze for mice consists of two opposing open arms (30 cm × 5 cm) and two enclosed arms (30 cm × 5 cm × 25 cm) connected by a central platform forming the shape of a plus sign. The dimensions of the central field that connects the open and closed arms are 5 cm × 5 cm. In this test, each mouse was individually placed at the central field of the apparatus with its head turned toward one of the closed arms. The behavior of each animal over 5 min was observed and recorded by means of a video camera (Sony Digital, Japan), which was fixed to the wall above the elevated plus maze. In this test, the following parameters were measured in drug-treated and control animals: time spent in the open arms and the percentage ratio between the number of entries into the open arms and the number of entries into all of the arms. To exclude the impact of excrements or smell left by a previous mouse on the behavior of the next mouse, the device was carefully cleaned after each testing session.

5.5.7. Locomotor activity test

The locomotor activity test was performed based on the method previously described by Kowalczyk et al. [28]. The locomotor activity test was performed using activity cages (40 cm × 40 cm × 30 cm, supplied with I.R. beam emitters) (Activity Cage 7441, Ugo Basile, Italy) connected to a counter to record light-beam interrupts. Sixty minutes before the experiment, the mice were pretreated with the test compound or vehicle and then individually placed in the activity cages in a sound-attenuated room. The movements of the animals (*i.e.*, the number of light-beam crossings) were counted during the next 30 min of the test. Before the test, the animals were habituated to the locomotor activity cages for 15 min.

5.5.8. Data analysis

Data analysis of *in vivo* results was performed using GraphPad Prism software (version 8.0, California, US). Results obtained in *in vivo* tests are expressed as the mean ± SEM or in percentages of activity (MES test, EPM test). Statistical analysis was performed using the Shapiro-Wilk normality test, followed by the analysis of variance (ANOVA) and followed by Dunnett's post hoc comparison to test differences between drug-treated groups and the control group. Repeated measures ANOVA followed by Bonferroni's multiple comparison were used to assess statistical significance among groups in the locomotor activity test. $P < 0.05$ was considered significant. In the ECT test, median current strength (CS_{50}) values with their 95% confidence limits were calculated and analyzed by computer log-probit analysis according to Litchfield and Wilcoxon [85].

Declaration of competing interest

The authors declare that they have no known competing financial interests or personal relationships that could have appeared to influence the work reported in this paper.

Acknowledgments

The chemistry studies were financially supported by the National Science Center in Poland as part of grant DEC-2012/05/B/NZ7/02705 and the Jagiellonian University Medical College grant K/DSC/001419. The *in vitro* studies were financially supported by the National Science Center in Poland as part of grant 2015/16/T/NZ7/00032. The molecular modeling studies were financially supported by the National Science Center, Poland, grant no. 2016/23/D/NZ7/01172. The *in vivo* studies were financially supported by the National Science Center in Poland as part of grants DEC-2012/05/B/NZ7/02705 (anticonvulsant, antidepressant-like and anxiolytic-like activities) and DEC-2014/15/B/NZ7/00930 (analgesic activity).

Appendix A. Supplementary data

Supplementary data to this article can be found online at https://doi.org/10.1016/j.ejmech.2021.113512.

References

[1] A.V. Kalueff, D.J. Nutt, Role of GABA in anxiety and depression 24 (2007) 495–517, https://doi.org/10.1002/da.
[2] K.K. Madsen, R.P. Clausen, O.M. Larsson, P. Krogsgaard-Larsen, A. Schousboe, H. Steve White, Synaptic and extrasynaptic GABA transporters as targets for anti-epileptic drugs, J. Neurochem. 109 (2009) 139–144, https://doi.org/10.1111/j.1471-4159.2009.05982.x.
[3] D.M. Treiman, GABAergic mechanisms in epilepsy, Epilepsia 42 (2001) 8–12, https://doi.org/10.1046/j.1528-1157.2001.042Suppl.3008.x.
[4] N.O. Dalby, Inhibition of γ-aminobutyric acid uptake: anatomy, physiology and effects against epileptic seizures, Eur. J. Pharmacol. 479 (2003) 127–137, https://doi.org/10.1016/j.ejphar.2003.08.063.
[5] P. Krogsgaard-Larsen, E. Falch, O.M. Larsson, A. Schousboe, GABA uptake inhibitors: relevance to antiepileptic drug research, Epilepsy Res. 1 (1987) 77–93, https://doi.org/10.1016/0920-1211(87)90012-X.
[6] R. Gosselin, M.R. Suter, R. Ji, I. Decosterd, R. Ji, I. Decosterd, Glial cells and chronic pain, Neuroscientist 16 (2010) 519–531, https://doi.org/10.1177/1073858409360822.
[7] T.J. Price, F. Cervero, M.S. Gold, D.L. Hammond, S.A. Prescott, Chloride regulation in the pain pathway, Brain Res. Rev. 60 (2009) 149–170, https://doi.org/10.1016/j.brainresrev.2008.12.015.
[8] K. Sałat, P. Kowalczyk, B. Gryzło, A. Jakubowska, K. Kulig, New investigational drugs for the treatment of neuropathic pain, Expet Opin. Invest. Drugs 23 (2014) 1093–1104, https://doi.org/10.1517/13543784.2014.916688.
[9] P. Nuss, Anxiety disorders and GABA neurotransmission: a disturbance of modulation, Neuropsychiatric Dis. Treat. 11 (2015) 165–175.
[10] L.E. Collins-Praino, S.J. Podurgiel, R. Kovner, P.A. Randall, J.D. Salamone, Extracellular GABA in globus pallidus increases during the induction of oral tremor by haloperidol but not by muscarinic receptor stimulation, Behav. Brain Res. 234 (2012) 129–135, https://doi.org/10.1016/j.bbr.2012.06.011.
[11] D. Zádori, A. Geisz, E. Vámos, L. Vécsei, P. Klivényi, Valproate ameliorates the survival and the motor performance in a transgenic mouse model of Huntington's disease, Pharmacol. Biochem. Behav. 94 (2009) 148–153, https://doi.org/10.1016/j.pbb.2009.08.001.
[12] K.L. Lanctôt, N. Herrmann, P. Mazzotta, L.R. Khan, N. Ingber, GABAergic function in alzheimer 's disease: evidence for the treatment of behavioural and psychological symptoms of dementia, Can. J. Psychiatr. 49 (2004) 439–453.
[13] A.S. Kristensen, J. Andersen, T.N. Jørgensen, L. Sørensen, J. Eriksen, C.J. Loland, K. Strømgaard, U. Gether, SLC6 neurotransmitter transporters: structure, function, and regulation, Pharmacol. Rev. 63 (2011) 585–640, https://doi.org/10.1124/pr.108.000869.
[14] A. Ortega, A. Schousboe, Glial amino acid transporters, Adv. Neurobiol. (2017), https://doi.org/10.1007/978-3-319-55769-4.
[15] Y. Zhou, S. Holmseth, R. Hua, A.C. Lehre, A.M. Olofsson, I. Poblete-Naredo, S.A. Kempson, N.C. Danbolt, The betaine-GABA transporter (BGT1, slc6a12) is predominantly expressed in the liver and at lower levels in the kidneys and at the brain surface, AJP Ren. Physiol. 302 (2012) 316–328, https://doi.org/10.1152/ajprenal.00464.2011.
[16] S.A. Kempson, Y. Zhou, N.C. Danbolt, The betaine/GABA transporter and betaine: roles in brain, kidney, and liver, Front. Physiol. 5 (2014) 1–16, https://doi.org/10.3389/fphys.2014.00159.
[17] K. Łątka, J. Jończyk, M. Bajda, γ-Aminobutyric acid transporters as relevant biological target: their function, structure, inhibitors and role in the therapy of different diseases, Int. J. Biol. Macromol. 158 (2020) 750–772, https://doi.org/10.1016/j.ijbiomac.2020.04.126.
[18] Y. Zhou, N.C. Danbolt, GABA and glutamate transporters in brain, Front. Endocrinol. 4 (2013) 1–14, https://doi.org/10.3389/fendo.2013.00165.
[19] Y. Zhou, S. Holmseth, C. Guo, B. Hassel, G. Höfner, H.S. Huitfeldt, K.T. Wanner, N.C. Danbolt, Deletion of the γ-aminobutyric acid transporter 2 (GAT2 and SLC6A13) gene in mice leads to changes in liver and brain taurine contents, J. Biol. Chem. 287 (2012) 35733–35746, https://doi.org/10.1074/jbc.M112.368175.
[20] S.B. Vogensen, L. Jørgensen, K.K. Madsen, N. Borkar, P. Wellendorph, J. Skovgaard-Petersen, A. Schousboe, H.S. White, P. Krogsgaard-Larsen, R.P. Clausen, Selective mGAT2 (BGT-1) GABA uptake inhibitors: design, synthesis, and pharmacological characterization, J. Med. Chem. 56 (2013) 2160–2164, https://doi.org/10.1021/jm301872x.
[21] B. Kragholm, T. Kvist, K.K. Madsen, L. Jørgensen, S.B. Vogensen, A. Schousboe, R.P. Clausen, A.A. Jensen, H. Bräuner-Osborne, Discovery of a subtype selective inhibitor of the human betaine/GABA transporter 1 (BGT-1) with a non-

competitive pharmacological profile, Biochem. Pharmacol. 86 (2013) 521–528, https://doi.org/10.1016/j.bcp.2013.06.007.
[22] S.B. Vogensen, L. Jørgensen, K.K. Madsen, A. Jurik, N. Borkar, E. Rosatelli, B. Nielsen, G.F. Ecker, A. Schousboe, R.P. Clausen, Structure activity relationship of selective GABA uptake inhibitors, Bioorg. Med. Chem. 23 (2015) 2480–2488, https://doi.org/10.1016/j.bmc.2015.03.060.
[23] M.E.K. Lie, S. Kickinger, J. Skovgaard, P. Gerhard, F.E. Rasmus, A. Schousboe, H.S. White, P. Wellendorph, Pharmacological characterization of a betaine/GABA transporter 1 (BGT1) inhibitor displaying an unusual biphasic inhibition profile and anti - seizure effects, Neurochem. Res. 10 (2020), https://doi.org/10.1007/s11064-020-03017-y.
[24] S. Kickinger, A. Al-Khawaja, A.S. Haugaard, M.E.K. Lie, F. Bavo, R. Löffler, M. Damgaard, G.F. Ecker, B. Frølund, P. Wellendorph, Exploring the molecular determinants for subtype-selectivity of 2-amino-1,4,5,6-tetrahydropyrimidine-5-carboxylic acid analogs as betaine/GABA transporter 1 (BGT1) substrate-inhibitors, Sci. Rep. 10 (2020) 1–15, https://doi.org/10.1038/s41598-020-69908-w.
[25] G.H. Fülep, C.E. Hoesl, G. Höfner, K.T. Wanner, New highly potent GABA uptake inhibitors selective for GAT-1 and GAT-3 derived from (R)- and (S)-proline and homologous pyrrolidine-2-alkanoic acids, Eur. J. Med. Chem. 41 (2006) 809–824, https://doi.org/10.1016/j.ejmech.2006.01.019.
[26] A. Kragler, G. Höfner, K.T. Wanner, Synthesis and biological evaluation of aminomethylphenol derivatives as inhibitors of the murine GABA transporters mGAT1-mGAT4, Eur. J. Med. Chem. 43 (2008) 2404–2411, https://doi.org/10.1016/j.ejmech.2008.01.005.
[27] X. Gong, Y. Shao, B. Li, L. Chen, C. Wang, Y. Chen, ??-Aminobutyric acid transporter-1 is involved in anxiety-like behaviors and cognitive function in knockout mice, Exp. Ther. Med. 10 (2015) 653–658, https://doi.org/10.3892/etm.2015.2577.
[28] K. Sałat, A. Podkowa, P. Kowalczyk, K. Kulig, A. Dziubina, B. Filipek, T. Librowski, Anticonvulsant active inhibitor of GABA transporter subtype 1, tiagabine, with activity in mouse models of anxiety, pain and depression, Pharmacol. Rep. 67 (2015) 465–472, https://doi.org/10.1016/j.pharep.2014.11.003.
[29] F.T. Kern, K.T. Wanner, Generation and screening of oxime libraries addressing the neuronal GABA transporter GAT1, ChemMedChem 10 (2015) 396–410, https://doi.org/10.1002/cmdc.201402376.
[30] T.G.M. Dhar, L.A. Borden, S. Tyagarajan, K.E. Smith, T.A. Branchek, R.L. Weinshank, C. Gluchowski, Design, synthesis and evaluation of substituted triarylnipecotic acid derivatives as GABA uptake inhibitors: identification of a ligand with moderate affinity and selectivity for the cloned human GABA transporter GAT- 3, J. Med. Chem. 37 (1994) 2334–2342, https://doi.org/10.1021/jm00041a012.
[31] K. Kataoka, K. Hara, Y. Haranishi, T. Terada, T. Sata, The antinociceptive effect of SNAP5114, a gamma-aminobutyric acid transporter-3 inhibitor, in rat experimental pain models, Anesth. Analg. 116 (2013) 1162–1169, https://doi.org/10.1213/ANE.0b013e318282dda7.
[32] K. Sałat, A. Podkowa, N. Malikowska, F. Kern, J. Pabel, E. Wojcieszak, K. Kulig, K.T. Wanner, B. Strach, E. Wyska, Novel, highly potent and in vivo active inhibitor of GABA transporter subtype 1 with anticonvulsant, anxiolytic, antidepressant and antinociceptive properties, Neuropharmacology 113 (2017) 331–342, https://doi.org/10.1016/j.neuropharm.2016.10.019.
[33] L.A. Borden, Gaba transporter heterogeneity: Pharmacology and cellular localization, Neurochem. Int. 29 (1996) 335–356. http://www.sciencedirect.com/science/article/pii/0197018695001581.
[34] T. Kvist, B. Christiansen, A.A. Jensen, H. Bräuner-Osborne, The four human gamma-aminobutyric acid (GABA) transporters: pharmacological characterization and validation of a highly efficient screening assay, Comb. Chem. High Throughput Screen. 12 (2009) 241–249, https://doi.org/10.2174/138620709787581684.
[35] J. Pabel, M. Faust, C. Prehn, B. Wörlein, L. Allmendinger, G. Höfner, K.T. Wanner, Development of an (S)-1-{2-[Tris(4-methoxyphenyl)methoxy] ethyl}piperidine-3-carboxylic acid [(S)-SNAP-5114] carba analogue inhibitor for murine γ-aminobutyric acid transporter Type4, ChemMedChem 7 (2012) 1245–1255, https://doi.org/10.1002/cmdc.201200126.
[36] A.M.C. Böck, G. Höfner, K.T. Wanner, N-substituted nipecotic acids as (S)-SNAP-5114 analogues with modified lipophilic domains, ChemMedChem 15 (2020) 756–771, https://doi.org/10.1002/cmdc.201900719.
[37] T. Kobayashi, A. Suemasa, A. Igawa, S. Ide, H. Fukuda, H. Abe, M. Arisawa, M. Minami, S. Shuto, Conformationally restricted GABA with bicyclo [3 . 1 . 0] hexane backbone as the first highly selective BGT - 1 inhibitor, ACS Med. Chem. Lett. 5 (2014) 889–893.
[38] M. Damgaard, A.S. Haugaard, S. Kickinger, A. Al-khawaja, M.E.K. Lie, G.F. Ecker, Development of non-GAT1-selective inhibitors: challenges and achievements, Adv. Neurobiol. 16 (2017) 315–332, https://doi.org/10.1007/978-3-319-55769-4.
[39] M.B. Zaręba P, B. Gryzło, G. Mazur, Development, recent achievements and current directions of research into GABA uptake inhibitors, Curr. Med. Chem. (2019), https://doi.org/10.2174/0929867325666191010120236, 10.21.
[40] S. Kickinger, A. Al-Khawaja, A.S. Haugaard, M.E.K. Lie, F. Bavo, R. Löffler, M. Damgaard, G.F. Ecker, B. Frølund, P. Wellendorph, Exploring the molecular determinants for subtype-selectivity of 2-amino-1,4,5,6-tetrahydropyrimidine-5-carboxylic acid analogs as betaine/GABA transporter 1 (BGT1) substrate-inhibitors, Sci. Rep. 10 (2020) 1–15, https://doi.org/10.1038/s41598-020-69908-w.
[41] M.E.K. Lie, S. Kickinger, J. Skovgaard, P. Gerhard, F.E. Rasmus, A. Schousboe, H.S. White, P. Wellendorph, Pharmacological characterization of a betaine/GABA transporter 1 (BGT1) inhibitor displaying an unusual biphasic inhibition profile and anti - seizure effects, Neurochem. Res. 10 (2020), https://doi.org/10.1007/s11064-020-03017-y.
[42] S. Kickinger, E. Hellsberg, A. Schousboe, G.F. Ecker, P. Wellendorph, Structural and molecular aspects of betaine-GABA transporter 1 (BGT1) and its relation to brain function Stefanie, Neuropharmacology (2019), https://doi.org/10.1016/j.Neuropharm.2019.05.021 (n.d.).
[43] K. Łątka, J. Jończyk, M. Bajda, Structure modeling of γ-aminobutyric acid transporters – molecular basics of ligand selectivity, Int. J. Biol. Macromol. 158 (2020) 1380–1389, https://doi.org/10.1016/j.ijbiomac.2020.04.263.
[44] A. Sarup, O.M. Larsson, A. Schousboe, GABA transporters and GABA-transaminase as drug targets, Curr. Drug Targets - CNS Neurol. Disord. 2 (2003) 269–277, https://doi.org/10.2174/1568007033482788.
[45] P. Zaręba, B. Gryzło, K. Malawska, K. Sałat, H. Gc, A. Nowaczyk, Ł. Fijałkowski, A. Rapacz, Novel mouse GABA uptake inhibitors with enhanced inhibitory activity toward mGAT3/4 and their effect on pain threshold in mice, Eur. J. Med. Chem. (2020), https://doi.org/10.1016/j.ejmech.2019.111920, 10.10.
[46] P. Kowalczyk, K. Sałat, G.C. Höfner, M. Mucha, A. Rapacz, A. Podkowa, B. Filipek, K.T. Wanner, K. Kulig, Synthesis, biological evaluation and structure-activity relationship of new GABA uptake inhibitors, derivatives of 4-aminobutanamides, Eur. J. Med. Chem. 83 (2014) 256–273, https://doi.org/10.1016/j.ejmech.2014.06.024.
[47] P. Kowalczyk, K. Sałat, G.C. Höfner, N. Guzior, B. Filipek, K.T. Wanner, K. Kulig, 2-Substituted 4-hydroxybutanamides as potential inhibitors of γ-aminobutyric acid transporters mGAT1-mGAT4: synthesis and biological evaluation, Bioorg. Med. Chem. 21 (2013) 5154–5167, https://doi.org/10.1016/j.bmc.2013.06.038.
[48] K.E. Andersen, C. Braestrup, F.C. Grønwald, A.S. Jørgensen, E.B. Nielsen, U. Sonnewald, P.O. Sørensen, P.D. Suzdak, L.J. Knutsen, The synthesis of novel GABA uptake inhibitors. 1. Elucidation of the structure-activity studies leading to the choice of (R)-1-[4,4-bis(3-methyl-2-thienyl)-3-butenyl]-3-piperidinecarboxylic acid (tiagabine) as an anticonvulsant drug candidate, J. Med. Chem. 36 (1993) 1716–1725, https://doi.org/10.1021/jm00064a005.
[49] K.E. Andersen, J.L. Sørensen, J. Lau, B.F. Lundt, H. Petersen, P.O. Huusfeldt, P.D. Suzdak, M.D. Swedberg, Synthesis of novel gamma-aminobutyric acid (GABA) uptake inhibitors. 5.(1) Preparation and structure-activity studies of tricyclic analogues of known GABA uptake inhibitors, J. Med. Chem. 44 (2001) 2152–2163.
[50] K. Stach, DE1203253, 1965.
[51] G. Chen, H. Xia, Y. Cai, D. Ma, J. Yuan, C. Yuan, Synthesis and SAR study of diphenylbutylpiperidines as cell autophagy inducers, Bioorg. Med. Chem. Lett 21 (2011) 234–239, https://doi.org/10.1016/j.bmcl.2010.11.029.
[52] P. Kowalczyk, G.H. Höfner, K.T. Wanner, K. Kulig, Synthesis and pharmacological evaluation of new 4 ,4-Diphenylbut-3-Enyl derivatives of 4-hydroxybutanamides as gaba uptake inhibitors, Acta Pol. Pharm. Drug Res. 69 (2012) 157–160.
[53] C. Zepperitz, G. Höfner, K.T. Wanner, MS-binding assays: kinetic, saturation, and competitive experiments based on quantitation of bound marker as exemplified by the GABA transporter mGAT1, ChemMedChem 1 (2006) 208–217, https://doi.org/10.1002/cmdc.200500038.
[54] M. Petrera, T. Wein, L. Allmendinger, M. Sindelar, J. Pabel, G. Höfner, K.T. Wanner, Development of highly potent GAT1 inhibitors: synthesis of nipecotic acid derivatives by suzuki-miyaura cross-coupling reactions, ChemMedChem 11 (2016) 519–538, https://doi.org/10.1002/cmdc.201500490.
[55] Q.R. Liu, B. López-Corcuera, S. Mandiyan, H. Nelson, N. Nelson, Molecular characterization of four pharmacologically distinct gamma-aminobutyric acid transporters in mouse brain [corrected], J. Biol. Chem. 268 (1993) 2106–2112.
[56] H. Nelson, S. Mandiyan, N. Nelson, Cloning of the human brain GABA transporter, FEBS Lett. 269 (1990) 181–184, https://doi.org/10.1016/0014-5793(90)81149-l.
[57] L.A. Borden, T.G. Dhar, K.E. Smith, T.A. Branchek, C. Gluchowski, R.L. Weinshank, Cloning of the human homologue of the GABA transporter GAT-3 and identification of a novel inhibitor with selectivity for this site, Recept. Channel 2 (1994) 207–213.
[58] L.A. Borden, K.E. Smith, E.L. Gustafson, T.A. Branchek, R.L. Weinshank, Cloning and expression of a betaine/GABA transporter from human brain, J. Neurochem. 64 (1995) 977–984, https://doi.org/10.1046/j.1471-4159.1995.64030977.x.
[59] B. Christiansen, A.K. Meinild, A.A. Jensen, H. Bräuner-Osborne, Cloning and characterization of a functional human γ-aminobutyric acid (GABA) transporter, human GAT-2, J. Biol. Chem. 282 (2007) 19331–19341, https://doi.org/10.1074/jbc.M702111200.
[60] S. Schmitt, G. Höfner, K.T. Wanner, Application of MS transport assays to the four human γ-aminobutyric acid transporters, ChemMedChem 10 (2015) 1498–1510, https://doi.org/10.1002/cmdc.201500254.
[61] N.O. Dalby, GABA-level increasing and anticonvulsant effects of three different GABA uptake inhibitors, Neuropharmacology 39 (2000) 2399–2407, https://doi.org/10.1016/S0028-3908(00)00075-7.
[62] K. Sałat, K. Kulig, GABA transporters as targets for new drugs, Fut. Sci. 3 (2011) 211–222.
[63] A. Schousboe, K.K. Madsen, H.S. White, GABA transport inhibitors and seizure Protection : the past and future, Future Med. Chem. 3 (2011) 183–187,

https://doi.org/10.4155/fmc.10.288.
[64] M. Chrościńska-krawczyk, M. Jargieło-baszak, M. Andres-mach, J.J. Łuszczki, Influence of caffeine on the protective activity of gabapentin and topiramate in a mouse model of generalized tonic-clonic seizures, Pharmacol. Rep. 68 (2009) 680–685.
[65] W. Loscher, Critical review of current animal models of seizures and epilepsy used in the discovery and development of new antiepileptic drugs, Seizure Eur. J. Epilepsy. 20 (2011) 359–368, https://doi.org/10.1016/j.seizure.2011.01.003.
[66] W. Löscher, Critical review of current animal models of seizures and epilepsy used in the discovery and development of new antiepileptic drugs, Seizure 20 (2011) 359–368, https://doi.org/10.1016/j.seizure.2011.01.003.
[67] W. Löscher, D. Schmidt, Modern antiepileptic drug development has failed to deliver: ways out of the current dilemma, Epilepsia 52 (2011) 657–678, https://doi.org/10.1111/j.1528-1167.2011.03024.x.
[68] W. Loscher, Critical review of current animal models of seizures and epilepsy used in the discovery and development of new antiepileptic drugs, Seizure Eur. J. Epilepsy. 20 (2011) 359–368, https://doi.org/10.1016/j.seizure.2011.01.003.
[69] M. Brodie, T. Covanis, A. Gil-nagel, H. Lerche, E. Perucca, G. Sills, S. White, Epilepsy & Behavior, Epilepsy Behav. 21 (2011) 490, https://doi.org/10.1016/j.yebeh.2011.04.053.
[70] U.B. Olsen, C.T. Eltorp, B.K. Ingvardsen, T.K. Jørgensen, J.A. Lundbæk, C. Thomsen, A.J. Hansen, ReN 1869 , a novel tricyclic antihistamine, is active against neurogenic pain and inf lammation 435 (2002) 43–57.
[71] P. Zwanzger, D. Eser, F. Padberg, T.C. Baghai, C. Schule, F. Rötzer, R. Ella, H.J. Möller, R. Rupprecht, Effects of tiagabine on cholecystokinin-tetrapeptide (CCK-4)-induced anxiety in healthy volunteers, Depress. Anxiety 18 (2003) 140–143, https://doi.org/10.1002/da.10099.
[72] D.P. Pham-Huu, J.R. Deschamps, S. Liu, B.K. Madras, P.C. Meltzer, Synthesis of 8-thiabicyclo[3.2.1]octanes and their binding affinity for the dopamine and serotonin transporters, Bioorg. Med. Chem. 15 (2007) 1067–1082, https://doi.org/10.1016/j.bmc.2006.10.016.
[73] C.K. Thoeringer, A. Erhardt, I. Sillaber, M.B. Mueller, F. Ohl, F. Holsboer, M.E. Keck, Long-term anxiolytic and antidepressant-like behavioural effects of tiagabine, a selective GABA transporter-1 (GAT-1) inhibitor, coincide with a decrease in HPA system activity in C57BL/6 mice, J. Psychopharmacol. 24 (2010) 733–743, https://doi.org/10.1177/0269881109103091.
[74] X. Gong, Y. Shao, B. Li, L. Chen, C. Wang, Y. Chen, γ-aminobutyric acid transporter-1 is involved in anxiety-like behaviors and cognitive function in knockout mice, Exp. Ther. Med. 10 (2015) 653–658, https://doi.org/10.3892/etm.2015.2577.
[75] S.H. Grimm, G. Höfner, K.T. Wanner, Development and validation of an LC-ESI-MS/MS method for the triple reuptake inhibitor indatraline enabling its quantification in MS Binding Assays, Anal. Bioanal. Chem. 407 (2015) 471–485, https://doi.org/10.1007/s00216-014-8312-8.
[76] S.H. Grimm, G. Höfner, K.T. Wanner, MS binding assays for the three monoamine transporters using the triple reuptake inhibitor (1R,3S)-Indatraline as native marker, ChemMedChem 10 (2015) 1027–1039, https://doi.org/10.1002/cmdc.201500084.
[77] D. Łażewska, M. Kaleta, S. Hagenow, S. Mogilski, G. Latacz, T. Karcz, A. Lubelska, E. Honkisz, J. Handzlik, D. Reiner, G. Satała, B. Filipek, H. Stark, K. Kieć-kononowicz, Novel naphthyloxy derivatives - potent histamine H3 receptor ligands. Synthesis and pharmacological evaluation, Bioorg. Med. Chem. 26 (2018) 2573–2585, https://doi.org/10.1016/j.bmc.2018.04.023.
[78] J.T. Litchfield, F. Wilcoxon, A simplified method of evaluating dose- effect experiments, J. Pharmacol. Exp. Therapeut. 96 (1949) 99–113.
[79] N.B. Eddy, D. Leimbach, And dithienylbutylamines, J. Pharmacol. Exp. Therapeut. 107 (1953) 383–393.
[80] T.M. Laughlin, K. V Tram, G.L. Wilcox, A.K. Birnbaum, Comparison of antiepileptic drugs tiagabine , lamotrigine , and gabapentin in mouse models of acute , prolonged , and chronic nociception, J. Pharmacol. Exp. Therapeut. 303 (2002) 1168–1175.
[81] R.D. Porsolt, M. Le Pichon, M. Jalfre, Depression_a new animal model sensitive to antidepressant treatments, Nature 266 (1977) 730–732, https://doi.org/10.1038/266730a0.
[82] L. Steru, R. Chermat, B. Thierry, P. Simon, The tail suspension test : a new method for screening antidepressants in mice, Pharmacology 85 (1985) 367–370.
[83] J.R.B. C Aron, P. Simon, C. Larousse, Evaluation of a rapid technique for detecting minor, Neuropharmacology 10 (1971) 459–469, https://doi.org/10.1016/0028-3908(71)90074-8.
[84] A.A. Walf, C.A. Frye, The use of the elevated plus maze as an assay of anxiety-related behavior in rodents, Nat. Protoc. 2 (2007) 322–328, https://doi.org/10.1038/nprot.2007.44.The.
[85] J.T. Litchfield, F. Wilcoxon, A simplified method of evaluating dose- effect experiments, J. Pharmacol. Exp. Therapeut. 96 (1949) 99–113.